EXOSOME MEDIATED DELIVERY OF PACLITAXEL FOR THE TREATMENT OF MULTI DRUG RESISTANT PULMONARY METASTASES

Myung Soo Kim

A dissertation submitted to the faculty at the University of North Carolina at Chapel Hill in partial fulfillment of the requirements for the degree of Doctor of Philosophy in the Division of Molecular Pharmaceutics in the Eshelman School of Pharmacy.

Chapel Hill
2016

Approved by:

Elena Batrakova

Leaf Huang

Alexander Kabanov

Robin O'Connor-Semmes

Chad Pecot

ABSTRACT

Myung Soo Kim: Exosome Mediated Delivery of Paclitaxel for the Treatment of Multi-Drug Resistant Pulmonary Metastases
(Under the direction of Elena Batrakova)

Exosomes have recently come into focus as "natural nanoparticles" for use as drug delivery vehicles because they lack many drawbacks inherent to other nanoformulations. Many potentially useful chemotherapeutics possess undesirable attributes such as low solubility in aqueous solutions, immunogenicity, or inefficient accumulation in target cancer cells due to multidrug resistance (MDR) mechanisms. Our objective was to assess the feasibility of an exosome-based drug delivery platform for a potent chemotherapeutic agent, paclitaxel (PTX), to treat MDR cancers expressing the sigma receptor. Herein, we developed and compared different methods of loading exosomes released by macrophages with PTX (exoPTX), vectorized to target the sigma receptor (exoPTX-AA), and characterized their size, stability, drug release, and *in vitro* antitumor efficacy. A reformation of exosomes upon sonication resulted in high loading efficiency, and sustained drug release. Importantly, incorporation of PTX into exosomes increased cytotoxicity more than 50 times in drug resistant $MDCK_{MDR1}$ (Pgp+) cells. Furthermore, exoPTX and exoPTX-AA demonstrated significantly greater cytotoxicity against all cell lines tested, as compared to Taxol and PTX. The biodistribution of exoPTX and exoPTX-AA and the antitumor effects of exoPTX were further evaluated in a model of murine Lewis Lung Carcinoma pulmonary metastases. Our studies demonstrated nearly complete co-localization of airway-delivered exosomes and intravenously delivered

vectorized exosomes with cancer cells, and a potent anticancer effect of exoPTX in this mouse model. We conclude that exoPTX-AA holds significant potential for the delivery of various chemotherapeutics to treat drug resistant cancers.

TABLE OF CONTENTS

LIST OF TABLES AND FIGURES

LIST OF ABBREVIATIONS AND SYMBOLS

°	Degrees
AA	Anisamide
AAV	Adeno-associated virus
AD	Alzheimer's Disease
AFM	Atomic force microscopy
APC	Antigen presenting cells
ATP	Adenosine triphosphate
BCA	Biochorionic acid assay
BODIPY-PC	2-decanoyl-1-(O-(11-(4,4-difluoro-5,7-dimethyl-4-bora-3a,4a-diaza--s-indacene-3-propionyl)amino)undecyl)-sn-glycero-3-phosphocholine
CAM	Cell adhesion molecule
CDC	Cardiosphere derived cells
CRC	Colorectal cancer
DAPI	4′,6-diamidino-2-phenylindole dihydrochloride
DC	Dendritic cells
DLS	Dynamic light scattering
DMEM	Dulbecco's modified eagle's medium

DOX	Doxorubicin
DSPE	1,2-Distearoyl-sn-glycero-3-phosphoethanolamine
DSPE-PEG	1,2-Distearoyl-sn-glycero-3-phosphoethanolamine conjugated to polyethylene glycol
DSPE-PEG-AA	1,2-Distearoyl-sn-glycero-3-phosphoethanolamine conjugated to polyethylene glycol and anisamide
EPR	enhanced permeability and retention effect
ER	endoplasmic reticulum
EtOH	ethanol
exoAA	exosomes vectorized to the sigma receptor using anisamide
exoDOX	exosomes loaded with doxorubicin
exoPTX	exosomes loaded with paclitaxel
exoPTX-AA	exosomes loaded with paclitaxel and vectorized to the sigma receptor using anisamide
FBS	Fetal bovine serum
GAPDH	Glyceraldehyde 3-phosphate dehydrogenase
GDNF	Glial cell-derived neurotrophic factor,
GMP	Good manufacturing processes
HPLC	High performance liquid chromatography
HSP	Heat shock protein

HUVEC	Human Umbilical Vein Endothelial Cells
i.n.	Intranasal
i.v.	Intravenous
IC50	The concentration of an inhibitor where the response (or binding) is reduced by half.
ISEV	International Society of Extracellular Vesicles
kDa	Kilo-daltons
LC	Loading Capacity; (Weight of Drug)/(Weight of Formulation)
LLC	Lewis Lung Carcinoma
MDR	Multi-drug resistance
MHC	Major histocompatibility complex
MI	Myocardial infarction
MiRNA	Micro RNA
MPS	Mononuclear Phagocyte System
mRNA	Messenger RNA
MS	Multiple Sclerosis
MSC	Mescenchymal stem cell
MTT	Colorimetric assay for assessing cell metabolic activity
MVB	Multivesicular bodies

NEP	Neprilysin
nm	Nanometers
NMR	Nuclear magnetic resonance imaging
NSCLC	Non-small cell lung cancer
NTA	Nanoparticle Tracking Analysis
OVA	Chicken egg ovalbumin
OVA-Exo	Exosomes released from OVA-pulsed DCs
PD	Parkinson’s Disease
pDNA	Plasmid DNA
PEG	Polyethylene glycol
Pep-Exo	OVA peptide that was directly loaded into exosomes
Pgp	P-glycoprotein, a drug efflux transporter
PTX	Paclitaxel
RES	Reticuloendothelial system
Rh123	Rhodamime 123
RNA	Ribonucleic acid
RRI	Resistance Reversal Index (IC50 of drug vs. IC50 of the formulation)
RVG	Rabies virus glycoprotein

SEC	Size exclusion chromatography
siRNA	Small interfering RNA
SMC	Smooth muscle cells
TLC	Thin layer chromatography
µl	Microliters
µm	Micrometers
VEGF	Vascular endothelial growth factor
WB	Western Blot

CHAPTER 1. PREPARATION OF EXOSOMAL FORMULATION OF PACLITAXEL VECTORIZED TO SIGMA RECEPTOR[1][2]

OVERVIEW

The recently emerged field of nanotechnology holds great promise for developing drug delivery systems with targeting and controlled-release characteristics for cancer treatment; there have been many new advances and innovations made in this field during the past decade [1]. A large proportion of chemotherapeutic drugs have low aqueous solubility, consequently requiring the use of specialized delivery vehicles (e.g. micelle, liposome, polymeric nanoparticles, or other types of nanoparticles) for parenteral administration. These nanosized delivery vehicles are often complex and may be difficult to manufacture, cause unwanted side effects (such as the excipient Cremophor EL in the commercial formulation of PTX, Taxol), and/or are immunogenic. The most common method of reducing the immunogenicity of nanoformulated drugs is to decorate the nanoparticle in a polyethylene glycol (PEG) corona, which reduces recognition by the reticuloendothelial system (RES) and aids in avoiding clearance.

[1] Some of this text previously appeared in an article in the Journal of Controlled Release. The original citation is as follows: Using exosomes, naturally-equipped nanocarriers, for drug delivery. Elena V. Batrakova, Myung Soo Kim. Review the "Americas" *Special Issue of the J Contr. Rel.* 2015 Aug 1. pii: S0168-3659(15)30042-0. doi: 10.1016/j.jconrel.2015.07.030.

[2] Some of this text previously appeared in an article in the journal Nanomedicine. The original citation is as follows: Development of Exosome-encapsulated Paclitaxel to Overcome MDR in Cancer cells. Myung Soo Kim, Matthew J. Haney, Yuling Zhao, Richa Gupta, Zhijian He, Natalia L. Klyachko, Aleksandr Piroyan, Marina Sokolsky, Alexander v. Kabanov, and Elena V. Batrakova. *Nanomedicine*, Nov 13. pii: S1549-9634(15)00202-6. doi: 10.1016/j.nano.2015.10.012. PMID: 26586551

Exosomes are membrane-derived vesicles ~40-200 nm in diameter[1], they may be found in extracellular bodily fluids (e.g. urine, saliva, cerebrospinal fluid) and in conditioned cell culture media[2]. They are released by a variety of cell types and are formed when multivesicular bodies inside the cells fuse with the plasma membrane and release intraluminal vesicles into the extracellular microenvironment as exosomes[2, 3]. Exosomes naturally function as intracellular messengers, carrying RNA and proteins between the cells[4]. Recently, exosomes have begun to be explored for use as drug delivery vehicles for non-native therapeutics such as nucleic acids[5-10], gene delivery using adeno-associated virus (AAV)[11-13], and small molecule drugs, such as curcumin[2, 14, 15], and doxorubicin[16]. It has been demonstrated that exosomes are able to deliver their intraluminal cargo into the cytosol of target cells[17]. In addition, allogenic exosomes may have an immune privileged status, which allows for decreased drug clearance compared to PEGylated nanoformulations. These unique features make exosomes an attractive option for use as a drug delivery vehicle for cancer treatment.

Lung cancer is one of the most lethal forms of cancer and has a high rate of metastasis and recurrence; non-small cell lung cancer (NSCLC) is responsible for ~85% of all lung cancers, and prognosis of metastatic NSCLC is poor, with chemotherapy providing only minimal increases in survival rates, with a 5 year survival rate of <15% [18, 19]. It has been shown that a variety of cancer types, including NSCLC, overexpress the sigma receptor [20]. The sigma receptor is a popular target for nanoformulations treating various types of cancer, including lung cancer, and has been targeted for the delivery of drugs such as siRNA or doxorubicin [21-23]. Anisamide has been shown to have high affinity for the sigma receptor and has thus been utilized to target the sigma receptor[23]. Furthermore, Kooijmans et al. have recently shown that the introduction of polyethylene glycol (PEGylation) to exosomes results in stealth properties which

significantly increases their circulation time in mice, thus, PEGylation of exosomes may be utilized to increase the accumulation of exosomes at tumor sites or at sites of inflammation, which have enhanced vascular permeability and retention (EPR effect) [24].

Herein, we have developed a new nanoformulation consisting of exosomes loaded with PTX, a commonly used chemotherapeutic agent, and given stealth properties as well as vectorized to target the sigma receptor by the addition of DSPE-PEG-AA.

Different methods of loading PTX into exosomes were assessed to identify the most efficient approach that provided the greatest loading capacity while minimizing any detrimental effects to the exosomal product. In this study, we show that loading PTX into exosomes under mild sonication conditions followed by a 60 min. incubation period at 37°C increased drug solubility while maintaining exosomal membrane integrity and morphology, as well as allowing for the retention of critical exosomal proteins necessary for cell adhesion and uptake. Next, the optimal formulation of exosomes vectorized to target the sigma receptor while maximizing drug loading capacity was determined. First, an introduction to exosomes, methods of isolation, natural functions, and their use in drug delivery applications is given below.

Introduction

Biogenesis, Isolation, and Characterization of Exosomes

The biogenesis, characterization, and functions of exosomes are exciting new fields of research that have triggered significant interest over the past three decades. Exosomes are 40 - 100 nm sized extracellular plasma-membrane derived vesicles actively secreted by most cell types, in particular, cells of the immune system such as dendritic cells [25], macrophages [26], B cells [27], and T cells [28]; as well as mesenchymal stem cells [29], endothelial [30] and

epithelial cells [31]. Exosomes are also secreted by a variety of cancer cells [32]. They are defined by the size, surface proteins, and lipid composition.

The unique properties of exosomes can be attributed to their biogenesis; they are initially produced by invagination of the endosomal membrane to create multivesicular bodies (MVB) (**Figure 1.1**).

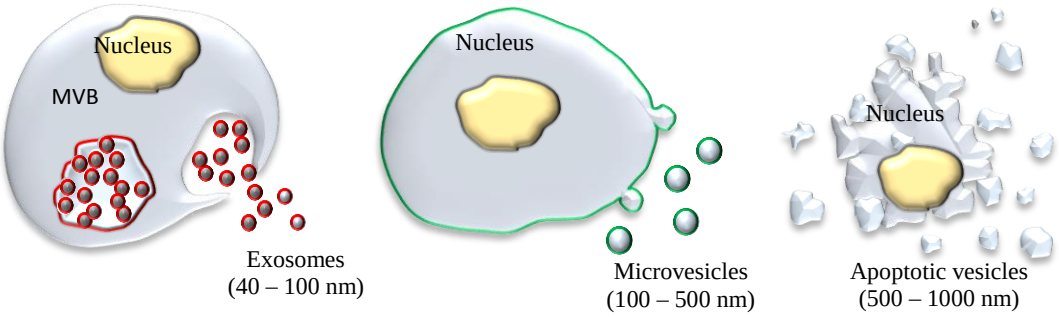

Figure 1.1. Schematic representation of different types of extracellular vesicles.

In contrast, exosomes' close relative, microvesicles, are greater in size (100 - 500 nm) and bud directly from the plasma membrane. Consequently, exosomes and microvesicles have endosomal (red) and plasma (green) membrane origin, respectively (**Figure 1.1**). Larger vesicles (500 - 1000 nm) are considered to be apoptotic vesicles (**Figure 1.1**). Many investigations, especially in the field of drug delivery, utilize both exosomes and microvesicles, defining them as extracellular vesicles, because a complete separation and purification of each type of vesicles is extremely laborious and difficult [33].

Exosomes can be characterized by size, protein and lipid content. Different techniques were developed for the characterization of exosomes. Among them are flow cytometry, western blotting, nanoparticle tracking analysis (NTA), dynamic light scattering (DLS), mass spectrometry (MS) and several microscopy techniques [34]. The International Society for Extracellular Vesicles (ISEV) published a position paper in 2014, in which the characterization

of exosomes is recommended by the presence of exosome-associated surface markers, as well as the absence of proteins not associated with exosomes [35]. Exosomal surface markers include TSG101, Alix, flotillin 1, tetraspanins (CD9, CD63, CD81), integrins (ITG**), and cell adhesion molecules (CAM) [35]. Exosomes are highly enriched in cholesterol, sphingomyelin, and hexosylceramides at the expense of phosphatidylcholine and phosphatidylethanolamine [36]. The fatty acids in exosomes are mostly saturated or monounsaturated. Together with the high concentration of cholesterol, this may account for lateral segregation of these lipids into exosomes during their formation at MVB. Exosomes can be isolated from conditioned cell culture media or bodily fluids by differential centrifugation, filtration paired with centrifugation, immunoaffinity or size exclusion chromatography, or polymer-based precipitation.

Differential Ultracentrifugation and Density Gradient Ultracentrifugation

This method is considered the "gold standard" for isolating exosomes. It involves applying a centrifugal force to a solution containing exosomes, *e.g.* conditioned cell culture media or biological fluids. First, a low speed centrifugation step (400 x *g*) is performed in order to remove cells and large cell debris. The supernatant is then subjected to 10,000 – 20,000 x *g* to remove large debris and intact organelles. Finally, the supernatant is again subjected to high speed centrifugation (100,000 - 150,000 x *g*) to pellet exosomes. It is worth noting that the type, quantity, and quality of exosomes isolated by this method is sensitive to the *g* force, rotor type, angle of rotor sedimentation, radius of centrifugal force, pelleting efficiency, and solution viscosity. One issue with differential ultracentrifugation is that it sediments exosomes as well as other vesicles, proteins, and/or protein-RNA aggregates. By including a sucrose density gradient, contaminants with densities different than exosomes may be separated from exosomes, allowing for recovery of a theoretically more pure fraction. Gradient centrifugation requires

extensive (62 – 90 h) centrifugation time [37], but provides a more uncontaminated exosome isolate than ultracentrifugation alone.

A fast and efficient method of exosome isolation was reported in [38]. Exosomes from monocyte-derived dendritic cells were rapidly purified (e.g. 4–6 h of a 2–3 L culture) based on their unique size and density. Ultrafiltration of the clarified supernatant through a 500-kDa membrane and ultracentrifugation into a 30% sucrose/deuterium oxide (D_2O) (98%) cushion (density 1.210 g/cm^3) reduced the volume and protein concentration approximately 200- and 1000-fold, respectively. The percentage recovery of exosomes ranged from 40% to 50% based on the exosome MHC class II concentration of the starting clarified supernatant [38]. While differential centrifugation has the potential for higher exosome yields, this method is subject to operator-dependent variability [38].

Immunoaffinity Chromatography

Immunoaffinity chromatography is a process in which antibodies, covalently attached to beads, filters, or other matrices, bind to specific surface proteins or antigens on the target particle and non-target particles remain unbound. The unbound fraction is discarded, and the desired bound fraction may be collected by washing the stationary phase, typically with a low pH buffer. For the isolation of exosomes, antibodies to exosomal surface markers such as TSG101 or tetraspanins are used (exosomal surface markers will be discussed further below). Tauro et al. showed that immunoaffinity chromatography is a more efficient method for isolating exosomes as compared to differential ultracentrifugation and density gradient ultracentrifugation [39]. However, because this method of exosomes isolation depends on antibody recognition of exosomal proteins, only a subset of all extracellular vesicles (those expressing the antibody-recognized protein) can be captured.

Size Exclusion Chromatography

Size exclusion chromatography (SEC) is a method wherein a solution consisting of a heterogeneous population of differently sized components is separated based on their size. A column containing heteroporous beads is used in SEC; components with a smaller hydrodynamic radius are able to pass through the many small pores, akin to a maze, resulting in a longer time to elute. Components with a larger hydrodynamic radius are unable to penetrate through as many pores, and thus elute earlier from the column. In this manner, exosomes may be separated from other vesicles and contaminants of different sizes. The advantages of SEC are that it preserves the integrity and biological activity of exosomes and other molecules being separated; because SEC is typically performed using gravity flow, vesicle structure and integrity remains intact. Furthermore, SEC has excellent reproducibility and sensitivity. However, because SEC uses gravity flow, it requires a long run time which limits its scalability for high-throughput applications.

Polymer Precipitation

Polymer precipitation has been used to isolate viruses and other macromolecules for more than 50 years, typically by use of a solution containing polyethylene glycol (PEG). The most commonly used commercial polymer precipitation-based product for exosome isolation is ExoQuick-TC™ from System Biosciences. Typically, to isolate exosomes, a precipitation solution consisting of PEG with a molecular weight of 8,000 Da is used. This precipitation solution is combined with biofluid containing exosomes and is incubated overnight at 4^0C. The mixture is then centrifuged at low speed to form a pellet containing exosomes. The product is relatively easy to use, and does not require specialized equipment or a lengthy run time. However, it has been shown that this method co-precipitates non-vesicular contaminants such as

lipoproteins, as well as polymer material [40]. These issues may be addressed by pre- and post-isolation steps. Pre-isolation involves the removal of subcellular particles such as lipoproteins. Post-isolation involves removal of the polymer, typically by using a Sephadex G-25 column [37].

Natural Functions of Exosomes and Their Intrinsic Biological Activity

Exosomes play a significant and diverse role in intercellular communication that is an essential process for the development and function of multicellular organisms. These extracellular vesicles were initially thought to be a mechanism for removing unneeded membrane proteins from reticulocytes. Recent studies have shown that they are specialized in long-distance intercellular communications [41, 42] facilitating transfer of proteins [43, 44], and functional mRNAs and microRNAs for subsequent protein expression in target cells [45, 46]. This mechanism of secretion, signaling and communication is a highly efficient, robust, and economic manner of exchanging information between cells. Thus, exosomes themselves exert unique biological activity, even without any loaded drug that may be used for therapeutic purposes.

Immune Regulation by Exosomes

Tumor cells are poorly immunogenic and this has hampered the development of effective cancer immunotherapy. By transporting ligands and receptors, exosomes can trigger an anti-tumor response by presenting tumor antigens to immune cells. Initially, tumor-derived exosomes that carry antigens have been suggested as a source of specific stimulus for the immune response against tumors [47]. These exosomes were shown to induce anti-tumor responses more efficiently than irradiated tumor cells, apoptotic bodies, or tumor cell lysates. For example,

mouse B lymphoma cells were reported to release exosomes that carry a number of heat shock proteins (HSP) that induced significant antitumor immune responses in T cells [48].

Later, it was demonstrated that tumor-derived exosomes can also possess immunosuppressive properties [49], promote oncogenesis, metastasis [50, 51], and drug resistance development [52-54]. Therefore, the attention was turned to the exosomes released by activated antigen presenting cells (APCs), such as dendritic cells (DCs), macrophages, T lymphocytes, and B cells. The presence of MHC class I and II, as well as T cell co-stimulatory molecules, on the surface of these exosomes could be an important mechanism of antigen presentation [55]. Furthermore, the immune response cells primed with antigens can package cellular components from cancer cells in exosomes that then promote immune responses [56-62]. In particular, exosomes secreted by DCs that were primed with acid-eluted tumor peptides were reported to eradicate established tumors in mice [56]. According to another study, DCs-secreted exosomes incubated with human breast adenocarcinoma cells (SK-BR-3) were able to induce tumor-sensitized T cells to secrete high levels of Interferon-γ (IFN-γ) [57]. Qazi et al. [58] reported a significant anti-cancer activity of exosomes secreted by DCs that were exposed to chicken egg ovalbumin (OVA). These exosomes elicited specific transgenic T cell proliferation *in vitro*. Interestingly, two different methods of OVA loading into exosomes were compared: OVA peptide that was directly loaded into exosomes (Pep-Exo), or exosomes released from OVA-pulsed DCs (OVA-Exo). Pep-Exo formulation was more efficient in specific transgenic T cell proliferation *in vitro*. However, only exosomes released from OVA-pulsed DCs were efficient *in vivo*, highlighting the importance of formulation strategies in some cases [58]. Noteworthy, DCs-derived exosomes may also exert undesirable effects, such as triggering the anti-donor T cell response that causes allograft rejection [63].

Along with the improving immune responses, exosomes released from T cells were shown to destroy tumor stroma, and prevent tumor invasion and metastases. In addition, cross-talk between T lymphocytes and endothelial cells through exosomes was reported [59]. Thus, T cell-derived exosomes were shown to modulate endothelial cell responses to vascular endothelial growth factor (VEGF) and alter tube formation and gene expression in target endothelial cells. Mechanistic studies revealed that overexpression of thrombospondin-1 and its receptor CD47 on exosomes derived from T cells allowed targeted and facilitated internalization of these extracellular vesicles into endothelial cells. CD47 transferred to the tumor vasculature by exosomes modulated tumor angiogenesis and inhibited pro-angiogenic signaling in endothelial cells [59]. Noteworthy, the induction of immune responses may be mediated not only by the bioactive lipids and proteins present in exosomes, but also by exosome-associated RNAs [60]. Contained inside exosomes, microRNAs (miRNAs) play a key role in mediating biological functions due to their prominent role in gene regulation. Thus, Aucher at al. [61] reported that human macrophages can transfer miRNAs to hepato-carcinoma cells and functionally inhibit proliferation of these cancerous cells. The transport of these miRNA was associated with extracellular vesicles.

Regarding infectious diseases, a succesful immunisation against difteria and *Leishmania* infections was achived by use of DC-derived exosomes that were exposed to difteria toxin [64] or *Leishmania major* [65] antigens, respectively. Furthermore, exosomes that were found in human breast milk can boost the immune response and alter the T cell balance toward a regulatory phenotype [66, 67]. This mechanism may be crucial for the development of the infants' immune system. Thus, exosomes are potent immune regulators, and may be utilized for

the design of vaccine adjuvants and therapeutic intervention strategies to modulate immune responses.

Protective and Regenerative Effects of Exosomes

Exosomes play a vital role in regulating a broad range of physiological and pathological cellular processes [68] that may be utilized for therapeutic purposes. Mesenchymal stem cells (MSCs) derived from bone marrow, adipose tissue, cord blood, and other origins have recently received much attention as potential therapeutic agents with regenerative properties [69-76]. It was reported that MSCs-derived exosomes produced significant cardio-protective paracrine effects against myocardial ischemia/reperfusion injury in pig and mouse models [69, 70]. These exosomes may also be beneficial in pulmonary hypertension (HP). HP is a kind of malignant pulmonary vascular disease characterized by an increase in pulmonary artery pressure, which may lead to heart failure and even death. MSCs-derived exosomes directly suppressed early pulmonary inflammation and vascular remodeling [71] through the suppression of hyper-proliferative pathways, including signal transducer and activator of transcription 3 (STAT3)-mediated signaling.

Exosomes secreted from cardiosphere-derived cells (CDCs) were shown to produce a range of diverse cardio-protective effects, including anti-inflammatory, anti-oxidative, anti-apoptotic, anti-fibrotic, and cardiomyogenic effects [76, 77]. CDCs-released exosomes stimulate angiogenesis, promote cardiomyocyte proliferation, and decreased programmed cell death *in vitro*. The regenerative capacity of these exosomes was demonstrated in a model of chronic myocardial infarction (MI) in rats [78]. These effects were attributed to the ability of exosomes to reduce collagen deposition and exert anti-fibrotic efficacy *via* paracrine mechanisms [79]. In addition, CDCs-released exosomes improved cardiac function, imparted structural benefits, and

increased viable mass after MI. The observed therapeutic effects were associated with normalized oxygen consumption, induced ATP production, and preserved mitochondrial integrity.

Exosomes derived from endothelial cells are a promising strategy to combat atherosclerosis [80]. Atherosclerosis, the underlying cause of myocardial infarction and stroke, occurs predominantly in predisposed spots in the large arteries. Systemic administration of exosomes released from human umbilical vein endothelial cells (HUVECs) reduced atherosclerotic lesions in mice fed a high-fat diet. It is known that shear stress and its central transcriptional regulator KLF2 elicit atheroprotective properties to the endothelium by regulating the expression of atheroprotective genes. Exosomes secreted by shear-stress-stimulated HUVECs were enriched in multiple miRNAs, prominently miR-143 and miR-145. HUVECs-released exosomes transported these miRNAs to smooth muscle cell (SMCs) which resulted in controlled target gene expression and reduction of atherosclerotic lesion formation in the mouse aorta [80].

MSCs-derived exosomes were shown to have neuroprotective effects in stroke. The release, as well as the content, of the MSC-generated exosomes can be modified by environmental conditions. Thus, stroke induces changes in the miRNA profile of MSCs-released exosomes [81, 82], especially in miRNAs that actively participate in the recovery process after stroke [83]. MSCs-derived exosomes transferred their therapeutic factors to recipient cells, and altered gene expression and thereby promoted neurite growth in rat primary neurons [73]. Hepatic regeneration was shown by use of MSC-derived exosomes in drug-induced liver injury models [84]. The higher survival rate was associated with up-regulation of the priming-phase genes during liver regeneration, which subsequently led to higher expression of proliferation proteins (PCNA and cyclin D1) in the exosomes-treated group. Therapeutic effects of exosomes

derived from human adipose tissue-derived MSCs were also reported for treatment of Alzheimer disease (AD) [72]. It was demonstrated that these exosomes carry enzymatically active neprilysin (NEP), the most important enzyme that degrades β-amyloid (Aβ) peptide plugs in the brain. MSCs-derived exosomes decreased both intracellular and extracellular Aβ levels in a neuroblastoma cell line N2A *in vitro*. Finally, Ju *et al*. showed protective effects of exosome-like nanoparticles isolated from crushed grapes [85]. Multivesicular bodies have been also identified in plants, and leaderless secreted proteins can be released in vesicles, as described recently [86]. Ju and colleagues observed that oral administration of exosome-like nanoparticles from grapes to mice led to the significant proliferation of the intestinal epithelium.

Using Exosomal Carriers for Therapeutics

Drug Loading into Exosomes

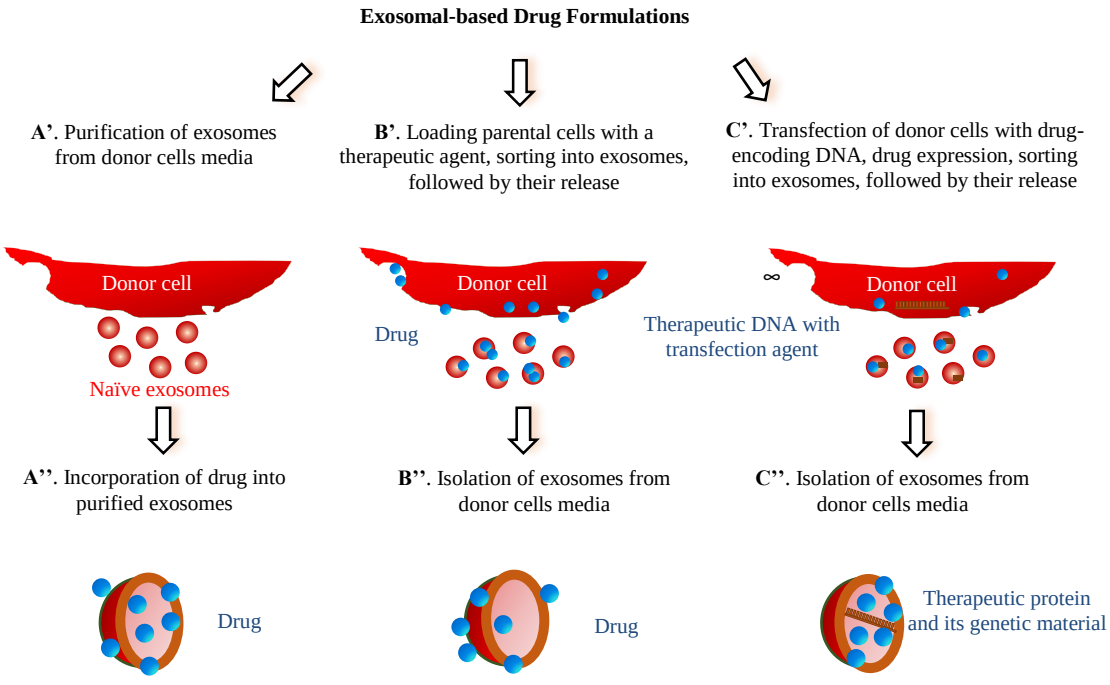

Figure 1.2 Different approaches for drug loading into exosomes.

These are several distinct approaches for loading of exosomal carriers with drugs (**Figure 1.2**): (**A**) loading naïve exosomes isolated from parental cells *ex vitro*; (**B**) loading parental cells

with a drug, which is then released in exosomes; and finally, (**C**) transfecting/infecting parental cells with DNA encoding therapeutically active compounds, which are then released in exosomes. Each of the approaches has its advantages and limitations, and may be dictated by the type of therapeutic agent.

Regarding *ex vitro* loading of naïve exosomes (**Figure 1.2, Path A**), different methods for drug incorporation were suggested. In most cases, lipophilic small molecules were passively loaded into exosomes during co-incubation with exosomes [87-93]. Thus, low molecular antioxidant, curcumin [89, 90], anticancer agents, Doxorubicin (Dox) [92, 93] and Paclitaxel (PTX) [94], and a model drug Rhodamine 123 [94] were loaded into exosomes by the incubation at room temperature (RT). The drug loading upon this loading procedure determined by HPLC varied from 7.2% for PTX to 11. 7% for Dox.

Exosomes naturally deliver mRNA, miRNA, various noncoding RNA, mitochondrial DNA, and genomic DNA [95, 96]. Therefore, they were suggested as carriers for nucleic acids transfer. Similar to the incorporation of genetic material into living cells, electroporation of purified exosomes was proposed for loading of exogenous RNA [5, 97-100]. Alvarez-Erviti et al. pioneered this method, electroporating siRNA into DC-derived exosomes [5]. The same method was used to load exosomes with miRNA to epidermal growth factor receptor (EGFR)-expressing breast cancer cells [101]. About 3,000 miRNA molecules were loaded *per* exosome. It should be taken into consideration that electroporation of extracellular vesicles with siRNA may be accompanied by extensive siRNA aggregate formation, which may cause overestimation of the amount of siRNA actually loaded into exosomes [102]. The authors suggested that electroporation is far less efficient than previously reported, and highlighted the necessity for

alternative methods to prepare siRNA-loaded exosomes. Exosomes are known to carry a negative surface charge, hence precluding electrostatic siRNA complexation. Pre-complexation of siRNA *via* cationic liposomes followed by fusion with isolated exosomes has been suggested for their loading with siRNA by Wahlgren *et al.* [103]. Furthermore, elevated temperature (37^0C) was may be used for improved siRNA loading into exosomes [104].

Exosomes are also known to be nature's way of delivering different proteins [105]. We suggested harnessing this mechanism for the delivery of a potent antioxidant, catalase, in exosomes [106]. Catalase is a large protein (MW 240 kDa that is susceptible to deactivation and rapid degradation, therefore the efficient incorporation of catalase in exosomes would be beneficial, but is not a simple task. We evaluated several loading methods. The amount of catalase loaded into exosomes increased as follows: incubation at RT < freeze/thaw cycles < sonication ≅ extrusion ≅ permeabilization with saponin. The highest loading capacity for catalase in exosomes was in the range of 20% - 26%. We hypothesized that the extensive reformation and reshaping of exosomes upon sonication and extrusion enabled catalase diffusion across relatively tight and highly structured lipid bilayers that resulted in the high loading efficiency of exosomal carriers. Furthermore, saponin treatment also increased catalase loading into exosomes. Saponin is an efficient permeabilization agent for cellular plasma membranes [107]. It is likely that, similar to whole cells, saponin can selectively remove membrane-bound cholesterol on exosomes, creating holes/pores in the exosomal lipid bilayers and thereby promoting catalase incorporation. Notably, aside from proteins, these methods for loading into exosomes can be applied to other therapeutic and imaging agents, in particular, gold nanoparticles [106].

As a second approach, parental cells can be loaded with exogenous compounds which then are released into the conditioned media inside exosomes (**Figure 1.2, Path B**). Thus, MSCs-

secreted exosomes were loaded with PTX by incubating the parental cells with the drug [108]. It was reported that the murine SR4987 cells that were used as MSCs model produced a significant amount of PTX-loaded exosomes as demonstrated by HPLC [108]. A similar result was reported for HepG2 cells that were incubated with different anticancer agents: PTX, Etoposide, Carboplatin, Irinotecan, Epirubicin, and Mitoxantrone [109]. Exosomes released from drug-treated HepG2 cells demonstrated strong anti-proliferative activity on the human pancreatic cell line CFPAC-1 and induced immunogenicity and HSPs-specific NK cell responses [109]. In another study, the breakdown of parental cells (monocytes /macrophages) loaded with anticancer agents, Dox, Gentamicin, 5-Fluoracil, or Carboplatin with subsequent isolation of exosome-like nanoparticles was also suggested [91]. An elegant approach to pack hydrophobic photosensitizers into exosomes was developed by professor Ji-Ho Park and his team in South Korea [110]. The researchers treated parental cells with synthetic membrane fusogenic liposomes loaded with hydrophobic therapeutics. The drug-loaded liposomes were efficiently incorporated into the membrane of exosomes in the parental cells and were consequently secreted from the cells.

We developed a new approach of loading parental cells (monocytes/macrophages) with catalase followed by isolation of drug-loaded exosomes from conditioned media (**Figure 1.2, Path B**) [106, 111]. To preserve the therapeutic protein against degradation in host cells and increase loading capacity, catalase was incorporated into a polymer-based nanocontainer before loading. Importantly, the formulation design of this polymer-based nanocontainer was different from the common approach, where a drug nanoformulation is prepared for systemic administration. Protective nanoparticles are typically size-restricted to avoid entrapment in MPS, focusing on small size nanoparticles with a PEG corona (to perpetuate a stealth effect). In

contrast, the best nanoformulation for loading into parental cells had a relatively large size (*c.a.* 200 nm) that resulted in improved accumulation in parental cells, and drug reshuffling into exosomes. The cross-linking of polymer-based nanoparticles with an excess of a non-biodegradable linker ensured low cytotoxicity of nanoformulation and efficient catalase protection in the parental cells [106, 112].

Finally, isolation of drug-loaded exosomes secreted from genetically-modified parental cells has been suggested as a third way of manufacturing exosome-based formulations (**Figure 1.2, Path C**) [33, 87, 111, 113]. As an example, OVA was loaded into exosomes when parental cells were transfected with OVAC1C2 fusion *c*DNA consisting of: (i) the cargo-encoding gene (OVA), and (ii) the gene encoding a protein known to localize to exosomes (C1C2) [113]. Our lab developed a new drug delivery system for different therapeutic proteins, where macrophages were transfected with plasmid DNA (*p*DNA) encoding therapeutic proteins, catalase [114], or glial cell-line derived neurotropic factor (GDNF) [111] to treat neurodegenerative disorders. An interesting approach for incorporation of adeno-associated virus (AAV) capsids into extracellular vesicles to diminish their immunogenicity and improve gene delivery was suggested by [115]. It was reported that during production, a fraction of released AAV vectors were associated with exosomes, termed vexosomes (vector-exosomes), which outperformed conventionally purified AAV vectors in transduction efficiency *in vitro*.

Therapeutic Effects of Drug-Loaded Exosomes

Since exosomal carriers can provide advantages of both cell-based drug delivery and nanotechnology, interest in using exosomes for therapeutic approaches has exploded in recent years. Similar to viruses, these remarkable carriers are capable of traveling from one cell to another, easily passing their contents across the cell membrane due to their unique

characteristics, and delivering their cargo in a biologically active form. Noteworthy, exosomes possess an intrinsic ability to cross biological barriers, including the most difficult to penetrate, blood brain barrier (BBB).

Exosomes have been exploited as drug delivery vehicles for low molecular drugs in several investigations [89-94, 108, 110]. In one of the first reports, exosomes loaded with an anti-inflammatory small molecule compound, curcumin, were shown to protect mice from lipopolysaccharides-induced brain inflammation [89, 90]. The incorporation of curcumin in exosomes improved its solubility, increased circulation time, preserved drug therapeutic activity, and improved brain delivery. In another study, exosomes loaded with different chemotherapeutics, Dox or PTX, were shown to traffic to tumor tissues and reduce tumor growth in mice without the adverse effects observed with the equipotent free drug [91-93]. Notable, the therapeutic effects of Dox-loaded exosomes were greater than the commercially available Dox-loaded liposomes, Doxil; the liposomal formulation was inefficient in reducing tumor growth in this model [91]. Pascucci et al. observed that PTX-treated MSCs mediated strong anti-tumorigenic effects because of their capacity to take up the drug and later release it in extracellular vesicles [108]. In this study, PTX-treated exosomes induced a dose-dependent inhibition of CFPAC-1 (human pancreatic adenocarcinoma) cell proliferation, as well as 50% inhibition of tumor growth. Next, exosomes loaded with hydrophobic photosensitizers exhibited superior phototherapeutic effects compared with the polymer-based synthetic nanoparticles [110]. This strategy allowed hydrophobic photosensitizers to significantly penetrate both spheroids and *in vivo* tumors, thereby enhancing the therapeutic efficacy. Finally, exosomes derived from brain endothelial cell line, bEND.3, were loaded with anticancer drugs and used for systemic delivery across the BBB to treat gliomas [94].

Another therapeutic avenue involves the use of exosomes to deliver exogenous siRNA [5, 97-100, 103, 116-118]. Wahlgren et al. reported the efficient silencing of the target *MAPK* gene in monocytes and lymphocytes using peripheral blood exosomes with incorporated exogenous siRNAs [103]. In another investigation, Shtam et al. introduced two different exogenous siRNAs against RAD51 and RAD52 into exosomes derived from HeLa cells [116]. In particular, the exosome-delivered siRNA against RAD51 was functional and caused the massive reproductive cell death of recipient cancer cells. The effect of exosome-siRNA gene silencing has also been validated in [117, 118]. As an example, extracellular vesicles were used to transport siRNA targeted to miR-150 [118]. miR150 is an oncomir due to its promotional effect on VEGF. It was demonstrated that the neutralization of miR-150 down-regulated VEGF levels in mice and attenuated angiogenesis.

The genetic modification of donor cells was also used for targeting exosomes to the disease site. As an example, targeting of exosomes to the brain was achieved by engineering the parental DCs to express lysosomal-associated membrane protein 2 (Lamp2b), fused to the neuron-specific peptide derived from rabies virus glycoprotein (RVG) [5]. Systemically administered RVG-targeted exosomes delivered glyceraldehyde 3-phosphate dehydrogenase (GAPDH) siRNA specifically to neurons, microglia, oligodendrocytes in the brain, resulting in specific gene knockdown. The therapeutic potential of exosome-mediated siRNA delivery was demonstrated by the strong mRNA (60%) and protein (62%) knockdown of BACE1, a therapeutic target in Alzheimer's disease, in wild-type mice [5].

Exosomes released from macrophages genetically-modified to express antioxidant, catalase, and glial cells-derived neurotrophic factor (GDNF) were suggested for the treatment of Parkinson’s disease (PD) [111, 114]. Mechanistic studies revealed that exosomes secreted from

genetically-modified parental cells contained the encoded therapeutic protein, as well as its genetic material (DNA and mRNA), and NF-κb, a transcription factor involved in the encoded gene expression [114]. Drug-loaded exosomes were able to efficiently transfer their contents to contiguous neurons resulting in *de novo* protein synthesis in target cells. Transfected brain tissues showed month-long expression of the encoded protein and prolonged attenuation of neuroinflammation (over 40 days) in mice with neuroinflammation [114]. Overall, these reports indicate that exosomes may function as exceptional gene delivery vectors that are safe, efficient, organ/cell-specific, and non-immunogenic. However, significant efforts are required to develop these therapies for clinical use.

Using Exosomal Drug Formulations in the Clinic

In clinical settings, several approaches may be applied to introduce exosome-based drug delivery systems. First, leukocytes harvested from peripheral blood by apheresis may be propagated and cultured, differentiated to specific cell types if necessary, and then exosomal carriers can be loaded with a therapeutic agent and re-administered back into the patient (**Figure 1.3**). One of the major challenges in developing this approach is whether the production of exosomes could be scalable or reproducible [119]. Indeed, the exosome yield *per* cell will impact the final production cost as well as clinical applications. In this respect, the choice of parental cells is critical. For example, MSCs are known to produce large amounts of exosomes, suggesting that these cells may be efficient for exosome production in a clinically applicable scale [120]. Next, extended culturing of donor cells may considerably increase exosomal production. For example, culturing DCs for extended time period [38], or at low pH [121] increased the exosomal production of exosomes 5-10 fold. In another study, the breakdown of parental cells (monocytes/macrophages) loaded with anticancer agents, and isolation of

exosome-like nanoparticles allowed a 100-fold higher production yield of the drug carriers [91]. Finally, specifically designed bioreactors that resemble bioreactors for tissue engineering [122] can be utilized for exosomes scale-up. Notably, exosomes can be concentrated, lyophilized, and reconstituted in aqueous solutions, as was reported in [106].

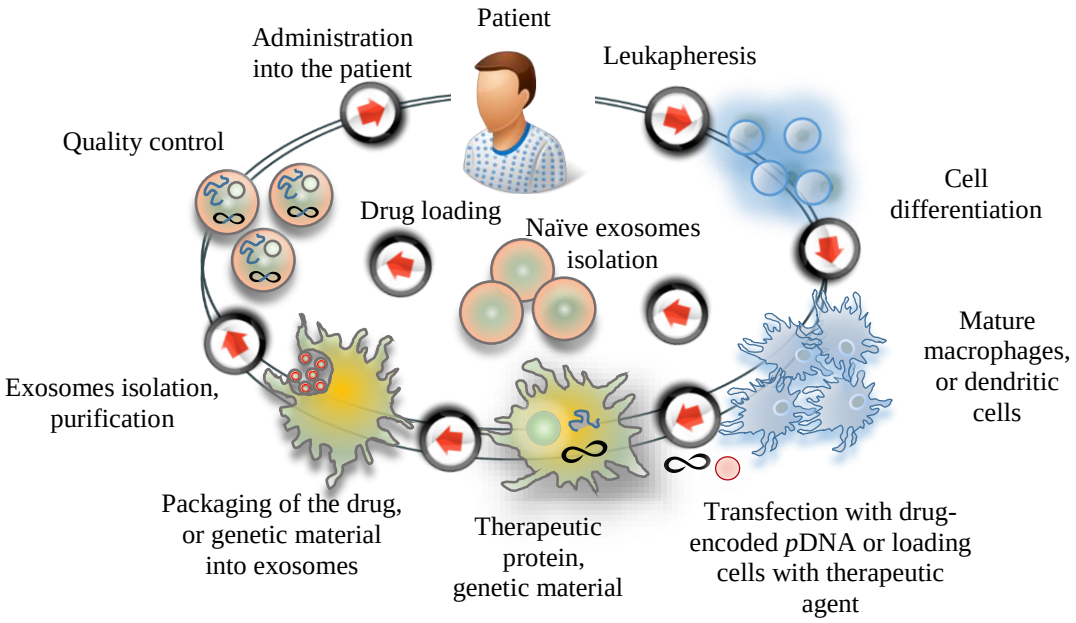

Figure 1.3. The flow of the production and delivery of exosomal drug formulations to the patient.

As an alternative approach, MSCs may be harvested from bone marrow, propagated in culture to obtain specific cell types, or even subtypes, and then exosomes may be loaded with a therapeutic agent. Although this approach would require a more invasive procedure, a significant amount of as well as storage of well-characterized exosomal carriers would be possible [123]. Furthermore, large scale production of therapeutically efficacious exosomes can be achieved through the immortalization of donor cells; for example, mesenchymal stem cells can be transfected by lentivirus carrying a MYC gene as reported in [124]. MYC is a regulator gene that codes for a transcription factor that plays a role in cell cycle progression. The transfection allows

for obtaining of immortalized cells, but does not alter the fundamental characteristics of these MSCs [124]. In this case, a library of various types of exosomal carriers for different drug formulations could be developed in the future, and stored in stock for emergency situations. Finally, exosomes may be isolated from other sources (bovine milk, crashed grapes, *etc.*), purified, loaded with a drug and used for oral or intranasal administration.

In fact, exosomes have already been approved for use in clinical trials, and our experience with exosome-based therapies in humans is rapidly expanding [125]. In particular, exosomes were purified from monocyte cultures from 15 patients with advanced metastatic melanoma. The good manufacturing procedures (GMP) process allowed harvesting about 5 x 10^{14} exosomal MHC class II carriers. Then, the exosomes were loaded with melanoma antigen *ex vitro,* and administered in an autologous fashion in an attempt to promote anti-melanoma immunity *via* therapeutic vaccination. It was reported that patients well-tolerated repeated administration of autologous exosomes for up to 21 months [126]. In a similar trial, non-small-cell-carcinoma lung cancer patients were injected with autologous exosomes weekly for 4 weeks, and similar low level immune responses were observed [127]. In another trial for the treatment of NSCLC, patients were given dendritic cell derived exosomes bearing IL-15Ra and NKG2D and also given cyclophosphamide after platinum-based chemotherapy. Finally, ascites-derived exosomes in combination with the granulocyte-macrophage colony-stimulating factor (GM-CSF) were utilized in the immunotherapy of colorectal cancer (CRC). A total of 40 patients with advanced CRC were enrolled in this clinical trial and received from 100 to 500 μg of exosomal formulations [128]. The exosomal-based therapies were safe, feasible, and efficient in induction of antigen-specific T lymphocyte response, however, several technical obstacles remain which must be overcome.

MATERIALS AND METHODS

Reagents

Paclitaxel (PTX) was purchased from LC Laboratories (Woburn, MA, USA). The stock solution was prepared in ethanol (EtOH) at a concentration of 10 mg/mL. Aliquots were stored at -20°C. Working solutions of PTX were prepared fresh according to experimental design by serial dilution in EtOH. A fluorescent dye, 2-decanoyl-1-(O-(11-(4,4-difluoro-5,7-dimethyl-4-bora-3a,4a-diaza-s-indacene-3-propionyl)amino)undecyl)-sn-glycero-3-phosphocholine (BODIPY-PC) was purchased from Molecular Probes. Cell culture medium and fetal bovine serum (FBS) were purchased from Gibco Life Technologies, Inc. (Grand Island, NY, USA). Culture flasks and dishes were purchased from Corning Inc. (Corning, NY, USA). ExoQuick-TC™ Exosome Precipitation Solution was obtained from System Biosciences (Mountain View, CA, USA).

Cells

RAW 264.7 macrophages (purchased from ATCC, Manassas, VA, USA) were cultured in Dulbecco's modified Eagle's medium (DMEM) high glucose (Gibco, Grand Island, NY, USA) supplemented with 10% fetal bovine serum (FBS; Thermo Fisher Scientific), 1% penicillin and streptomycin at 37°C and 5% CO2.

Exosome Isolation

For all studies, exosome-depleted media was prepared by ultracentrifugation of fetal bovine serum (FBS) at 120,000 x g for 110 min to remove all vesicular content prior to addition to media with 1% penicillin and streptomycin. Exosomes were harvested from the supernatants of RAW 264.7 cells cultured in exosome-depleted media using the ExoQuick-TC™ Kit (System BioSciences; Mountain View, CA, USA). Briefly, > 90% confluent RAW 264.7 cells were

cultured in exosome-depleted media for 2 days at 37°C and 5% CO_2. 50 mL conditioned cell culture media were centrifuged at 300 x g for 10 min (Thermo CL-10 centrifuge with O-G26/1 rotor, Thermo Fisher Scientific, Waltham, MA, USA) in order to remove cells and cellular debris. The supernatant was then taken, filtered with a .22 μm PES filter, and ExoQuick-TC™ Exosome Precipitation Solution (System Biosciences, Mountain View, CA, USA) was added to the filtered supernatant and the mixture was vortexed and incubated overnight at 4°C. After overnight incubation, the mixture was vortexed again and subsequently centrifuged at 1500 x g for 30 min. and 5 min. to pellet exosomes. The supernatant was discarded and the exosome pellet was resuspended in PBS. Freshly-prepared exosomes or exosomes stored at -20°C were used for all experiments.

Drug Loading into Exosomes

For PTX loading into exosomes, purified exosomes (~10^{11} exosomes) were first mixed with PTX in 1 mL PBS. First, PTX was dissolved in ethanol (EtOH, 10 mg/mL drug in EtOH stock solution) and added to 1 mL exosomes. Different methods of drug loading were investigated: incubation at room temperature (RT), electroporation, and sonication. For the incubation method, the mixture was incubated at 37°C for 1 hour with shaking. For the electroporation method, exosomes were mixed with PTX and added to a chilled 4 mm electroporation cuvette. The mixture was then electroporated using an Eppendorf Eporator (Eppendorf AG, Hamburg, Germany) at 1000 kV for 5 ms, and then incubated at 37°C for 30 min to allow for recovery of the exosomal membrane. For the sonication method, the PTX-exosome mixture was sonicated using a Model 505 Sonic Dismembrator with 0.25" tip (Thermo Fisher Scientific, USA) with the following settings: 20% amplitude, 6 cycles of 30 s on/off for three minutes with a two minute cooling period between each cycle. After sonication, PTX-

loaded exosomes (exoPTX) solution was incubated at 37°C for 60 min to allow for recovery of the exosomal membrane.

Excess free PTX was separated from exoPTX, respectively, by size exclusion chromatography using a NAP-10 Sephadex G25 column (GE Healthcare, Buckinghamshire, UK) according to the manufacturer's recommended protocol. Briefly, 750 µL of exoPTX were added to the NAP-10 column and the void volume was discarded. 250 µL of PBS was then added to the column and allowed to enter the gel bed completely and the eluate was discarded. 1.2 mL of PBS was then added to the column and the eluate containing purified exoPTX was collected and stored at -20°C.

Quantification of Drug Loading

The amount of PTX loaded into exosomes was measured by a high performance liquid chromatography (HPLC) method. Briefly, exoPTX or exoPTX-AA (10^{10} exosomes/0.1mL) in a microcentrifuge tube was placed on a heating block set to 75°C to evaporate solvent. After all solvent had evaporated, an equal volume of acetonitrile was added to the microcentrifuge tube and the mixture was vortexed, sonicated, and vortexed again. The sample was then centrifuged at 13,000 rpm (Thermo Legend Micro 21, Thermo Fisher Scientific, Waltham, MA, USA) for 10 min. Following centrifugation, the supernatant was taken and filtered through a Corning Regenerated Cellulose .2 µm syringe filter and transferred into HPLC autosampler vials. 20 µL aliquots were injected into the HPLC system (Agilent 1200, Agilent Technologies, Palo Alto, CA, USA). All analyses were performed using a C18 column (Supelco Nucleosil C18, 250 mm x 4.6 mm, 5 µm, 100 Å, Sigma-Aldrich,) with a mobile phase of H2O:acetonitrile (45:55, v/v) at a flow rate of 1 mL/min at 30°C. Absorbance was measured at 227 nm to monitor the elution of PTX. The area under the PTX peak was measured for each sample and compared with known

concentration of standard. A calibration curve was constructed by plotting peak area versus concentrations of paclitaxel and was found to be linear within the tested concentration range (r^2 = .997). Exosomal protein content was measured using the Pierce BCA Protein Assay Kit (Thermo Fisher Scientific, Waltham, MA, USA) according to the manufacturer's recommended protocol. Loading capacity is expressed by μg protein of exosomes.

Synthesis of DSPE-PEG-AA

The synthesis was carried out according to the published synthetic protocol with little adjustment[23]. Briefly, to synthesize the N-(2-bromoethyl)-4-methoxy-benzamide, 4-methyoxybenzoyl chloride (1g, 5.8 mmol) in 50 mL of pre-warmed benzene was mixed with an aqueous solution of 2-bromoethylamine hydrobromide (1.32g, 6.4 mmol). The emulsion was shaken and cooled in running water during the dropwise addition of 5% aqueous solution of sodium hydroxide. The precipitate was solidified out of the reaction mixture within a few minutes to an amorphous mass. The mixture was continuously stirred for 1h, after which time the sold amide was filtered with suction and washed once with benzene and air dried for 2-3h. Then, the synthesized N-(2-bromoethyl)-4-methoxy-benzamide (100 mg, 0.4 mmol) was reacted with DSPE-PEG-NH2 (100 mg, 23.3 μmol) in acetonitrile (5 mL) in the presence of DIPEA (30 uL, 0.2 mmol) at 65-70 °C for 16h. After evaporating the solvent, 5 mL of methanol was added to dissolve the pellet followed by excess ether (50mL) and it was the kept at -80 °C overnight. The precipitate was collected after centrifugation and recrystallized twice. The overall yield was 70%. The products was characterized by NMR and TLC as reported elsewhere[129].

Preparation of Vectorized Exosomes

Vectorized exosomes targeted to sigma receptor using DSPE-PEG-AA and loaded with PTX (exoPTX-AA) were prepared as follows: exosomes were isolated as described above and

then 10mg/mL DSPE-PEG-AA was added to the exosome solution. 100μL of 10mg/mL PTX in EtOH was also added to the mixture of exosomes with DSPE-PEG-AA when preparing exoPTX-AA. The mixture was then sonicated by the same method used by our lab previously [130]. Briefly, the mixture was sonicated using a Model 505 Sonic Dismembrator with .25" tip (Thermo Fisher Scientific, USA) with the following settings: 20% amplitude, 6 cycles of 30 s on/off. After sonication, the solution was incubated at 37°C for 60 min to allow for recovery of the exosomal membrane. Excess free PTX and DSPE-PEG-AA were separated from exoPTX-AA or exoAA by size exclusion chromatography using a NAP-10 Sephadex G50 column (GE Healthcare, Buckinghamshire, UK) according to the manufacturer's recommended protocol. Briefly, 750 μL of exoPTX-AA was added to the NAP-10 column packed with Sephadex G50 and the void volume was discarded. 250 μL of PBS was then added to the column and allowed to enter the gel bed completely. 1.2 mL of PBS was then added to the column and the eluate containing purified exoPTX-AA was collected and stored at -20°C. Loading capacity was determined by HPLC and formulations were evaluated to determine which provided the greatest drug loading.

Characterization of Exosomes

Nanoparticle Tracking Analysis (NTA). Exosomes were identified and characterized using NanoSight LM 10 instrument (NanoSight Ltd., Amesbury, UK). The settings were optimized and kept constant between samples, and each video was analyzed using the Nanosight system to obtain the size and concentration of exosomes. The stability of exosomes was monitored by measuring size over a period of time under various conditions (4°C, room temperature, or 37°C). Prior to measurement, exosomes were diluted 1:1000 to yield a particle

concentration in the region of ~10^8 particles/mL, in accordance with the manufacturer's recommendations. All samples were analyzed in triplicate.

Dynamic Light Scattering (DLS). The average hydrodynamic diameter and zeta potential of exosomes was measured by DLS using a Malvern Zetasizer Nano ZS system (Malvern, Worcestershire, UK) equipped with He–Ne laser (5 mW, 633 nm) as the light source at 22°C. All samples were analyzed in triplicate.

Atomic Force Microscopy (AFM). The morphology of exoPTX was investigated by AFM imaging. ExoPTX formulations were diluted in PBS and a drop of the sample was placed on a glass slide and dried under a flow of argon gas. The AFM imaging instrumentation was operated as described earlier[131].

Western Blot Analysis. The levels of proteins constitutively expressed in exosomes, Alix and flotillin 1, as well as the lymphocyte function associated antigen-1 (LFA1, subunit CD11a), were examined by western blot (WB). Protein concentrations were determined using BCA kit (Pierce Biotechnology, Rockford, IL). The protein bands were detected with Alix, flotillin 1, and CD11a primary monoclonal antibodies, (Abcam, Cambridge, UK; 1:1000 dilution), and secondary HRP-conjugated rabbit anti-goat IgG-HRP (Santa Cruse, CA, USA; 1:5000 dilution).

The TSG101 levels were visualized by TSG101 monoclonal antibodies, Abcam (Cambridge, MA, USA). The protein bands were visualized by chemiluminescent substrate (Pierce Biotechnology, Rockford, IL, USA) and quantified using ImageJ software (National Institute of Health, Bethesda, MD, USA)[132]. To correct for loading differences in cellular lysates and exosomal fractions, the levels of proteins were normalized to constitutively expressed β-actin in cells with goat polyclonal antibodies to β-actin (Abcam, ab8229; 1:500 dilution); and

TSG101 in exosomes with goat polyclonal antibodies to TSG101 (Santa Cruz, SC6037; 1:200 dilution).

Membrane Fluidity Measurements. BODIPY-PC, a fluorescent dye was used as a probe to examine the fluidity properties of exosomal membranes as described earlier[133]. Briefly, 30 μL exosomes with concentration $4x10^{11}$ particles/mL were mixed with 20 μL BODIPY-PC (0.03 mg/ml) and supplemented with 70 μL deionized water; the mixture was incubated for 45 min at 37°C in darkness. Unbound label was removed using a ZebaTM column (Life Technologies). BODIPY-PC is a hydrophobic fluorescent compound which incorporates into the hydrocarbon regions of lipid membranes. Transfer of BODIPY-PC from the aqueous environment into the lipid bilayers results in a drastic increase of the fluorescence emission for this probe. Furthermore, once the probe is incorporated into lipid membranes, its fluorescence polarization is strongly dependent on the microenvironment, with decreases in membrane microviscosity resulting in increased fluorescent polarization. Fluorescence intensities were measured with Spectramax M5 microplate reader (Molecular Devices, Sunnyvale, CA, USA). An excitation wavelength of 495 nm and an emission wavelength of 502 nm were used for both probes.

RESULTS

Isolation and Characterization of Exosomes from RAW 264.7 Macrophages

Exosomes were collected from the conditioned media of RAW 264.7 macrophages using a polymer purification method (ExoQuick-TC™) and were characterized by protein content, size, and morphology. Exosomes had elevated expression of exosome-associated proteins (Alix, TSG101, and Flotillin) as compared to cell lysate, which had greater levels of β-actin (**Figure 1A**).

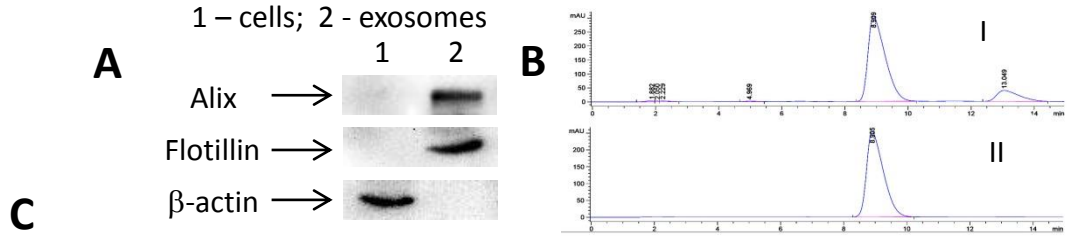

C

Sample/ Method	Size by NTA (nm)	Z-Average size (nm)	Zeta Potential (mV)	Loading Capacity (%)
Naive	110.2 ± 3.3	70.8 ± 2.8	-10.74 ± 1.13	n/a
Incubation	178.7 ± 5.8	132.2 ± 2.3	-9.33 ± .44	1.44 ± 0.38
Electroporation	159.0 ± 3.6	145.3 ± 1.0	-8.47 ± .55	5.3 ± 0.48
Sonication	217.9 ± 10.1	287.7 ± 0.7	-14.07 ± 0.94	28.29 ± 1.38

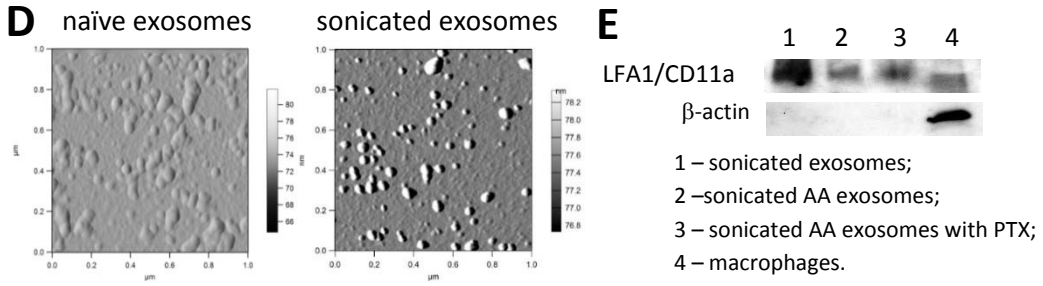

Figure 1.4. Characterization of PTX exosomal formulations. 264.7 macrophages were collected from conditioned media, and the exosome protein content was confirmed by western blot (**A**). Exosomes were loaded with PTX by various methods: co-incubation at RT; electroporation, and sonication. The size of the exosomes with incorporated PTX was measured by NTA and DLS (**C**). The amount of PTX incorporated into exosomes was assessed by HPLC (**B**). The loading efficiency of exosomes with PTX increased in a row: incubation at RT < electroporation<< sonication (**C**). The morphology of drug-loaded exosomes was examined by AFM (**D**). Images revealed small spherical naïve exosomes, and PTX-loaded exosomes. The bar: 200 nm. LFA1/CD11a expression in exosomes as assessed by Western Blot (**E**).

Exosomes were also found to express the lymphocyte function associated antigen-1 (LFA1, subunit CD11a) (**Figure 1E**), which assists in cell uptake and may bind to endothelial cell adhesion molecules which are overexpressed on activated endothelial cells such as those found in tumors[134]. Naïve empty exosomes had a narrow size distribution, with an average particle diameter of 110.4 ± 4.2 nm and 70.8 ± 2.8 nm as revealed by NTA and DLS, respectively (**Figure 1C**); and a round morphology as shown by AFM imaging (**Figure 1D**).

Manufacture and Characterization of Exosomal Formulations of PTX (exoPTX)

PTX was incorporated into exosomes using three different methods: a) incubation at RT, b) electroporation, and c) mild sonication, as described in the Materials and Methods section. ExoPTX formulations were purified from non-incorporated drug by size-exclusion chromatography and analyzed by HPLC to determine the loading capacity (LC) of exosomal carriers. The typical HPLC profile for PTX extracted from exosomes (I) and PTX standards (II) are shown in **Figure 1.4B**. HPLC analysis revealed that the amount of PTX loaded into exosomes increased as follows: incubation at RT < electroporation << sonication (**Figure 1.4C**)**.** We suggested that a reorganization of exosomes caused by ultrasound treatment may result in reorganization/reshuffling of exosomal membranes that enables PTX diffusion across relatively tight and highly structured lipid bilayers. Indeed, fluorescence polarization measurements revealed significant increases (more than 2x) in membrane fluidization upon sonication (**Figure 1.5**), which allowed the high loading efficiency of exosomal carriers. Noteworthy, after one hour, the membrane microviscosity was restored. As such, exosomes were incubated for one hour at 37°C after sonicating in order to restore exosome membrane integrity.

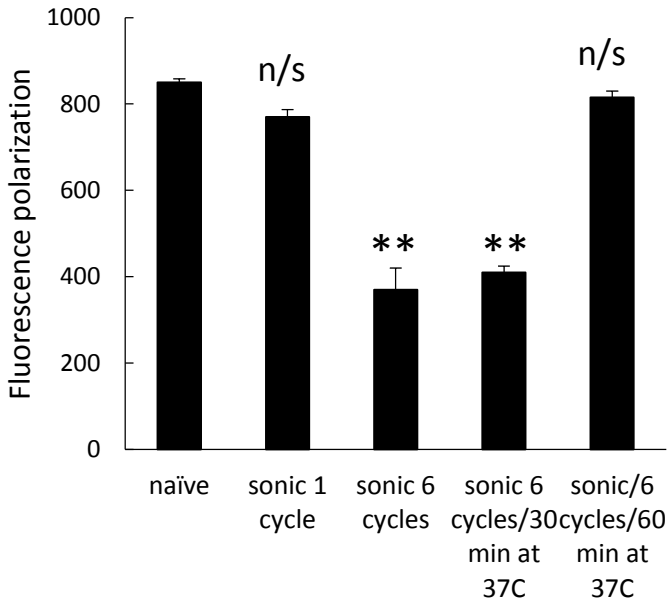

Figure 1.5. Effect of sonication on fluidity of exosomal membranes. Exosomes isolated from RAW 264.7 macrophages concomitant media were labeled with BODIPY-PC fluorescent dye as described in Materials section, and subjected to one or 6 cycles of ultrasound treatment. The fluorescence polarization was measured right after the sonication, or following 30 min or 1 hour incubation period at 37C. Values are means ± SEM (n = 4). Symbols indicate the relative level of significance compared with naive exosomes.

Interestingly, DLS studies revealed that the size of exoPTX nanoformulations increased similarly, with the smaller being exoPTX nanoparticles obtained by electroporation or incubation at RT, and the larger being exosomes loaded with PTX by sonication (**Figure 1.4C**). Noteworthy, NTA analysis confirmed these results indicating that the size of exoPTX obtained by sonication is about 1.5x greater than naïve empty exosomes (**Figure 1.4C**). Interestingly, exosomes sonicated in the absence of PTX (average size 326.0 ± 23.5 nm by NTA, and 356.1 ± 3.5 nm by DLS) were even larger than exosomes sonicated with PTX solution (217.9 ± 10.1 nm). We hypothesized that incorporation of PTX into exosomal membranes stabilized these aggregates. Furthermore, all mentioned loading procedures did not significantly alter the zeta potential of the nanocarriers (**Figure 1.4C**). It is known that the anionic phospholipid phosphatidylserine is abundant on cell membranes and contributes to the surface charge of

individual cellular membranes. We speculated that all of the PTX loading procedures caused no major alterations the lipid content of exosomal membranes. Thus, AFM imaging showed that exosomes retained their round morphology upon sonication (**Figure 1.4D**), suggesting that this procedure did not significantly disrupt the structure of exosomes.

Overall, the mild sonication procedure provided the highest amount of drug loading; the obtained LC of 28.29 ± 1.38% was much higher than the LC of commercially available formulations of PTX, Taxol (~1% LC) or Abraxane (~10% LC). We hypothesized that the application of ultrasound creates pores in exosomes which allows for PTX to incorporate into the hydrophobic lipid bilayer of the exosome without destroying the exosome membranes. Because of the high LC, exoPTX produced by sonication was selected for further experiments.

Manufacture and Characterization of Exosomal Formulations of PTX Vectorized to the Sigma Receptor (exoPTX-AA)

The sigma receptor is overexpressed by many types of cancer, including NSCLC, making

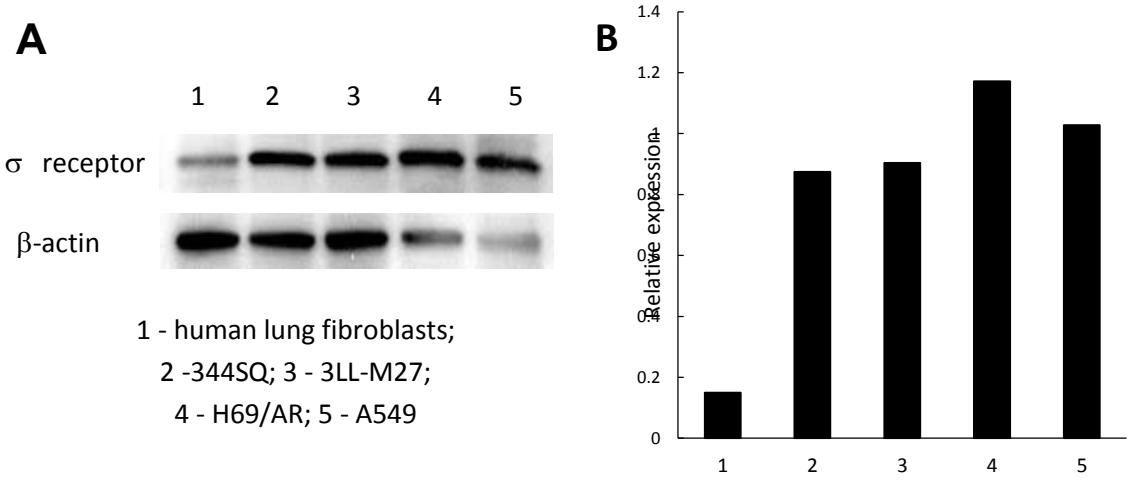

Figure 1.6. Overexpression of σ receptor in lung cancer cells. (**A**) Western blot analysis revealed a significant amount of σ receptor in cancer cells, but not in normal lung fibroblasts. (**B**) Relative expression of target receptors to β-actin.

it an attractive target for cancer therapy [20-23]. In order to validate the sigma receptor as a target for our Lewis Lung Carcinoma 3LL-M27 cell line used in our mouse model of metastatic lung cancer, a Western Blot was performed to look for the presence of the sigma receptor in 3LL-M27 cells. Western Blot analysis revealed overexpression of the sigma receptor in target 3LL-M27 cells (**Figure 1.6A**), indicating that the choice of anisamide (a sigma receptor ligand) as a vector to target 3LL-M27 cells is appropriate.

A

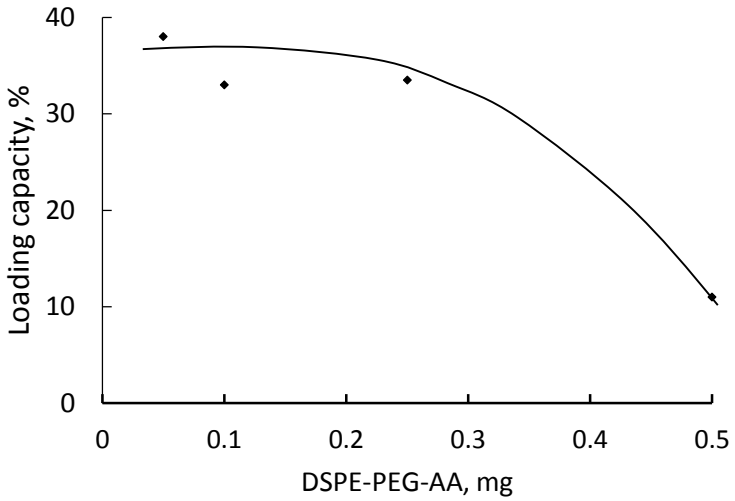

B

Sample	Z-Average Size (nm)	Zeta Potential (mV)	Loading Capacity (%)
exoPTX	287.7 ± 0.7	-14.07 ± 0.94	28.29 ± 1.38
exoPTX-AA	304.5 ± 3.85	-4.37 ± 0.09	33.42 ± 3.22

Figure 1.7 Optimization and Characterization of exoPTX-AA. (A) Varying amounts of DSPE-PEG-AA were added to exosome with 1mg paclitaxel, and the mixture was sonicated to produce vectorized and paclitaxel-loaded exosomes (exoPTX-AA). HPLC analysis of each formulation revealed the loading capacity (LC), and the formulation providing the greatest LC while maximizing the amount of DSPE-PEG-AA was chosen (.25mg DPSE-PEG-AA). (B) The exoPTX-AA formulation was characterized by DLS to obtain the Z-average size and zeta potential. LC was determined by HPLC.

We hypothesize that reorganization of exosomes caused by ultrasound treatment may result in the reorganization/reshuffling of the exosomal membrane, enabling PTX and DSPE-PEG-AA diffusion across relatively tight and highly structured lipid bilayers. Exosomes were

loaded with PTX and vectorized to target the sigma receptor using the sonication method developed by our lab [29]. Varying amounts of vector were added to exosomes with paclitaxel in order to determine the optimal formulation providing the greatest loading capacity while maximizing the amount of vector. HPLC analysis of the formulations revealed that the optimal amount of DSPE-PEG-AA to add in order to achieve the greatest loading capacity was 0.25 mg, thus this formulation was chosen for further study (**Figure 1.7A**). HPLC analysis revealed that the loading capacity of the optimal formulation of exoPTX-AA was 33.42 ± 3.22%, similar to the loading capacity achieved by exoPTX alone without vector (28.29 ± 1.38%) (**Figure 1.7B**).

Further characterization by DLS showed that exoPTX had a smaller size (287.7 ± 0.7nm) than exoPTX-AA (304.5 ± 3.85 nm) (**Figure 1.7B**). We hypothesize that this size increase as measured by DLS is due to the presence of the long PEG chains of DSPE-PEG-AA on the surface of exoPTX-AA, as well as the insertion of DSPE lipids into the exosomal lipid membrane. The surface charge of exoPTX was found to be -14.07 ± 0.94 mV, whereas exoPTX-AA had a surface charge of -4.37 ± 0.09 mV (**Figure 1.7B**). We hypothesize that this decrease in observed surface charge may be due to shielding of the exosomal membrane surface charge by DSPE-PEG-AA.

DISCUSSION

Although various drug nanoformulations have been developed to improve the therapeutic effect of drugs, there are still issues that significantly diminish their application in clinic, *e.g.* toxicity and rapid clearance by the mononuclear phagocyte system (MPS) [135]. In fact, the safety of drug nanoformulations is the subject of substantial criticism. In this respect, exosomes, naturally-produced nanosized vesicles secreted by a variety of cells, represent an important tool for both diagnostic and therapeutic purposes. Exosomes consist of cellular membranes with a variety of adhesion proteins on their surface [136] which allow for efficient transport of exosomal cargo into target cells. Exosomes have been reported for use as drug delivery vehicles for nucleic acids [5, 8, 10, 103, 117, 137] and small molecule drugs such as curcumin [89, 90], anticancer agents (Dox [92, 93] and PTX [94]). The low molecular-weight compounds were loaded into exosomes or exosome-like vesicles by co-incubation at RT. These studies demonstrated the feasibility of using an exosomal formulation for cancer therapy as well as for neurodegenerative disorders. We also reported recently the development of a new exosome-based formulation of potent antioxidant, catalase, to treat Parkinson's disease [106]. A large protein, catalase (M_W 240 K), was loaded into exosomes using different procedures: sonication, extrusion, and permeabilization of exosomal membranes with saponin. The extensive reformation and reshaping of exosomes upon sonication and extrusion, as well as the creation of holes/pores in the exosome lipid bilayer by saponin, enabled catalase to diffuse across relatively tight and highly structured lipid bilayers and resulted in high loading efficiency of exosomal carriers [106].

PTX is a potent chemotherapeutic used to treat many forms of cancer, however, its effectiveness for clinical use is hampered by its low aqueous solubility. There have been

significant efforts to formulate PTX into various nanoformulations to increase solubility and improve pharmacokinetics, including polymer based nanoparticles and liposomes. However, these systems possess several undesirable properties such as the presence of toxic excipients and/or rapid clearance by the endothelial system (RES).

In the present study, we utilized various methods for PTX incorporation into exosomes: incubation at RT, electroporation, and mild sonication. Mild sonication of exosomes in the presence of PTX, provided the greatest loading capacity (28.29% ± 2.58%). PTX is a highly hydrophobic compound, therefore we hypothesized that this drug is incorporated into the hydrophobic inner region of the phospholipid bilayer of exosomes. Indeed, exosome membranes display a high rigidity that was significantly decreased upon sonication. We hypothesized that the membrane fluidization allowed PTX incorporation into lipid bilayers resulting in the high loading capacity of exosomal carriers. The precise location of PTX in exosomes will be investigated in future studies. Importantly, drug located in the inner bilayer of exosomes may also be available for use: as the exosomal membrane fuses with the cell or endosomal membrane, its intraluminal cargo may be released into the cytosol. Next, we assessed the optimal concentration of DSPE-PEG-AA to add to exosomes which would provide the greatest drug loading capacity. DSPE is a lipid, thus we hypothesize that DSPE would insert into the lipid bilayer of the exosomal membrane upon sonication. The optimal formulation of exoPTX-AA was found to have a loading capacity (33.42% ± 3.22%) similar to that of exoPTX (28.29% ± 2.58%) and a slightly larger size (304.5 ± 3.85 nm for exoPTX-AA vs. 287.7 ± 0.7 nm for exoPTX). The size increase may be due to the presence of long PEG chains on the surface of exoPTX-AA, as well as an increased surface area due to insertion of the DSPE lipid into the exosomal membrane. A slight decrease in zeta potential for exoPTX-AA as compared to

exoPTX was also observed, again, this may be caused by shielding of the exosomal membrane by long PEG chains on the surface of exoPTX-AA.

CHAPTER 2. *IN VITRO* CHARACTERIZATION OF exoPTX AND exoPTX-AA[3]

OVERVIEW

Multiple drug resistance (MDR) is a factor which severely limits the efficacy of a variety of chemotherapeutics, including paclitaxel. MDR may be intrinsic or acquired [1,2] and is mediated by different mechanisms, in particular, the overexpression of the drug efflux transporter P-glycoprotein (Pgp). As a result, the response rate following treatment remains very low for many types of malignancies, including acute leukemias, malignant gliomas, metastatic breast cancer, and other cancers [1-3]. Prior treatment with antineoplastic agents is a serious adverse prognostic factor for many cancers due to the acquiring of drug resistance, resulting in low long-term survival rates for patients with recurring cancers [3,4]. To date, there has been limited success in overcoming drug resistance in cancers through the use of novel small molecule chemotherapeutics [7,8], or nanoformulations of existing chemotherapeutics. In addition, various Pgp inhibitors, such as quinine or cyclosporine A, have been co-administered with chemotherapeutic agents [138, 139]. These efforts did result in improved patient outcomes, however, the non-specific inhibition of Pgp frequently increased drug toxicity due to alteration of drug elimination pathways in the liver, kidney, *etc*. [140].

[3] Some of this text previously appeared in an article in the journal Nanomedicine. The original citation is as follows: Development of Exosome-encapsulated Paclitaxel to Overcome MDR in Cancer cells. Myung Soo Kim, Matthew J. Haney, Yuling Zhao, Richa Gupta, Zhijian He, Natalia L. Klyachko, Aleksandr Piroyan, Marina Sokolsky, Alexander v. Kabanov, and Elena V. Batrakova. *Nanomedicine*, Nov 13. pii: S1549-9634(15)00202-6. doi: 10.1016/j.nano.2015.10.012. PMID: 26586551

Herein, we have developed a new nanoformulation consisting of exosomes loaded with PTX (exoPTX), a commonly used chemotherapeutic agent, and vectorized to target the sigma receptor. The main objectives of this study were: (i) to assess the feasibility of using exoPTX for MDR-related anticancer therapy, (ii) to identify mechanisms underlying inhibitory effects of exosomes on drug efflux pump in Pgp expressing cancer cells, (iii) to prepare and assess the targeting ability of exosomes vectorized to the sigma receptor, and (iv) to assess the intracellular fate of exosomes and vectorized exosomes.

Results showed that exoPTX were readily taken up by multiple cancer cell types and exhibited greater cytotoxicity than Taxol *in vitro,* especially in MDR cancer cells. Vectorized exosomes were able to successfully be taken up by target cancer cells expressing the sigma receptor by receptor mediated endocytosis, and their intracellular fate was not altered by the addition of the vector. Finally, vectorized exosomes loaded with paclitaxel (exoPTX-AA) exhibited greater cytotoxicity than Taxol and similar cytotoxicity to exoPTX *in vitro*. Overall, exosome-based PTX formulations have the potential to be a versatile strategy to treat drug resistant cancers.

MATERIALS AND METHODS

Reagents

Paclitaxel (PTX) was purchased from LC Laboratories (Woburn, MA, USA). The stock solution was prepared in ethanol (EtOH) at a concentration of 10 mg/mL. Aliquots were stored at -20°C. Doxorubicin (DOX) was purchased from LC Laboratories (Woburn, MA, USA). The stock solution was prepared in DMSO at a concentration of 2 mg/mL and aliquots were stored at 4°C. Working solutions of PTX or DOX were prepared fresh according to experimental design by serial dilution in an appropriate medium. A lipophilic fluorescent dye, 1,1'-dioctadecyl-3,3,3',3'-tetramethylindo-carbocyanine perchlorate (DIL), was purchased from Invitrogen (Carlsbad, CA, USA). Rhodamine 123 (R123), 4′,6-diamidino-2-phenylindole dihydrochloride (DAPI), and Triton X-100 were obtained from Sigma-Aldrich (St. Louis, MO, USA). Cell culture medium and fetal bovine serum (FBS) were purchased from Gibco Life Technologies, Inc. (Grand Island, NY, USA). Culture flasks and dishes were from Corning Inc. (Corning, NY, USA). Fluorescent polystyrene nanoparticles (Fluoro-Max G100) were obtained from Thermo Fisher Scientific (Waltham, MA, USA). ExoQuick-TC™ Exosome Precipitation Solution was obtained from System Biosciences (Mountain View, CA, USA). ER Tracker Blue-White DPX, LysoTracker Green DND-26, and MItoTracker Deep Red were purchased from Thermo Fisher (Thermo Fisher Scientific, Waltham, MA, USA).

Cells

RAW 264.7 macrophages, Madin-Darby canine kidney $MDCK_{WT}$ and $MDCK_{MDR1}$ cells (purchased from ATCC, Manassas, VA, USA) were cultured in Dulbecco's modified Eagle's medium (DMEM) high glucose (Gibco, Grand Island, NY, USA) supplemented with 10% fetal bovine serum (FBS; Thermo Fisher Scientific), 1% penicillin and streptomycin at 37°C and 5%

CO2. Murine Lewis lung carcinoma cell subline (3LL-M27), a highly metastatic lung clone, was a generous gift from Dr. L. Pelletier (CHUL, Laval University, QC, Canada), and were cultured in DMEM high glucose supplemented with 10% FBS, 10 mM HEPES, 1% penicillin and streptomycin at 37°C and 5% CO2.

Pgp protein levels in sensitive and resistant cancer cells were determined by western blot as previously reported [22] using monoclonal antibodies to Pgp, C219 (Dako Corp., Carpinteria, CA, USA; at dilution 1:100), and secondary horseradish peroxide donkey anti-mouse IgG antibodies (Amersham Life Sciences, Cleveland, OH, USA; at dilution 1:1500). To correct for loading differences, the Pgp levels were normalized to the constitutively expressed β-actin (stained with monoclonal antibodies to β-actin, anti-β-1-chicken integrin (Sigma Chemical Co., at dilution 1:200)). Specific bands were visualized using a chemiluminescence kit (Pierce, Rockford, IL, USA).

Exosome Isolation

For all studies, exosome-depleted media was prepared by ultracentrifugation of fetal bovine serum (FBS) at 120,000 x g for 110 min to remove all vesicular content prior to addition to media. Exosomes were harvested from the supernatants of RAW 264.7 cells cultured in exosome-depleted media using the ExoQuick-TC™ Kit (System BioSciences; Mountain View, CA, USA). Briefly, > 90% confluent RAW 264.7 cells were cultured in exosome-depleted media for 2 days. 50 mL conditioned cell culture media were centrifuged at 300 x g for 10 min (Thermo CL-10 centrifuge with O-G26/1 rotor, Thermo Fisher Scientific, Waltham, MA, USA) in order to remove cells and cellular debris. The supernatant was then taken, filtered with a .22 µm PES filter, and ExoQuick-TC™ Exosome Precipitation Solution (System Biosciences, Mountain View, CA, USA) was added to the filtered supernatant and the mixture was vortexed

and incubated overnight at 4°C. After overnight incubation, the mixture was vortexed again and subsequently centrifuged at 1500 x g for 30 min. and 5 min. to pellet exosomes. The supernatant was discarded and the exosome pellet was resuspended in PBS. Freshly-prepared exosomes or exosomes stored at -20°C were used for all experiments.

Drug Loading into Exosomes

For PTX and DOX loading into exosomes, purified exosomes (~10^{11} exosomes) were first mixed with PTX or DOX in 1 mL PBS. First, PTX was dissolved in ethanol (EtOH, 10 mg/ml drug in EtOH stock solution) and added to 1 mL exosomes. DOX stock solution was prepared in DMSO (2 mg/mL) and added to 1mL exosomes. The PTX-exosome or DOX-exosome mixture was then sonicated using a Model 505 Sonic Dismembrator with .25" tip (Thermo Fisher Scientific, USA) with the following settings: 20% amplitude, 6 cycles of 30 s on/off for three minutes with a two minute cooling period between each cycle. After sonication, PTX-loaded exosomes (exoPTX) or DOX-loaded exosomes (exoDOX) solution was incubated at 37°C for 60 min to allow for recovery of the exosomal membrane.

Excess free PTX or DOX was separated from exoPTX or exoDOX, respectively, by size exclusion chromatography using a NAP-10 Sephadex G25 column (GE Healthcare, Buckinghamshire, UK) according to the manufacturer's recommended protocol. Briefly, 750 µL of exoPTX or exoDOX were added to the NAP-10 column and the void volume was discarded. 250 µL of PBS was then added to the column and allowed to enter the gel bed completely and the eluate was discarded. 1.2 mL of PBS was then added to the column and the eluate containing purified exoPTX or exoDOX was collected and stored at -20°C.

For mechanistic studies, two fluorescent dyes used as model Pgp substrates, Rhodamine 123 (Rh123) and Doxorubicin, were incorporated into exosomes as described above. Doxorubicin was chosen as it is actually an antinreoplastic agent and a Pgp substrate.

ExoPTX Stability

The stability of exoPTX was assessed at 4°C, RT, and at 37°C. Briefly, samples of exoPTX were stored at different temperatures for varying lengths of time. After each time point, samples were analyzed by NTA to assess their size.

Quantification of Drug Loading

The amount of PTX loaded into exosomes was measured by a high performance liquid chromatography (HPLC) method. Briefly, exoPTX (10^{10} exosomes/0.1mL) in a microcentrifuge tube was placed on a heating block set to 75°C to evaporate solvent. After all solvent had evaporated, an equal volume of acetonitrile was added to the microcentrifuge tube and the mixture was vortexed, sonicated, and vortexed again. The sample was then centrifuged at 13,000 rpm (Thermo Legend Micro 21, Thermo Fisher Scientific, Waltham, MA, USA) for 10 min. Following centrifugation, the supernatant was taken and filtered through a Corning Regenerated Cellulose .2 µm syringe filter and transferred into HPLC autosampler vials. 20 µL aliquots were injected into the HPLC system (Agilent 1200, Agilent Technologies, Palo Alto, CA, USA). All analyses were performed using a C18 column (Supelco Nucleosil C18, 250 mm x 4.6 mm, 5 µm, 100 Å, Sigma-Aldrich,) with a mobile phase of H2O:acetonitrile (45:55, v/v) at a flow rate of 1 mL/min at 30°C. Absorbance was measured at 227 nm to monitor the elution of PTX. The area under the PTX peak was measured for each sample and compared with known concentration of standard. A calibration curve was constructed by plotting peak area versus concentrations of paclitaxel and was found to be linear within the tested concentration range (r2 = .997).

Exosomal protein content was measured using the Pierce BCA Protein Assay Kit (Thermo Fisher Scientific, Waltham, MA, USA) according to the manufacturer's recommended protocol. Loading capacity is expressed by μg protein of exosomes.

Synthesis of DSPE-PEG-AA

The synthesis was carried out according to the published synthetic protocol with little adjustment[23]. Briefly, to synthesize the N-(2-bromoethyl)-4-methoxy-benzamide, 4-methyoxybenzoyl chloride (1g, 5.8 mmol) in 50 mL of pre-warmed benzene was mixed with an aqueous solution of 2-bromoethylamine hydrobromide (1.32g, 6.4 mmol). The emulsion was shaken and cooled in running water during the dropwise addition of 5% aqueous solution of sodium hydroxide. The precipitate was solidified out of the reaction mixture within a few minutes to an amorphous mass. The mixture was continued stirred for 1h, after which time the solid amide was filtered with suction and washed once with benzene and air dry for 2-3h. Then, the synthesized N-(2-bromoethyl)-4-methoxy-benzamide (100 mg, 0.4 mmol) was reacted with DSPE-PEG-NH2 (100 mg, 23.3 μmol) in acetonitrile (5 mL) in the presence of DIPEA (30 uL, 0.2 mmol) at 65-70 °C for 16h. After evaporating the solvent, 5 mL of methanol was added to dissolve the pellet followed by excess ether (50ml) and it was the kept at -80 °C overnight. The precipitate was collected after centrifugation and recrystallized twice. The overall yield was 70%. The products was characterized by NMR and TLC as reported elsewhere[129].

Preparation of Exosomes Vectorized to the Sigma Receptor

Vectorized exosomes targeted to sigma receptor using DSPE-PEG-AA (exoAA) and non-vectorized control exosomes with DSPE-PEG (exoPEG) were prepared as follows: exosomes were isolated as previously described and then varying volumes of 10mg/mL DSPE-PEG or DSPE-PEG-AA were added to the exosome solution (for exoPEG and exoAA, respectively).

100µL of 10mg/mL PTX in EtOH was also added to the mixture when preparing exoPTX-AA. The mixture was then sonicated by the same method used by our lab previously [29]. Briefly, the mixture was sonicated using a Model 505 Sonic Dismembrator with .25" tip (Thermo Fisher Scientific, USA) with the following settings: 20% amplitude, 6 cycles of 30 s on/off. After sonication, the exoAA or exoPEG solution was incubated at 37°C for 60 min to allow for recovery of the exosomal membrane. Excess free DSPE-PEG or DSPE-PEG-AA was separated from exoPEG or exoAA, respectively, by size exclusion chromatography using a NAP-10 column packed with Sepharose 6b (GE Healthcare, Buckinghamshire, UK) according to the manufacturer's recommended protocol. Briefly, 750 µL of exoPEG or exoAA were added to the NAP-10 column packed with Sephadex 6b and the void volume was discarded. 250 µL of PBS was then added to the column and allowed to enter the gel bed completely. 1.2 mL of PBS was then added to the column and the eluate containing purified exoPEG or exoAA was collected and stored at -20°C.

Drug Release

To measure PTX release, freshly prepared exoPTX were placed in a 300K MWCO Float-A-Lyzer G2 device (Spectrum Laboratories, Houston, TX, USA). The device was then placed in PBS under sink conditions at RT with stirring. Samples were taken at time points from inside the dialysis tube and were analyzed by HPLC as described above. The amount of PTX released from exoPTX was expressed as a percentage of total PTX and plotted as a function of time.

Preparation of Liposomes

Liposomes were prepared by a reverse phase evaporation method. Briefly, 2 mg of phospholipids (95 molar % of phosphatidyl choline and 5% of PEG-PE) were dissolved in 6 mL of chloroform:diisopropyl ether in a 1:1 mixture. Then, 1 mL of 5 mM calcein solution in PBS

filtered through a 450 nm syringe filter and was added to the mixture. The mixture was then intensively vortexed and bath sonicated to form a stable emulsion. Organic solvents were evaporated on a rotary evaporator, forming the liposome aqueous dispersion. 200-250 µL of Millipore water was added to the mixture at this point in case some water had also evaporated. Evaporation was continued to get an almost-clear dispersion. The volume was then adjusted to 1000 µL by addition of a small amount of water. The dispersion was vortexed and bath sonicated to get a clear solution. Liposomes were sequentially extruded 21 times through 200 nm polycarbonate filters using a hand extruder (Avanti Polar Lipids, Alabaster, AL, USA). Liposomes were purified through a Sepharose CL4B column to remove non-encapsulated fluorophore. The volume of the sample was doubled after column separation. Calcein loaded liposomes were used within 24 h after column separation.

Accumulation of Exosomes and Exosome-incorporated PTX in Cancer Cells

To quantify the amount of exosomes taken up by cells, exosomes were first stained with a lipophilic fluorescent dye, DiL. Briefly, the supernatant of RAW 264.7 macrophage conditioned media free of cells and cellular debris was filtered with a .22 µm PES filter and incubated with DiL dye (4 µM) at 37°C for 20 min. After 20 min, ExoQuick-TC™ Exosome Precipitation Solution was added to the filtered supernatant and the mixture was vortexed and incubated overnight at 4°C. After overnight incubation, the mixture was vortexed again and subsequently centrifuged at 1500 x g for 30 min. and 5 min. to pellet exosomes. The supernatant was discarded and the exosome pellet was resuspended in PBS. Freshly-prepared fluorescently labeled exosomes or exosomes stored at -20°C were used for all experiments.

3LL-M27 cells were seeded overnight at 10,000 cells/well on borosilicate chamber slides. DiL-labeled exosomes, or fluorescently-labeled polystyrene nanoparticles (Fluoro-Max G100,

Thermo Fisher Scientific, USA), were added in equal numbers (~10^8 particles/well) and incubated with the cells at 37°C and 5% CO2 for 3 or 24 hrs. After each time point, the media was removed and cells were washed 3x with PBS and fixed by incubating with Formal-Fixx (Thermo Fisher Scientific) for 15 min at 23°C. Then, Formal-Fixx was removed, and cells were washed with PBS, and fluorescence in each sample was measured by Shimadzu RF5000 fluorescent spectrophotometer (Shimadzu Scientific Instruments, Columbia, MD).

To study the effect of PTX incorporation into exosomes on the level of drug accumulation in cancer cells, 3LL-M27, $MDCK_{WT}$, or $MDCK_{MDR1}$ cells were seeded overnight at 100,000 cells/well in a 24-well plate. ExoPTX or Taxol were added in equimolar amounts to the cells and incubated for 72h. The media was then removed; 3LL-M27 cells were detached using a cell scraper and MDCK cells were washed with PBS and incubated with 0.25% trypsin for 5-15 min at 37°C. The cell suspension was then mechanically lysed via sonication and analyzed for PTX content by HPLC as described above and protein content by BCA assay according to the manufacturer's recommended protocol.

Confocal Studies

Exosomes were labeled with DiL as described above. Fluorescently-labeled exosomes, liposomes, or polystyrene nanoparticles (~108 particles/well) were incubated with 3LL-M27 cells grown in chamber slides ($1x10^5$ cells/chamber) for 3 h. Following incubation, cells were washed with PBS and fixed with Formal-Fixx. Accumulation of fluorescently-labeled exosomes was visualized by a confocal fluorescence microscopic system ACAS-570 (Meridian Instruments, Okimos, MI, USA) with argon ion laser and corresponding filter set. Digital images were obtained using the CCD camera (Photometrics, Tucson, AZ, USA).

Effect of Pgp Inhibitor, Verapamil, on the Uptake of Exosome-incorporated Drugs

To assess the ability of exosome-incorporated drugs to overcome Pgp-mediated drug efflux, the accumulation of a Pgp substrate, Doxorubicin (Dox), incorporated into exosomes by sonication, was evaluated in MDR cancer cells ($MDCK_{MDR1}$). The accumulation levels of these fluorescent probes were assessed by spectrofluorimetry. For this purpose, Pgp-overexpressing $MDCK_{MDR1}$ cells and their parental sensitive $MDCK_{WT}$ cells were seeded overnight at 100,000 cells/well in a 96-well plate. Then, the cells were pre-incubated in assay buffer or verapamil (300 μM) for 30 min at 37°C. Cells were then treated with the free probe, or the probe incorporated into exosomes (exoDox), with or without verapamil, for 2 hours. Cells were then washed 3x with cold PBS and supplemented with 1% Triton X-100 to lyse the cells.

Next, to evaluate whether exosomes inhibit Pgp-mediated drug efflux in resistant cancer cells, a fluorescent probe and Pgp substrate, Rhodamine 123 (R123), was used in accumulation studies. Briefly, $MDCK_{WT}$ and $MDCK_{MDR1}$ cell monolayers were pretreated with verapamil, or empty exosomes, or assay buffer, washed 3x times with PBS, and R123 solution (3.2 uM) was added to the cells for 2 hours. Cells were then washed 3x with cold PBS and supplemented with 1% Triton X-100 to lyse the cells. A standard curve of R123 or DOX was prepared in 1% Triton X-100 and the fluorescence of samples was measured (*ex = 505 nm, *em = 540 nm for R123, and *ex = 480 nm, *em = 594 nm for Dox). Samples in 1% Triton X-100 were analyzed by BCA for protein content. The accumulation levels were expressed as μg R123 or DOX/μg protein. All experiments were carried out in triplicate.

***In Vitro* Cytotoxicity**

The *in vitro* antitumor efficacy of exoPTX was assessed using a standard MTT (3-(4,5-dimethyl-2-thiazolyl)-2,5-diphenyl-2-H-tetrazoliumbromide) assay with three cancer cell lines,

3LL-M27, $MDCK_{WT}$ and $MDCK_{MDR1}$, and compared to Taxol. Briefly, the cells were seeded in 96-well plates at a density of 5,000 cells per well, followed by 48-hour incubation at 37°C and 5% CO2. The cells were incubated with serial dilutions of exoPTX, or Taxol for 48 hours. Then, 25 µL MTT reagent (5 mg/mL) was added to wells. After 1-3 h incubation at 37C and 5% CO2 in the dark, plates were centrifuged at 1500 rpm for 10 min and media was removed from the wells. 100 µL of DMSO was then added to each well to solubilize formazan crystals and the plates were shaken at 200 rpm for 15 min. in the dark. Absorbance was measured at 570 nm using Spectramax M5 microplate reader (Molecular Devices, Sunnyvale, CA, USA), and IC50 values were determined using GraphPad Prism Software version 5.01 (GraphPad Software, San Diego, CA, USA). Each concentration point was determined from samplings from eight separate wells. SEM values were less than 10%. Data are expressed as mean ± SEM.

Receptor Competitive Inhibition

In order to assess the ability of exoPTX-AA to target the sigma receptor and be taken up by cells expressing the sigma receptor, a receptor competitive inhibition study was performed. Briefly, 3LL-M27 cells expressing sigma receptor were seeded overnight at 50,000 cells/well in a black/clear bottom 96-well plate. Cells were pre-treated with anisamide (AA) at varying concentrations for 30min at 37°C. Media was then removed from wells and cells were treated with a solution of DiD labeled exoAA with varying concentration of AA. After 1h, media was removed from wells and cells were washed 3x with PBS. PBS was then removed from wells and 1% Triton X-100 added to wells to lyse cells. The plate was then placed in -80°C for 5min., followed by shaking at 37°C for 30min. Excitation/emission was read at 640nm/670nm using a Spectramax M5 microplate reader (Molecular Devices, Sunnyvale, CA, USA), and the number of exosomes taken up at each concentration of AA was determined by comparing the

fluorescence against a known concentration of standard. A calibration curve was constructed by plotting fluorescence versus concentrations of DiD exoAA in 1% Triton X-100 and was found to be linear within the tested concentration range (r^2 = .998). Cellular protein content was measured using the Pierce BCA Protein Assay Kit (Thermo Fisher Scientific, Waltham, MA, USA) according to the manufacturer's recommended protocol and results were expressed as number of exosomes per µg protein versus concentration of AA. Each concentration point was determined from samplings from three separate wells. SEM values were less than 10%. Data are expressed as mean ± SEM.

Effect of Proteinase K Treatment on Exosome Uptake

Exosomes possess a variety of surface proteins which are believed to play a role in cell uptake and adhesion, such as LFA-1[134]. In order to explore the role of surface proteins on exosome uptake, naïve exosomes, sonicated exosomes (exoSONIC), or exoAA were diluted to the same concentration of exosomes (~10^{11} exosomes/mL) and treated with Proteinase K. Briefly, 10µL of 10mg/mL proteinase K or PBS (as a control) were added to 1mL naïve exosomes, exoSONIC, or exoAA and incubated at 37°C for 30 min. Excess free enzyme was separated from digested exosomes by size exclusion chromatography using a NAP10 column packed with Sepharose CL-6B to the same volume/height according to the manufacturer's recommended instructions. Briefly, 750µL exosomes were added to the column and the void volume was discarded. 250 µL of PBS was then added to the column and allowed to enter the gel bed completely and the eluate was discarded. 1.2 mL of PBS was then added to the column and the eluate containing purified exosomes was collected and stored at -20°C. Exosomes were then labeled with DiL dye as described above. 3LL-M27 cells were seeded overnight in a black/clear bottom 96-well plate (Corning Costar, Corning, NY, USA) at 50,000 cells/well.

Undigested and digested exosomes were diluted to the same concentration and added to wells for varying lengths of time. After 2h, media was removed from wells and wells were washed 3x with PBS. PBS was then removed from the wells and 50µL of 1% Triton X-100 (Sigma-Aldrich, St. Louis, MO, USA) was added to each well. The 96-well plate was then placed at -80°C for 5 min., followed by incubation at 37°C for 30 min. with shaking. Excitation and emission was read at 540nm and 570nm, respectively, using a Spectramax M5 microplate reader (Molecular Devices, Sunnyvale, CA, USA), and compared against a known concentration of standard. A calibration curve was constructed by plotting peak area versus concentrations of DiL labeled exosomes, exoSONIC, or exoAA, and was found to be linear within the tested concentration range (r^2 = .999). Exosomal protein content was measured using the Pierce BCA Protein Assay Kit (Thermo Fisher Scientific, Waltham, MA, USA) according to the manufacturer's recommended protocol. Results were expressed as number of exosomes per µg protein versus time.

Intracellular Distribution of Exosomes and Exosomal Proteins and Lipids

In order to assess the intracellular distribution of exosomes, 3LL-M27 cells were seeded at 500,000 cells/well in chamber slides and incubated overnight. Exosomes or exoAA were labeled with DiL as described above and added to wells for varying times. Media was then removed from wells and pre-warmed staining solution (ER Tracker Blue-White DPX, LysoTracker Green DND-26, or MitoTracker Deep Red) were added to wells according to the manufacturer's recommended instructions. Media was then removed from wells and washed 3x with PBS. Cells were then fixed by the addition of Formal-Fixx for 20min. at 37°C followed by washing 3x with PBS. Exosomes and organelles were visualized by confocal fluorescence microscopic system ACAS-570 (Meridian Instruments, Okimos, MI, USA) with argon ion laser

and corresponding filter set. Excitation/emission were set and measured at 540nm/570nm for DiL labeled exosomes and exoAA, and 358nm/461nm or 490nm/520nm or 640nm/670nm for ER Tracker Blue-White DPX, LysoTracker Green DND-26, and MitoTracker Deep Red, respectively.

Statistical Analysis

For the all experiments, data are presented as the mean ± SEM. Tests for significant differences between the groups were performed using a t-test or one-way ANOVA with multiple comparisons (Fisher's pairwise comparisons) using GraphPad Prism 5.0 (GraphPad software, San Diego, CA, USA). A minimum *p*-value of 0.05 was chosen as the significance level.

RESULTS

Drug Release and Stability of Exosomes Loaded with Paclitaxel

The release of PTX from exosomes loaded with PTX by sonication was evaluated by HPLC by placing exoPTX in dialysis membranes with a cut-off of 300 kDa under sink conditions and measuring PTX content inside the dialysis tube at varying timepoints (**Figure 2.1A**). ExoPTX showed burst release within the first one hour, and then displayed a sustained release profile thereafter.

Next, the aggregation stability of exosomes in an aqueous solution was assessed at three temperatures: 4°C, RT, and 37°C. The size of exosomes was not altered over a period of one month at all temperatures tested (**Figure 2.1B**). This provides a clinical link for exosomal drug

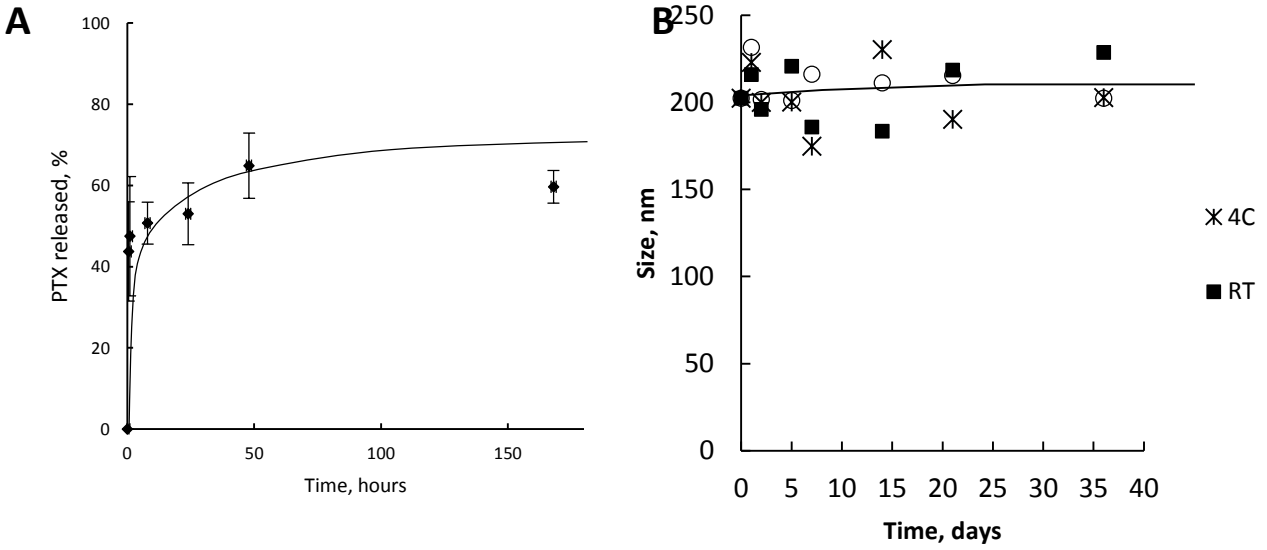

Figure 2.1 Characteristics of exosomal PTX formulation. (A) A release profile of exoPTX formulation obtained by sonication. (B) Exosomes released from Raw 264.7 macrophages were loaded with PTX as described in the materials and methods section, and the size of nanoparticles was measured at 4°C, RT, and 37°C over the course of a month. No significant changes in size of the exoPTX were registered at all conditions.

formulations, indicating that multiple lots of exosomal PTX may be prepared and stored prior to administration to the patient.

Accumulation and Therapeutic Efficacy of exoPTX and exoPTX-AA in Target Cancer Cells *In Vitro*

The ability to deliver the drug payload into target cells is crucial for the therapeutic efficacy of exosomal formulations. First, we studied accumulation levels of fluorescently-labeled exosomes in murine Lewis lung carcinoma cells (3LL-M27), and compared them to commonly used liposomes or polystyrene (PS) nanoparticles with the same size and level of fluorescence (**Figure 2.2**). These nanocarriers (liposomes and PS nanoparticles) have been utilized in many investigations for the delivery of different anticancer agents[141].

For this purpose, exosomes were isolated from RAW 264.7 macrophages conditioned media, labeled with red fluorescent dye (DIL), and incubated with 3LL-M27 cells for various lengths of time. In parallel, liposomes or polystyrene nanoparticles (red, 100 nm) were incubated with 3LL-M27 cells for the same duration. Confocal images revealed a profound accumulation of

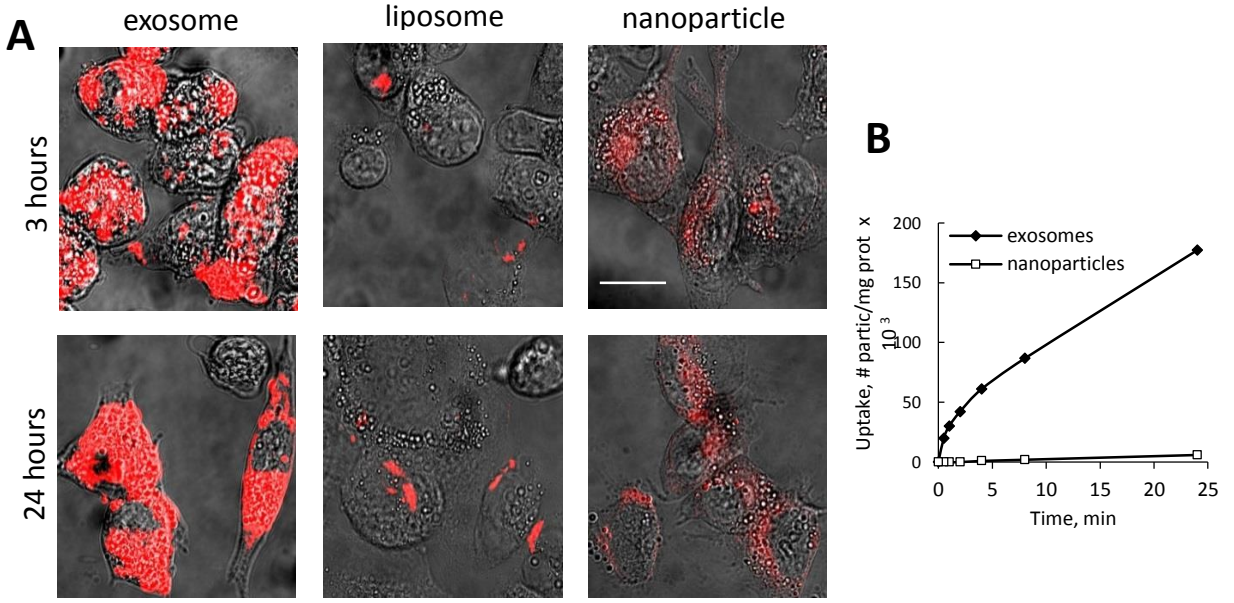

Figure 2.2 A profound accumulation of exosomes in 3LL-M27 cells in vitro. A: 3LL-M27 cells were incubated for 3 or 24 hours with fluorescently-labeled (red) exosomes, or liposomes, or polymer nanoparticles, washed with PBS, and the uptake of nanocarriers in cancer cells was visualized by confocal microscopy. The accumulation studies (**B**) confirmed superior uptake of exosomes in 3LL-M27 cancer cells *vs.* polystyrene nanoparticles. All nanoformulations were used at the same fluorescence intensity. Bar: 10 μm.

exosomes in cancer cells and limited uptake of liposomes and polystyrene nanoparticles (**Figure 2.2A).** Exosomes consist of cellular membranes with numerous adhesive proteins and specific vector ligands (e.g. tetraspanins, integrins, LFA1, CD11b and CD18 receptors) on their surface [30, 31]. They efficiently adhere to and fuse with target cells to deliver their cargo. The efficient uptake of exosomal carriers by cancer cells was further confirmed and quantitated by accumulation studies (**Figure 2.2 B**). The exosomal carriers were taken up about 30 times better than synthetic polystyrene nanoparticles. This suggests that PTX loaded into exosomes can be delivered to cancer cells in therapeutically sufficient quantities.

To assess the therapeutic effect of exoPTX, the cytotoxicity of exoPTX was determined in various cancer cell lines using a standard MTT assay [32]. To evaluate the role of drug loading into exosomes, a resistant MDR cell line expressing the drug efflux transporter, Pgp ($MDCK_{MDR1}$), and their sensitive counterpart ($MDCK_{WT}$) were employed in these experiments, along with murine 3LL-M27 Lewis Lung Carcinoma cells.

The incorporation of PTX into exosomes significantly increased its cytotoxicity as compared to PTX alone and to the commercially available PTX formulation, Taxol (**Table 2.1**). It is worth noting that the increase in PTX cytotoxicity afforded by exoPTX was greater in Pgp-overexpressing cells than their sensitive counterparts ($MDCK_{MDR1}$ and $MDCK_{WT}$, respectively). Thus, the effects of various PTX formulations were expressed in the form of a "Resistance Reversion Index" (RRI), i.e. ratio of IC50 of PTX alone, and in nanoformulation ($IC50_{PTX}/IC50_{exoPTX}$, or $IC50_{PTX}/IC50_{taxol}$). Both PTX formulations caused significant sensitization of MDR cells with respect to PTX. However, the RRI for exoPTX was ten times greater than for Taxol. We hypothesized that exoPTX may alter drug intracellular trafficking and bypass the drug efflux system more efficiently than Taxol (the increase in cytotoxicity for

exoPTX may also be due to the facilitated endosomal release of PTX from exosomes in cancer cells).

Drug	Cell Line	IC_{50} (ng/mL)	RRI
exoPTX	3LL-M27	13.57 ± 1.33	9.32
	MDCK WT	23.33 ± 3.77	18.38
	MDCK MDR1	187.5 ± 38.65	>53.33
Taxol	3LL-M27	23.16 ± 1.88	5.46
	MDCK WT	69.54 ± 11.50	6.17
	MDCK MDR1	1708.67 ± 299.93	>5.85
Paclitaxel	3LL-M27	126.41 ± 31.31	1
	MDCK WT	428.77 ± 63.37	1
	MDCK MDR1	>10,000	1

Table 2.1. Cytotoxicity of different PTX formulations in cancer cells. The RRI was calculated as IC_{50} of PTX *vs.* IC_{50} of exoPTX or Taxol.

To prove this hypothesis, we examined the accumulation levels of a fluorescent probe and Pgp substrate, Dox, incorporated into exosomes (exoDox). Pgp-overexpressing resistant $MDCK_{MDR1}$ cells, and their sensitive counterparts, $MDCK_{WT}$ cells were used in this experiment. First, to characterize these cancer cells, elevated Pgp expression levels in $MDCK_{MDR1}$ cells, and low, if any, Pgp levels in $MDCK_{WT}$ cells were confirmed by western blot (**Figure 2.3A**). Next, the uptake of free Dox and the exosome-incorporated drug, exoDox, was compared in the presence/absence of Pgp inhibitor, verapamil (**Figure 2.3B**). As expected, the incorporation of Dox into exosomes significantly increased drug accumulation levels in both sensitive and resistant cancer cells. Inhibition of Pgp-mediated drug efflux by verapamil elevated accumulation levels of free Dox in MDR cells, and did not alter drug accumulation in their sensitive counterparts. Interestingly, pre-treatment with verapamil did not significantly increase exoDox accumulation levels in resistant $MDCK_{MDR1}$ cancer cells, indicating that the

incorporation of drug into exosomes allowed it to bypass this resistance mechanism (**Figure 2.3B**).

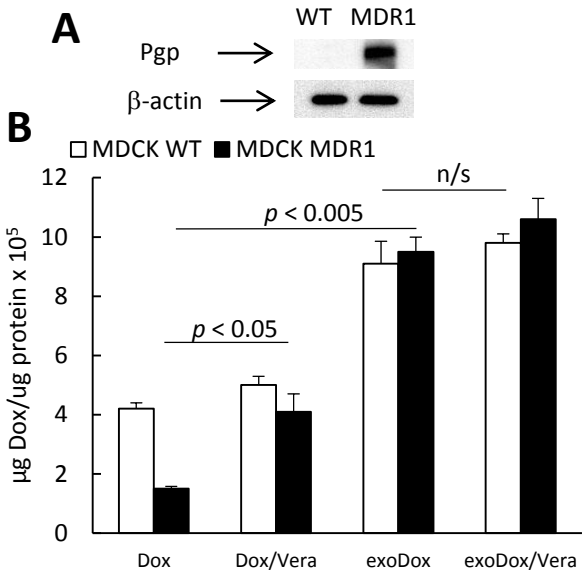

Figure 2.3. Effect of Pgp inhibition on Dox accumulation in resistant and sensitive cancer cells. $MDCK_{MDR1}$ and $MDCK_{WT}$ cells grown on 24-well plates were incubated with free Dox or exoDox formulations for two hours, washed, and the levels of fluorescence were analyzed in cell lysates. The incorporation of the drug into exosomes significantly increased accumulation of Dox in sensitive and resistant cancer cells. No significant difference between exoDox accumulation with or without verapamil was found. Values are means ± SEM (n = 4). Symbols indicate the relative level of significance compared with free Dox or Dox in exosomes.

We demonstrated earlier that the incorporation of Pgp substrates, such as R123 or Dox, into block-copolymer-based nanocarriers, i.e. Pluronic micelles, increased drug accumulation in resistant cancer cells. The mechanism of Pluronic effects is related to the inhibition of the Pgp drug efflux transporter by polymer chains incorporated into the membranes of resistant cancer cells 22, 33-35[142-145]. To exclude the possibility that exosomes may inhibit Pgp-mediated efflux by their fusion with cellular membranes, accumulation of R123 in both resistant and sensitive MDCK cancer cells was assessed. For this purpose, $MDCK_{WT}$ and $MDCK_{MDR1}$ cell monolayers were pretreated with a Pgp inhibitor, verapamil (positive control), or empty exosomes, or media (negative control), and then were treated with R123 solutions for two hours (**Figure 2.4**). (R123 does not incorporate into exosomes upon incubation at RT, as was

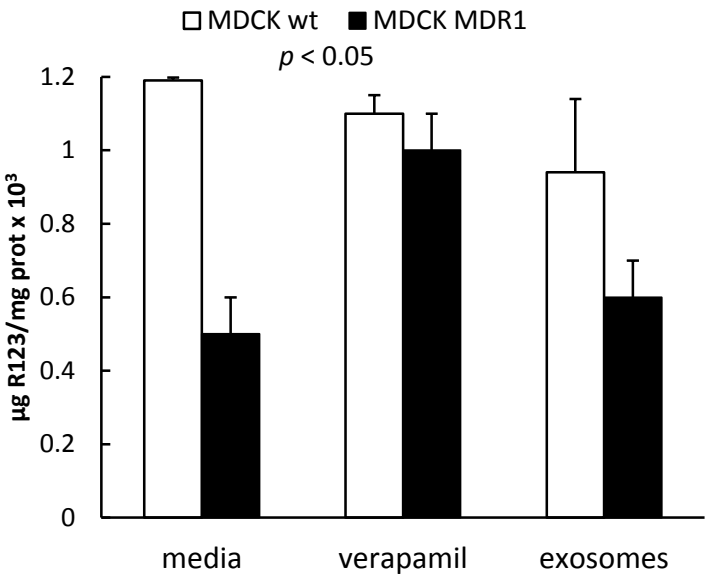

Figure 2.4 Exosomes do not inhibit Pgp-mediated drug efflux in resistant cancer cells. Resistant $MDCK_{MDR1}$ cells and their sensitive counterparts $MDCK_{WT}$ were pretreated with verapamil, a well-known Pgp inhibitor, or empty exosomes, or media as a control. Then, cells were supplemented with R123 solutions for two hours, washed, and accumulation of a Pgp substrate, R123, was examined by fluorescence. Verapamil significantly increased R123 accumulation in resistant cancer cells and did not alter the R123 uptake in sensitive $MDCK_{WT}$ cells. Contrary to verapamil, exosomes pretreatment did not affect accumulation levels of R123in resistant $MDCK_{MDR1}$ cells, indicating that exosomes themselves did not inhibit Pgp efflux mechanism. Values are means ± SEM (n = 6). Symbols indicate the relative level of significance compared with R123 uptake in verapamil or exosome-free media.

confirmed in preliminary studies (**Figure 2.5**)).

R123 accumulation levels in resistant $MDCK_{MDR1}$ cells were increased almost five times in verapamil pre-treated cells. In contrast, pre-treatment with empty exosomes did not affect R123 accumulation in $MDCK_{MDR1}$ cells. As expected, neither pre-treatment with verapamil, nor with empty exosomes, altered R123 accumulation levels in sensitive $MDCK_{WT}$ cells. This indicates that exosomes themselves do not appear to have any inhibitory effect on Pgp-mediated drug efflux;, rather, we hypothesize that they allow incorporated drugs to bypass the Pgp efflux

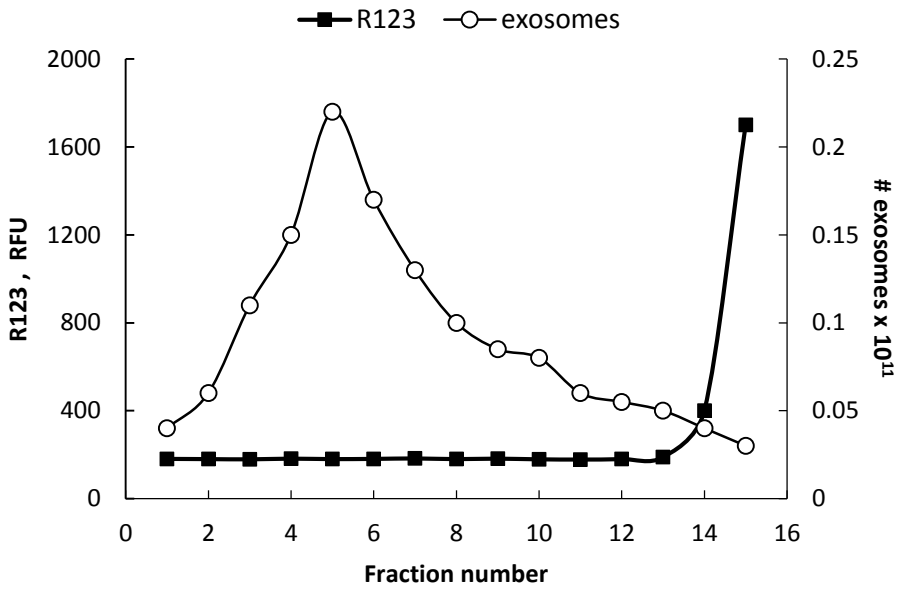

Figure 2.5 R123 does not incorporate into exosomes upon incubation at RT. Exosomes (10^{11} particles/ml) were supplemented with R123 solution and incubated at RT as described in the Materials and methods section. Non-incorporated R123 was separated on from exosomes by size exclusion chromatography using a NAP-10 Sephadex G25 column. Fractions were collected from a column and analyzed by fluorescence (for R123) and NTA (for exosomes). The chromatography profile showed two separated peaks; the free R123 was eluted from the column at a much later time than the exosomes.

protein through endocytosis-mediated transport and/or fusion with plasma membranes.

Vectorized Exosomes Are Targeted to Cells Expressing Sigma Receptor

The ability to delivery a drug payload specifically to target cancer cells while avoiding normal healthy cells is essential in achieving therapeutic efficacy as well as minimizing side effects. To this end, the ability of exosomes vectorized to the sigma receptor to target and be taken up by cells expressing the sigma receptor was assessed by a receptor competitive inhibition study (**Figure 2.6**). Exosomes were isolated from RAW 264.7 macrophages conditioned media, labeled with a fluorscent dye (DiL), and vectorized to the sigma receptor with DSPE-PEG-AA to produce vectorized exosomes (exoAA). Cells were pre-treated with varying concentrations of anisamide (AA) for 30min. and then incubated with fluorescently labeled exoAA with varying concentrations of AA for 1h. Protein content was determined by BCA assay and fluorescence

was measured and compared against a known standard to determine the number of exoAA per μg protein and the number of exoAA per μg protein was plotted against the concentration of AA. Results showed a dose-dependent response to competitive inhibition by AA, indicating that vectorized exosomes are targeted to and taken up by cells expressing sigma receptor, and that vectorized exosomes are taken by cells via receptor-mediated endocytosis.

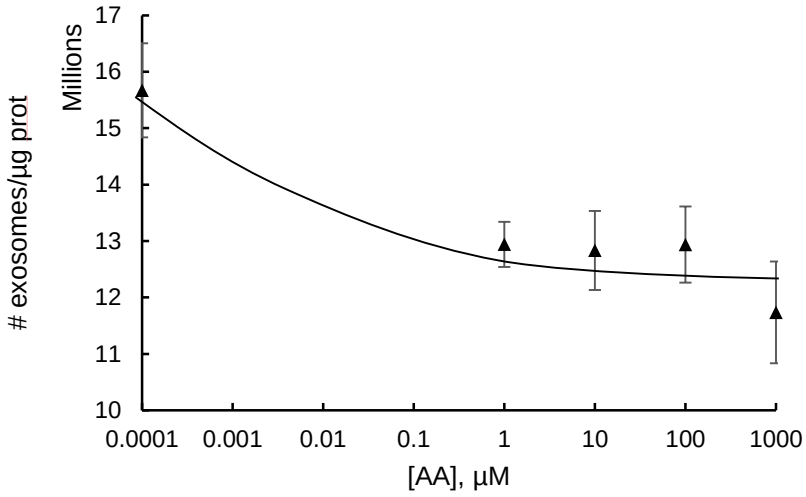

Figure 2.6 Receptor Competitive Inhibition Study. Fluorescently labeled exosomes were incubated with varying concentrations of anisamide (AA) and added to 3LL-M27 cells. After 1h, fluorescence levels were measured and normalized to μg protein. Results show a dose-dependent response to competitive inhibition by AA.

Effect of Proteinase K Treatment on Exosome Uptake

To explore the role of exosomal surface proteins in exosome uptake, exosomes were isolated from RAW 264.7 macrophage conditioned media, labelled with DiL dye, treated with proteinase K (or PBS as a control) to digest the exosomal surface proteins, and incubated with 3LL-M27 cells for varying lengths of time. Afterwards, fluorescence levels were measured and the amount of exosomes/μg protein was quantified (**Figure 2.7**).

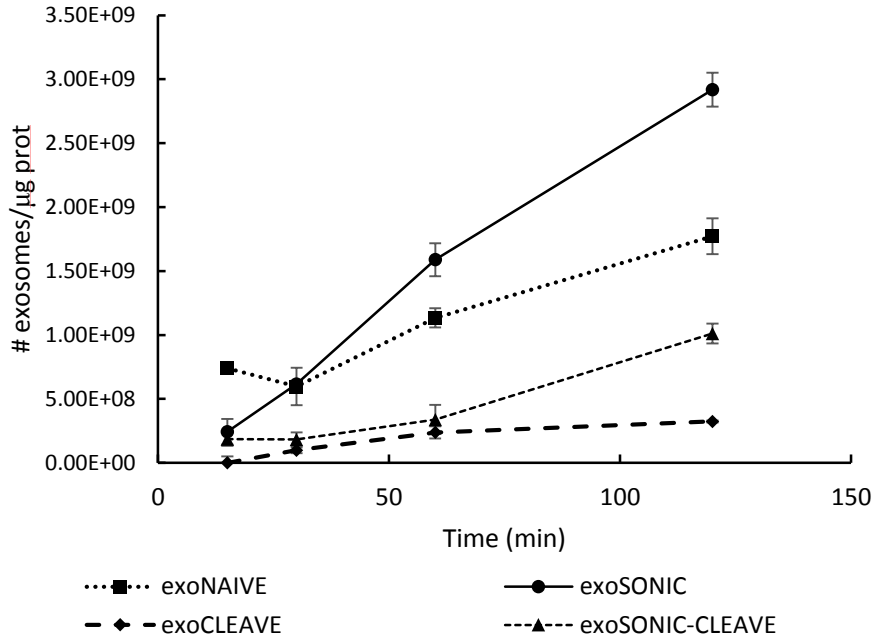

Figure 2.7 Exosome Uptake with/without Proteinase K Treatment. Naïve exosomes or empty sonicated exosomes with or without treatment by Proteinase K to digest exosomal surface proteins, such as LFA1, important in adhesion and uptake to target cancerous and inflamed cells, were evaluated for their uptake into 3LL-M27 cells. Results showed that Proteinase K treatment (exoCLEAVE and exoSONIC-CLEAVE) significantly decreased exosome uptake, highlighting the importance of exosomal surface proteins in cell adhesion and uptake.

Results showed that, for both naïve exosomes and sonicated exosomes, digestion of exosomal surface proteins by Proteinase K resulted in a decrease of exosome uptake by target 3LL-M27 cells. This finding highlights the importance and role of exosomal surface proteins in exosome uptake.

Intracellular Distribution of Exosomes

Exosomes are known to function as intracellular messengers, delivering proteins and nucleic acids[4] from cell to cell. However, the fate of their cargo remains unknown. Thus, we explored the intracellular fate of exosomes in murine Lewis Lung Carcinoma cells (3LL-M27). The fate of both naïve exosomes as well as exoAA targeted to the sigma receptor were assessed. For this purpose, exosomes were isolated with RAW 264.7 macrophages conditioned media,

labeled with red fluorescent dye (DiL), and vectorized to the sigma receptor as needed as described above.

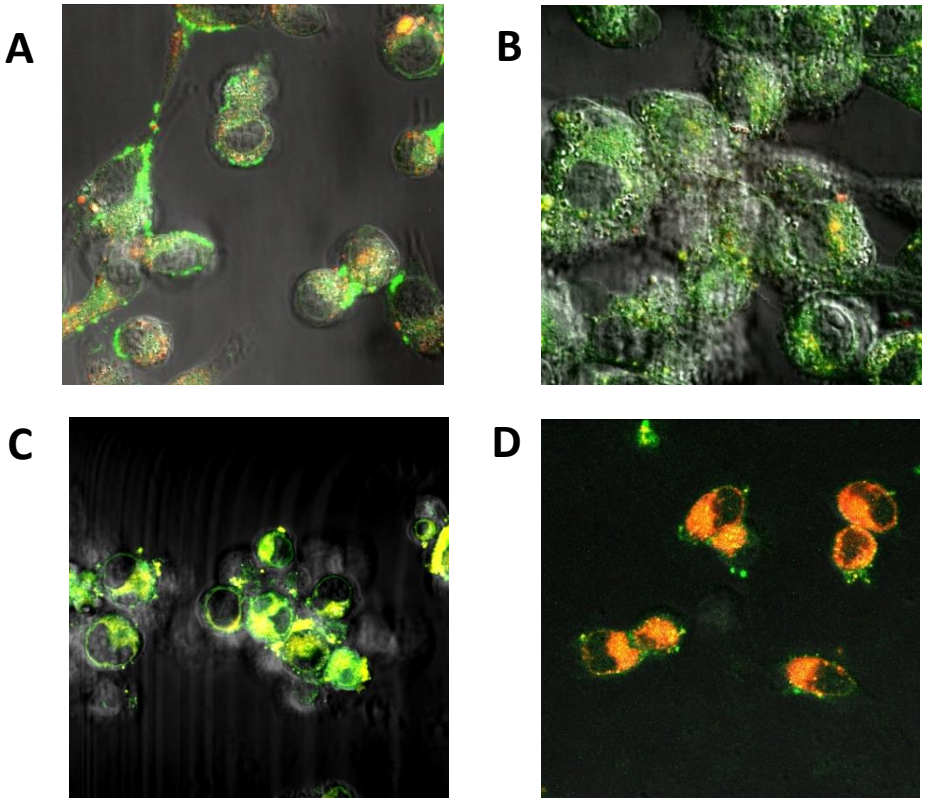

Figure 2.8 Intracellular Distribution of Exosomes. Fluorescently labeled (DiL, red) exosomes (**A, B**) or vectorized exosomes (**C, D**) were incubated with 3LL-M27 cells for 1h. Afterwards, cells were washed and stained with ER Tracker (**A, C**), LysoTracker (**B**), or MitoTracker (**D**), shown in green. Areas of colocalization are shown in yellow.

Exosomes or exoAA were then incubated with 3LL-M27 cells for various lengths of time, followed by staining of the mitochondria, lysosomes, or endoplasmic reticulum (ER). Confocal images revealed that both exosomes and exoAA were preferentially distributed to the ER (**Figure 2.8**). Furthermore, confocal images also revealed that vectorization of exosomes did not alter the intracellular distribution pattern of exosomes.

DISCUSSION

PTX is a potent chemotherapeutic used to treat many forms of cancer; however, its effectiveness for clinical use is hampered by its low aqueous solubility. In addition, PTX is a substrate for the drug efflux transporter, Pgp, which significantly reduces its therapeutic efficacy in resistant tumors [146]. There have been significant efforts to formulate PTX into various nanoformulations to increase solubility, improve pharmacokinetics, and avoid efflux by Pgp, including polymer based nanoparticles and liposomes. However, these systems possess several undesirable properties such as the presence of toxic excipients and/or rapid clearance by the RES.

The aggregation stability of exoPTX formulations is imperative for their use in clinic. We report here that our exoPTX formulation was stable at various conditions (4°C, RT, and 37°C) for over a month, which confirms previous reports about the long-term stability [147] of exosomes. In addition, exosomes may be lyophilized and reconstituted, while retaining their morphology and other characteristics [106].

Exosomes possess an extraordinary ability to interact with and accumulate in target cancer cells. Confocal microscopy studies indicated that exosomes are taken up in considerably greater numbers than liposomes or polystyrene nanoparticles. Because exosomes are taken up in a unique manner, we hypothesized that incorporation of PTX into exosomes may not only increase its solubility, but also may allow for overcoming of Pgp mediated resistance to PTX. To validate this hypothesis, we first validated the ability of exosomes to improve drug accumulation and overcome Pgp-mediated drug efflux in *in vitro* studies with a fluorescent probe, Dox, which is known to be a Pgp substrate. Incorporation of Dox into exosomes significantly increased Dox accumulation in MDR cells as compared to free Dox. Next, we compared the cytotoxicity of our

exoPTX formulation in resistant cancer cells and their sensitive counterparts. Strikingly, the increase in cytotoxicity afforded by the exosome formulation of PTX was more than twenty times greater in resistant cells (*RRI* > 53.33) than sensitive cells (*RRI* = 18.35). The Taxol formulation showed little difference in resistant (*RRI* = 5.85) and sensitive cancer cells (*RRI* = 6.17). This effect may be attributed to the difference in route of internalization of exoPTX as compared to Taxol. Exosomes and micelles, such as those found in Taxol, are taken up by endocytosis, but exosomes have superior uptake due to the presence of adhesion proteins such as tetraspanins, integrins, immunoglobulins, proteoglycans, and lectins [136] which are not found on artificial nanoparticles. Furthermore, exosomes consist of cellular membranes that may fuse with the plasma and/or endocytic membranes and deliver their cargo, bypassing Pgp-mediated efflux. Finally, the obtained data indicated that exosomes themselves did not inhibit Pgp, as pretreatment with empty exosomes did not increase accumulation of the Pgp substrate, R123, in resistant cancer cells.

It was suggested that the MDR efflux transporters are likely to contribute to the production of drug-loaded exosomes during their biogenesis in resistant cancer cells. Thus, Safaei et al. reported that cisplatin-resistant cells release exosomes with 2.6 times higher cisplatin content than cisplatin sensitive cells [148]. A study by Yamagishi and co-workers suggests that Pgp may be also involved in the increased lysosomal sequestration of accumulated drugs [149]. Pgp associated with the endosomal membrane excretes the internalized drug into the endosomal lumen, where newly formed exosomes are literally incubated with the drug and become "drug-loaded" before being released from the cell. The same effect was reported with PTX incorporated into exosomes during their biogenesis in Pgp-overexpressing bone marrow mesenchymal stromal cells (SR4987) [108]. We hypothesized that exoPTX accumulated in the

MDR cancer cells may bypass not only efflux by Pgp transporter located on the plasma membrane, but also avoid accumulation in lysosomes and multivesicular bodies of cancer cells, and therefore reduce drug elimination and increase its therapeutic efficacy in resistant tumors.

The intracellular fate of exosomes and their cargo is of paramount importance for drug delivery applications, thus, we explored the intracellular fate of exosomes and vectorized exosomes targeted to the sigma receptor in target Lewis Lung Carcinoma 3LL-M27 cells. Both exosomes and vectorized exosomes shared a similar fate, with the greatest accumulation in the ER, followed by lysosomes and finally the mitochondria.

This work demonstrates that exosomes are an exceptionally potent carrier for PTX. We developed an efficient method of drug loading into and vectorizing exosomes without significantly altering their structure, and we showed that vectorized exosomes loaded with PTX efficiently accumulate in cancer cells and produce a potent anticancer effect. Furthermore, the apparent ability of exosomes to circumvent the protective properties of drug efflux by Pgp is an exciting finding which implies that exosomes may be valuable in treating drug resistant cancers. These findings indicate that an exosomal based formulation of PTX could be a valuable tool in the future for anticancer therapy. This data warrants further evaluation of this formulation in an *in vivo* model of cancer.

CHAPTER 3. BIODISTRIBUTION AND THERAPEUTIC EFFICACY OF EXOSOME BASED PTX FORMULATIONS IN A MOUSE MODEL OF PULMONARY METASTASES[4]

OVERVIEW

Metastatic lung cancer is one of the most common and aggressive forms of cancer, typically diagnosed during a relatively late stage in its progression which results in little to no chance for a cure. Stage 4 metastatic lung cancer is one of the greatest threats to public health, lung metastases are identified in 30 – 55% of all cancer patients. As a result, lung cancer is the leading of cause of cancer-related deaths in the world, responsible for more deaths than breast, colon, and prostate cancers combined[150]. The lungs are the most common site of metastases and tumor relapse following treatment of the primary tumor mass.

Regrettably, efficient and targeted delivery of antineoplastic agents to pulmonary metastases poses a significant challenge to the scientific and healthcare communities. Resection is the current standard for metastatic cancer, but because pulmonary metastases are distributed throughout the pulmonary parenchyma, their excision is difficult if not impossible. Thus, successful treatment of pulmonary metastases demands an innovative approach to the design of

[4] Some of this text previously appeared in an article in the journal Nanomedicine. The original citation is as follows: Development of Exosome-encapsulated Paclitaxel to Overcome MDR in Cancer cells. Myung Soo Kim, Matthew J. Haney, Yuling Zhao, Richa Gupta, Zhijian He, Natalia L. Klyachko, Aleksandr Piroyan, Marina Sokolsky, Alexander v. Kabanov, and Elena V. Batrakova. *Nanomedicine*, Nov 13. pii: S1549-9634(15)00202-6. doi: 10.1016/j.nano.2015.10.012. PMID: 26586551

drug delivery systems for this application. We propose the utilization of exosomes released by autologous macrophages for the targeted delivery of paclitaxel to pulmonary metastases. The combination of targeting ability with the long circulation time of exosomal-based drug formulations offers a powerful and novel delivery platform for anticancer therapy.

Herein, we have assessed the *in vivo* biodistribution and efficacy of exosomes loaded with PTX in a murine model of metastatic pulmonary cancer. The objectives of this study were: (i) to assess the ability of exosomes to travel to and delivery their drug payload to pulmonary metastases, (ii) to assess the ability of vectorized exosomes to travel to and target pulmonary metastases, and (iii) to assess the *in vivo* therapeutic efficacy of paclitaxel loaded in exosomes in a murine model of pulmonary metastases.

Our results showed that exosomes were able to travel to sites of pulmonary metastases when administered intranasally or intravenously, and were also able to deliver their drug payload to target cancer cells. Furthermore, exosomes loaded with paclitaxel (exoPTX) showed greater *in vivo* therapeutic efficacy in a murine model of pulmonary metastases as compared to a commercially available PTX formulation, Taxol. Taken together, our results indicate that an exosomal based formulation of paclitaxel with targeting moieties represents a promising new innovation in anticancer therapy for the treatment of pulmonary metastases and other types of metastatic cancers.

MATERIALS AND METHODS

Reagents

Paclitaxel (PTX) was purchased from LC Laboratories (Woburn, MA, USA). The stock solution was prepared in ethanol (EtOH) at a concentration of 10 mg/mL. Aliquots were stored at -20°C. Doxorubicin (DOX) was purchased from LC Laboratories (Woburn, MA, USA). The stock solution was prepared in DMSO at a concentration of 2 mg/mL and aliquots were stored at 4°C. Working solutions of PTX or DOX were prepared fresh according to experimental design by serial dilution in an appropriate medium. A lipophilic fluorescent dye, 1,1'-dioctadecyl-3,3,3',3'-tetramethylindo-carbocyanine perchlorate (DIL), was purchased from Invitrogen (Carlsbad, CA, USA). A fluorescent duy, 2-decanoyl-1-(O-(11-(4,4-difluoro-5,7-dimethyl-4-bora-3a,4a-diaza-s-indacene-3-propionyl)amino)undecyl)-sn-glycero-3-phosphocholine (BODIPY-PC) was purchased from Molecular Probes. Doxorubicin, Rhodamine 123 (R123), 4′,6-diamidino-2-phenylindole dihydrochloride (DAPI), and Triton X-100 were obtained from Sigma-Aldrich (St. Louis, MO, USA). Cell culture medium and fetal bovine serum (FBS) were purchased from Gibco Life Technologies, Inc. (Grand Island, NY, USA). Culture flasks and dishes were from Corning Inc. (Corning, NY, USA). ExoQuick-TC™ Exosome Precipitation Solution was obtained from System Biosciences (Mountain View, CA, USA). ER Tracker Blue-White DPX, LysoTracker Green DND-26, and MItoTracker Deep Red were purchased from Thermo Fisher (Thermo Fisher Scientific, Waltham, MA, USA).

Cells

RAW 264.7 macrophages (purchased from ATCC, Manassas, VA, USA) were cultured in Dulbecco's modified Eagle's medium (DMEM) high glucose (Gibco, Grand Island, NY, USA) supplemented with 10% fetal bovine serum (FBS; Thermo Fisher Scientific), 1%

penicillin and streptomycin at 37°C and 5% CO2. Murine Lewis lung carcinoma cell subline (3LL-M27), a highly metastatic lung clone, was a generous gift from Dr. L. Pelletier (CHUL, Laval University, QC, Canada), and were cultured in DMEM high glucose supplemented with 10% FBS, 10 mM HEPES, 1% penicillin and streptomycin at 37°C and 5% CO2.

To utilize exosomes from autologous macrophages, bone marrow derived macrophages (BMM) were obtained by differentiation of bone marrow stem cells extracted from murine femurs (C57Bl/6 mice) as described in[151]. The cells were then cultured for 10 days in media supplemented with 1000 U/mL macrophage colony-stimulating factor (M-CSF, Sigma-Aldrich, MO, CAS Number 81627-83-0). The purity of monocyte culture was determined by flow cytometry using FACS Calibur (BD Biosciences, San Jose, CA).

Animals

The experiments were performed with female C57BL/6 mice (Charles River Laboratories, Durham, NC, USA) eight weeks of age in strict accordance with the recommendations in the Guide for the Care and Use of Laboratory Animals of the National Institutes of Health. The protocol was approved by the Committee on the Ethics of Animal Experiments of the University of North Carolina at Chapel Hill. The animals were kept five per cage with an air filter cover under light- (12-hours light/dark cycle) and temperature-controlled (22 ± 1^{o} C) environment. All manipulations with the animals were performed under a sterilized laminar hood. Food and water were given *ad libitum*.

Exosome Isolation

For all studies, exosome-depleted media was prepared by ultracentrifugation of fetal bovine serum (FBS) at 120,000 x g for 110 min to remove all vesicular content prior to addition to media. Exosomes were harvested from the supernatants of RAW 264.7 cells cultured in

exosome-depleted media using the ExoQuick-TC™ Kit (System BioSciences; Mountain View, CA, USA). Briefly, > 90% confluent RAW 264.7 cells were cultured in exosome-depleted media for 2 days. 50 mL conditioned cell culture media were centrifuged at 300 x g for 10 min (Thermo CL-10 centrifuge with O-G26/1 rotor, Thermo Fisher Scientific, Waltham, MA, USA) in order to remove cells and cellular debris. The supernatant was then taken, filtered with a .22 µm PES filter, and ExoQuick-TC™ Exosome Precipitation Solution (System Biosciences, Mountain View, CA, USA) was added to the filtered supernatant and the mixture was vortexed and incubated overnight at 4°C. After overnight incubation, the mixture was vortexed again and subsequently centrifuged at 1500 x g for 30 min. and 5 min. to pellet exosomes. The supernatant was discarded and the exosome pellet was resuspended in PBS. Freshly-prepared exosomes or exosomes stored at -20°C were used for all experiments.

Drug Loading into Exosomes

For PTX and DOX loading into exosomes, purified exosomes (~10^{11} exosomes) were first mixed with PTX or DOX in 1 mL PBS. First, PTX was dissolved in ethanol (EtOH, 10 mg/ml drug in EtOH stock solution) and added to 1 mL exosomes. DOX stock solution was prepared in DMSO (2 mg/mL) and added to 1mL exosomes. The PTX-exosome or DOX-exosome mixture was then sonicated using a Model 505 Sonic Dismembrator with .25" tip (Thermo Fisher Scientific, USA) with the following settings: 20% amplitude, 6 cycles of 30 s on/off for three minutes with a two minute cooling period between each cycle. After sonication, PTX-loaded exosomes (exoPTX) or DOX-loaded exosomes (exoDOX) solution was incubated at 37°C for 60 min to allow for recovery of the exosomal membrane.

Excess free PTX or DOX was separated from exoPTX or exoDOX, respectively, by size exclusion chromatography using a NAP-10 Sephadex G25 column (GE Healthcare,

Buckinghamshire, UK) according to the manufacturer's recommended protocol. Briefly, 750 µL of exoPTX or exoDOX were added to the NAP-10 column and the void volume was discarded. 250 µL of PBS was then added to the column and allowed to enter the gel bed completely and the eluate was discarded. 1.2 mL of PBS was then added to the column and the eluate containing purified exoPTX or exoDOX was collected and stored at -20°C.

Quantification of Drug Loading

The amount of PTX loaded into exosomes was measured by a high performance liquid chromatography (HPLC) method. Briefly, exoPTX (10^{10} exosomes/0.1mL) in a microcentrifuge tube was placed on a heating block set to 75°C to evaporate solvent. After all solvent had evaporated, an equal volume of acetonitrile was added to the microcentrifuge tube and the mixture was vortexed, sonicated, and vortexed again. The sample was then centrifuged at 13,000 rpm (Thermo Legend Micro 21, Thermo Fisher Scientific, Waltham, MA, USA) for 10 min. Following centrifugation, the supernatant was taken and filtered through a Corning Regenerated Cellulose .2 µm syringe filter and transferred into HPLC autosampler vials. 20 µL aliquots were injected into the HPLC system (Agilent 1200, Agilent Technologies, Palo Alto, CA, USA). All analyses were performed using a C18 column (Supelco Nucleosil C18, 250 mm x 4.6 mm, 5 µm, 100 Å, Sigma-Aldrich,) with a mobile phase of H2O:acetonitrile (45:55, v/v) at a flow rate of 1 mL/min at 30°C. Absorbance was measured at 227 nm to monitor the elution of PTX. The area under the PTX peak was measured for each sample and compared with known concentration of standard. A calibration curve was constructed by plotting peak area versus concentrations of paclitaxel and was found to be linear within the tested concentration range (r2 = .997). Exosomal protein content was measured using the Pierce BCA Protein Assay Kit (Thermo Fisher

Scientific, Waltham, MA, USA) according to the manufacturer's recommended protocol. Loading capacity is expressed by µg protein of exosomes.

Synthesis of DSPE-PEG-AA

The synthesis was carried out according to the published synthetic protocol with little adjustment[23]. Briefly, to synthesize the N-(2-bromoethyl)-4-methoxy-benzamide, 4-methyoxybenzoyl chloride (1g, 5.8 mmol) in 50 mL of pre-warmed benzene was mixed with an aqueous solution of 2-bromoethylamine hydrobromide (1.32g, 6.4 mmol). The emulsion was shaken and cooled in running water during the dropwise addition of 5% aqueous solution of sodium hydroxide. The precipitate was solidified out of the reaction mixture within a few minutes to an amorphous mass. The mixture was continued stirred for 1h, after which time the solid amide was filtered with suction and washed once with benzene and air dry for 2-3h. Then, the synthesized N-(2-bromoethyl)-4-methoxy-benzamide (100 mg, 0.4 mmol) was reacted with DSPE-PEG-NH2 (100 mg, 23.3 µmol) in acetonitrile (5 mL) in the presence of DIPEA (30 uL, 0.2 mmol) at 65-70 °C for 16h. After evaporating the solvent, 5 mL of methanol was added to dissolve the pellet followed by excess ether (50ml) and it was the kept at -80 °C overnight. The precipitate was collected after centrifugation and recrystallized twice. The overall yield was 70%. The products was characterized by NMR and TLC as reported elsewhere[129].

Preparation of Exosomes Vectorized to Sigma-receptor

Vectorized exosomes targeted to sigma receptor using DSPE-PEG-AA (exoAA) and non-vectorized control exosomes with DSPE-PEG (exoPEG) were prepared as follows: exosomes were isolated as previously described and then varying volumes of 10mg/mL DSPE-PEG or DSPE-PEG-AA were added to the exosome solution (for exoPEG and exoAA, respectively). 100µL of 10mg/mL PTX in EtOH was also added to the mixture when preparing exoPTX-AA.

The mixture was then sonicated by the same method used by our lab previously [29]. Briefly, the mixture was sonicated using a Model 505 Sonic Dismembrator with .25" tip (Thermo Fisher Scientific, USA) with the following settings: 20% amplitude, 6 cycles of 30 s on/off. After sonication, the exoAA or exoPEG solution was incubated at 37°C for 60 min to allow for recovery of the exosomal membrane. Excess free DSPE-PEG or DSPE-PEG-AA was separated from exoPEG or exoAA, respectively, by size exclusion chromatography using a NAP-10 column packed with Sepharose 6b (GE Healthcare, Buckinghamshire, UK) according to the manufacturer's recommended protocol. Briefly, 750 µL of exoPEG or exoAA were added to the NAP-10 column packed with Sephadex 6b and the void volume was discarded. 250 µL of PBS was then added to the column and allowed to enter the gel bed completely. 1.2 mL of PBS was then added to the column and the eluate containing purified exoPEG or exoAA was collected and stored at -20°C.

Biodistribution of Airway Delivered Exosomes in Mice with Pulmonary Metastases

C57BL/6 mice (n = 4) were injected intra tail vein (*i.v.*) with 8FlmC-FLuc-3LL-M27 cells ($5x10^6$ cells/mouse in 100 µl saline) and tumor lung metastases were allowed to establish for 10-12 days. In parallel, exosomes isolated from autologous macrophages conditioned media were stained with a fluorescent lipophilic dye DiD as described above. Twelve days following cancer cells *i.v.* injection, DiD-labeled exosomes were administered intranasally (*i.n.,* 10^7 particles/10µl x 2) to mice with lung metastases. Four hours later, mice were sacrificed and perfused according to a standard protocol. Lungs were extracted and sectioned on a microtome at a thickness of 20 µm; nuclei were stained with DAPI (300 mM, 5 min). The images of lung sections were examined by a confocal fluorescence microscopic system ACAS-570 and corresponding filter set, and processed using ImageJ software.

Colocalization of Drug Delivered via Exosomes with Pulmonary Metastases

C57BL/6 mice (*n* = 4) were injected intra tail vein (*i.v.*) with GBM8FlmC-3LL-M27 cells ($5x10^6$ cells/mouse in 100 µl saline) and tumor lung metastases were allowed to establish for 10-12 days. In parallel, exosomes isolated from autologous macrophages conditioned media were loaded with Dox as described above. Twelve days following cancer cells *i.v.* injection, mice with metastases were injected *i.n.* with non-labeled exosomes loaded with Dox by sonication as described above (10^7 particles/10µl x 2). Four hours later mice were sacrificed, perfused; lungs were extracted, sectioned, and co-localization of Dox with pulmonary metastases was visualized by confocal microscopy.

Biodistribution of Intravenously Injected Vectorized Exosomes in Mice with Pulmonary Metastases

C57BL/6 mice (*n* = 4) were injected intra tail vein (*i.v.*) with GFP/3LL-M27 cells ($2x10^6$ cells/mouse in 100 µl saline) and tumor lung metastases were allowed to establish for 10-12 days. In parallel, exosomes isolated from autologous macrophages conditioned media were stained with a fluorescent lipophilic dye DiD and vectorized to the sigma receptor as described above. Twelve days following cancer cells *i.v.* injection, DiD-labeled exosomes were administered *i.v.* (10^8 particles/100µl) to mice with lung metastases. Four hours later, mice were sacrificed and perfused according to a standard protocol. Lungs were extracted and sectioned on a microtome at a thickness of 20 µm; nuclei were stained with DAPI (300 mM, 5 min). The images of lung sections were examined by a confocal fluorescence microscopic system ACAS-570 and corresponding filter set.

Therapeutic Efficacy of exoPTX Against Pulmonary Metastases

The antineoplastic effects of exoPTX were evaluated in a mouse model of pulmonary metastases. For this purpose, C57BL/6 mice were *i.v.* injected with 8FlmC-FLuc-3LL-M27 cancer cells ($5x10^6$ cells/100 µl/ mouse). Forty eight hours later, mice were treated *i.n.* with exoPTX (10^7 particles/10 µl x 2), or Taxol (50 mg/kg/mouse), or saline as a control (n = 7)10 times every other day. Tumor progression was monitored by luminescence using IVIS system. To reduce fluorescence quenching by fur and autofluorescence from solid diet, C57Bl/6 mice were shaved and kept on liquid diet for 48 hours prior to the imaging studies. For background fluorescence level evaluation, all animals were imaged before the injections in the IVIS 200 Series imaging system (Caliper, Xenogen Co., Life Sciences). The animals were imaged at various time points (1 – 22 days) post-treatment as described [152]. The chemoluminescent signal was quantified by Living Image® 2.50 software. To assess amount of cancer metastases at day 21, mice were sacrificed, perfused, and lung slides obtained on microtome (Thermo Scientific) were examined by confocal microscopy.

RESULTS

Co-localization of Airway-delivered Exosomes with Pulmonary Metastases in Lewis Lung Carcinoma (LLC) mouse model

To establish an *in vivo* model of pulmonary metastases, C57BL/6 mice were injected intra-tail vein ($5x10^6$ cells/100 µL) with 3LL-M27 cells. Twenty days later, mice were sacrificed, perfused, and lungs were isolated, sectioned, and stained with Hematoxylin and Eosin (H&E). Multiple metastases were detected in whole lungs (**Figure 3.1A**). Histological evaluations revealed that the structure of alveoli in tumor-bearing lungs was disrupted by tumor cells (**Figure 3.1B**).

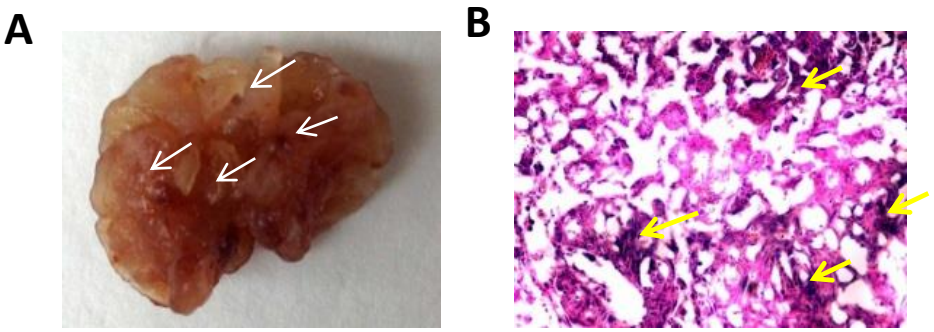

Figure 3.1. Lung metastasis model of Lewis Lung Carcinoma (3LL-M27). C57BL/6 mice were *i.v.* injected with 3LL/M27 cells. 21 days following the injection, multiple metastases (arrows) were detected on gross images of tumor-bearing lungs (**A**), and lung sections (**B**).

To visualize the ability of exosomes to target and deliver their payload to cancer metastases, confocal imaging studies were conducted in an LLC mouse model. 3LL-M27 cells were transduced with lentiviral vectors encoding the optical reporter mCherry (8FlmC) fluorescent protein and Luciferase (Luc). To induce metastases, C57BL/6 mice were injected with 8FlmC-FLuc-3LL-M27 (red, **Figure 3.2A**) intra-tail vein as described in the Materials and Methods section. 22 days later, autologous exosomes stained with a fluorescent dye, DiD

(green), were administered intranasally (*i.n.*, 10^7 particles/10µl) to C57BL/6 mice (**Figure 3.2B**). Four hours later, mice were sacrificed, perfused; lungs were sectioned on microtome and examined by confocal microscopy. Nuclei were stained with DAPI (blue, **Figure 3.2C**). Confocal images revealed 97.9± 2.0% of exosomes (**Figure 3.2D**) were co-localized with lung metastases, indicating efficient targeting of exoPTX *in vivo.*

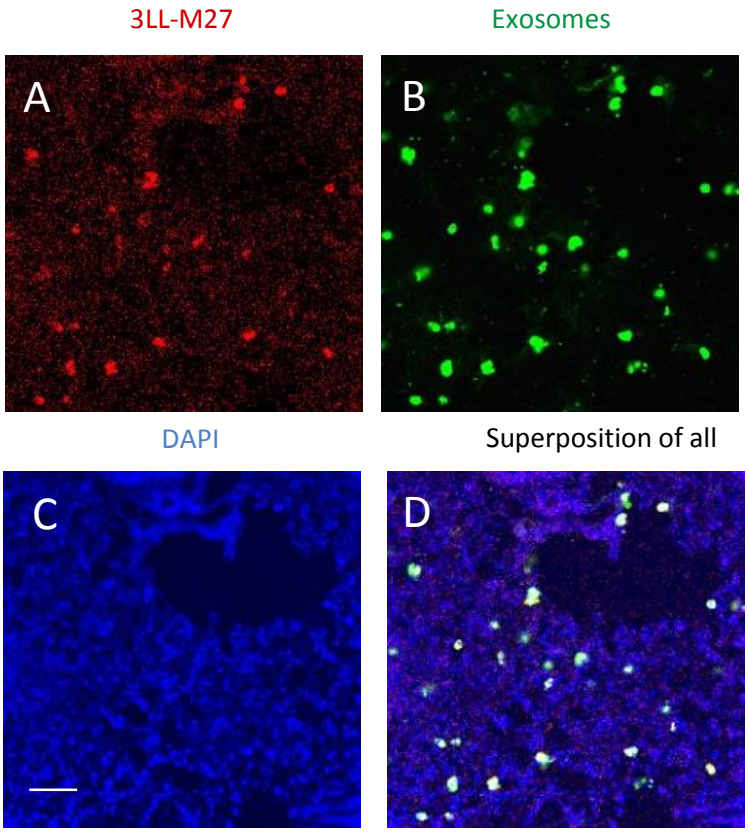

Figure 3.2. Co-localization of airway-delivered exosomes with pulmonary metastases. Exosomes were isolated from macrophages conditioned media, and labeled with fluorescent dye, DiD (green). C57BL/6 mice were i.v. injected with 8FlmC-FLuc-3LL-M27 (red). 22 days later, the mice with established pulmonary metastases (red) were *i.n.* injected with DiD-labeled exosomes (green). 4 hours later, mice were euthanized, perfused, lungs were sectioned, and stained with DAPI (blue). The confocal images revealed near complete co-localization of exosomes with metastases (yellow). Bar: 50 µm.

A similar experiment was performed with exoDox formulation in order to visualize drug delivery to pulmonary metastases (**Figure 3.3**). Non-labeled exosomes loaded with Dox (green,

Figure 3.3B) were *i.n.* administered to mice with established 8FlmC-FLuc-3LL-M27 metastases (red, **Figure 3.3A**). Four hours later, mice were euthanized, perfused, and lung sections were taken and stained with the nuclei marker DAPI (blue). Confocal images revealed a substantial amount of Dox in the lungs co-localized with cancer cells (yellow, **Figure 3.3C**). These results indicate that airway-administered exosomes reached pulmonary metastases and delivered their drug payload to target cancer cells.

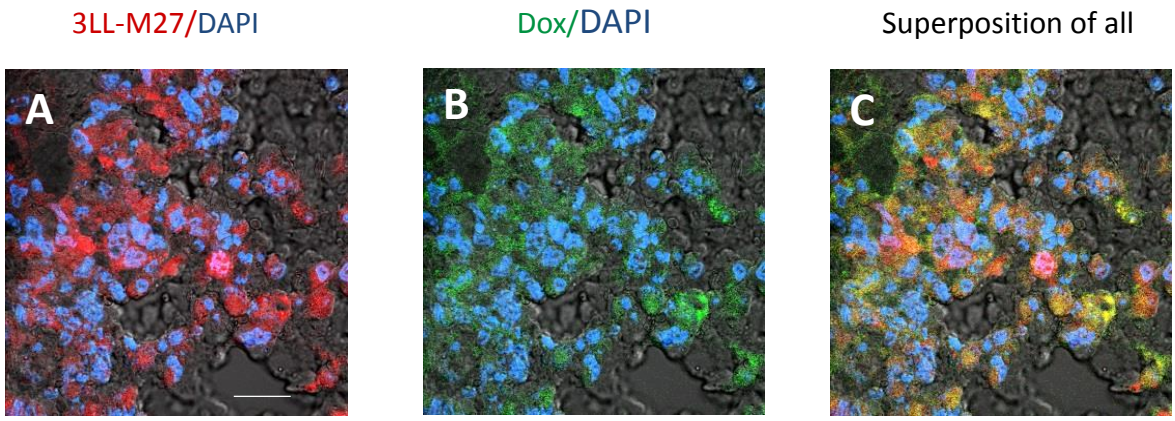

Figure 3.3. Co-localization of airway-delivered exoDox with pulmonary metastases. Exosomes were isolated from macrophages conditioned media, and loaded woth Dox (green). C57BL/6 mice were *i.v.* injected with 3LL-M27 cells transduced with lentiviral vectors encoding the optical reporter mCherry (8FlmC) fluorescent protein (red, **A**). 21 days later, the mice with established pulmonary metastases (red) were *i.n.* injected with DID-labeled exosomes (**B**, green). 4 hours later, mice were euthanized, perfused, lungs were sectioned, and stained with DAPI (blue). The confocal images revealed a significant co-localization of exosome-delivered Dox with metastases (yellow, **C**). Bar: 20 µm.

Co-localization of Intravenously-delivered Vectorized Exosomes with Pulmonary Metastases in Lewis Lung Carcinoma (LLC) mouse model

In order to assess the ability of vectorized exosomes to target sigma receptor expressing pulmonary metastases, confocal images were conducted in an LLC mouse model. 3LL-M27 cells were transduced with lentiviral vectors encoding the optical reporter GFP fluorescent protein. To induce metastases, C57BL/6 mice were injected with GFP/3LL-M27 intra-tail vein as described in the Materials and Methods section. 7 days later, autologous non-vectorized (**Fig.**

3.4.A-C) and vectorized exosomes (**Fig. 3.4.D-F**) stained with a fluorescent dye, DiD (red), were administered intravenously (10^7 particles/10µl) to C57BL/6 mice. Four hours later, mice were sacrificed, perfused; lungs were sectioned on microtome and examined by confocal microscopy.

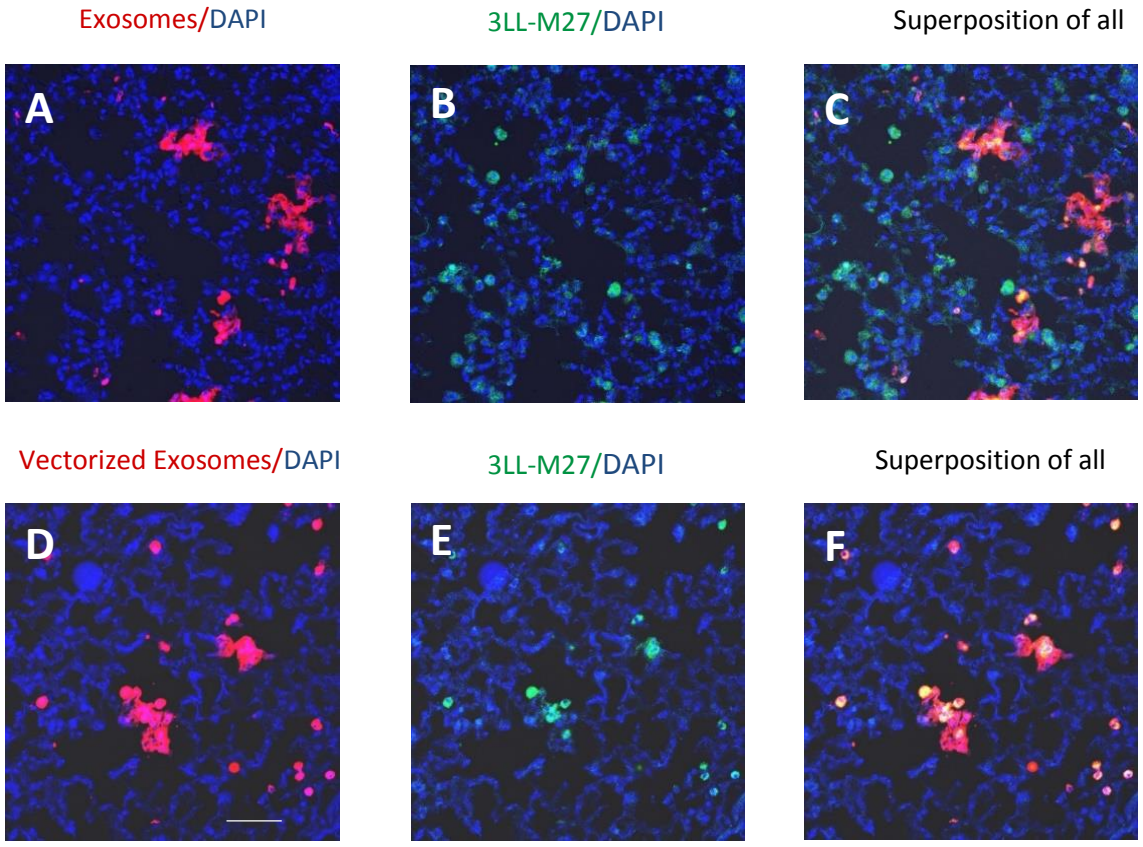

Figure 3.4. Co-localization of intravenously-delivered vectorized exosomes with pulmonary metastases. Exosomes were isolated from macrophages conditioned media, and labelled with DiD dye (red, **A, D**). C57BL/6 mice were *i.v.* injected with 3LL-M27 cells transduced with lentiviral vectors encoding the optical reporter GFP fluorescent protein (green, **B, E**). 7 days later, the mice with established pulmonary metastases (green) were *i.v.* injected with DiD-labeled exosomes (red, **A)** or vectorized exosomes (red, **D**). 4 hours later, mice were euthanized, perfused, lungs were sectioned, and stained with DAPI (blue). The confocal images revealed a significant co-localization of vectorized exosomes with metastases (94.4 + 0.8%) and minimal colocalization of non-vectorized exosomes with metastases (21.8 + 0.2%) (yellow, **F**). Bar: 20 µm.

Nuclei were stained with DAPI. Confocal images revealed a minimal amount of non-vectorized exosomes were colocalized with lung metastases (21.8 + 0.2%) whereas a substantial amount of vectorized exosomes were co-localized with lung metastases (94.4 + 0.8%) (yellow, **Figure 3.4C**), indicating efficient *in vivo* targeting of vectorized exosomes when administered *i.v.*

Noteworthy, vectorized exosomes showed a few, if any, colocalization with healthy cells in the lungs of control healthy mice (**Figure 3.5C**), suggesting that vectorized exosomes might have minimal off-target effects.

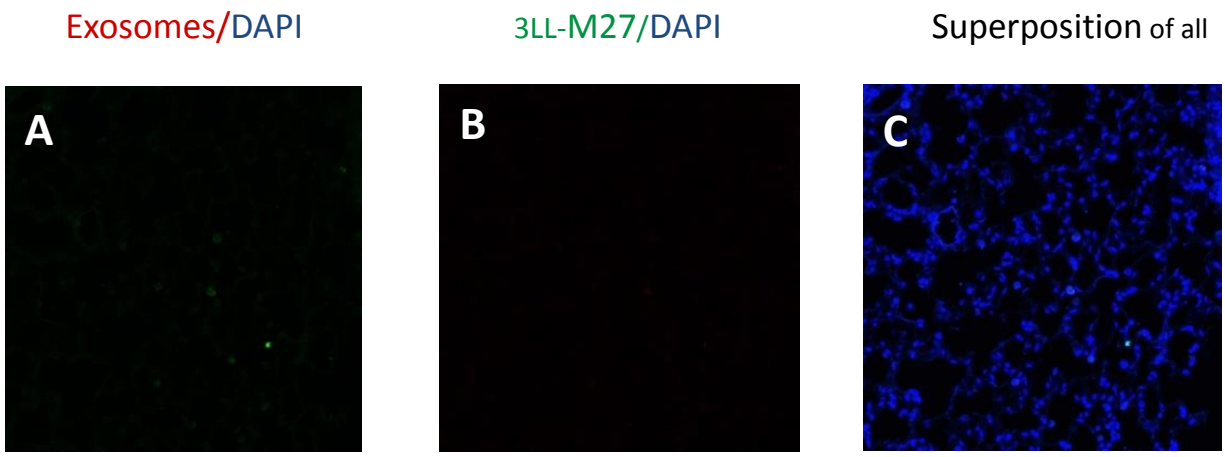

Figure 3.5. Intravenously-delivered vectorized exosomes do not colocalize with healthy lung cells. Exosomes were isolated from macrophages conditioned media, and labelled with DiD dye (red, **A**). Healthy C57BL/6 mice were *i.v.* injected with DiD-labeled vectorized exosomes (red, **A**). 4 hours later, mice were euthanized, perfused, lungs were sectioned, and stained with DAPI (blue). The confocal images revealed no co-localization of vectorized exosomes with healthy lung cells (yellow, **C**). Bar: 20 µm.

Therapeutic Efficacy of exoPTX Against Pulmonary Metastases

To provide insight into the potential of exosome-based therapeutic delivery, the antineoplastic effects of exoPTX were evaluated in an LLC mouse model of pulmonary metastases. This model is particularly relevant to the present investigation, as it was demonstrated that 3LL-M27 tumor cells have high expression levels of the MDR1 gene and Pgp expression *in vivo* [153].

For this purpose, C57BL/6 mice were *i.v.* injected with 8FlmC-FLuc-3LL-M27 cells as described in the Materials and Methods section. 48 hours later, mice were *i.n.* administered exoPTX (10^7 particles/10 µl x 2,), or Taxol, or saline as a control ten times every other day.

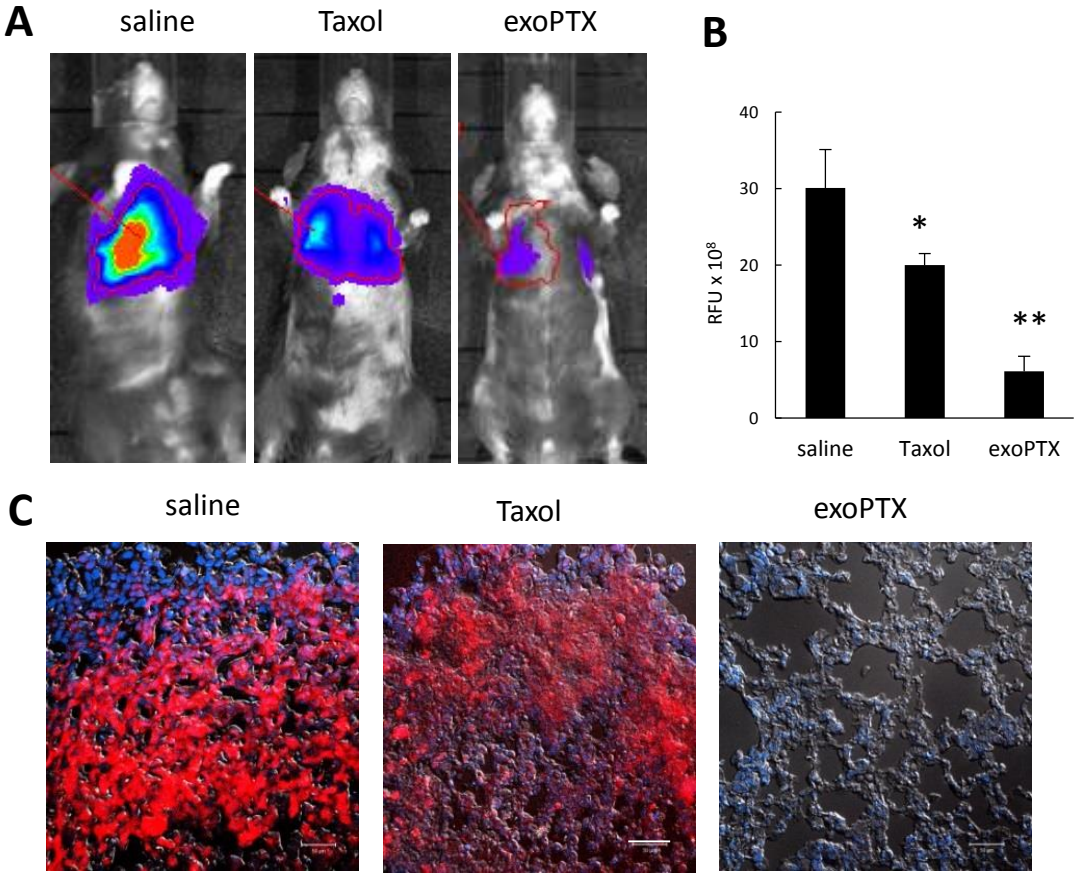

Figure 3.6. Inhibition of metastases growth in mouse lungs upon exoPTX treatment. C57Bl/6 mice were *i.v.* injected with 8FlmC-FLuc-3LL-M27 (red) cells to establish pulmonary metastases. 48 hour later mice were treated with exoPTX, or Taxol, or saline as a control, and the treatment was repeated every other day for a total of ten treatments. Representative IVIS images from each group were taken at day 22 (**A**). Statistical significance of metastases luminescence levels from IVIS images in lungs of treated animals compared to control mice injected with saline is shown by asterisk (*$p < 0.05$; **$p < 0.005$), calculated by one-way ANOVA (**B**). Errors are mean ± SEM, $N = 7$. Symbols indicate the relative level of significance compared with control mice treated with saline. At the endpoint, mice were sacrificed, perfused, and lung slides were examined by confocal microscopy (C). Bar: 10 µm.

Progression of pulmonary metastases in treated mice was monitored by IVIS by observing the luminescence of transduced cancer cells. Representative fluorescent and light images of dorsal planes of the injected animals at day 22 are shown on (**Figure 3.4A**). A

significant ($p < 0.05$) inhibition in the metastases growth by exoPTX treatment was demonstrated (**Figure 3.4B**). Taxol treatment was shown to inhibit metastases growth as compared to non-treated controls (saline), although to a lesser extent than exoPTX treatment.

We further examined the anti-tumor efficacy of PTX formulations on pulmonary metastases growth by confocal microscopy. C57BL/6 mice with established 8FlmC-FLuc-3LL-M27 pulmonary metastases were treated with exoPTX, Taxol or saline as described above. At the end point of the experiment (day 22), the mice were sacrificed, perfused, and lungs were sectioned on microtome. The lung sections were visualized using confocal microscopy. A marked number of fluorescent transduced cancer cells (red) were detected in the lungs of animals treated with Taxol (**Figure 3.6C**), while only a few cancer cells were observed in the lungs of exoPTX treated animals. This suggests the superior antineoplastic efficacy of our exosomal PTX formulation as compared to Taxol (**Figure 3.6C**).

Altogether, our exoPTX formulation showed potent inhibition of pulmonary metastases growth in mice and represents a novel and promising strategy for the treatment of drug resistant cancers.

DISCUSSION

Using exosomes as drug delivery vehicles takes advantage of their natural carriage and extraordinary ability to interact with target cells. It offers several benefits over common drug administration regimens. Herein, the therapeutic efficacy of exoPTX formulation against pulmonary metastases was demonstrated in an LLC mouse model. Intriguingly, airway-delivered exosomes showed near complete co-localization with cancer metastases in this model. We hypothesized that macrophage-released exosomes have specific proteins located on their surface which allows for their preferential accumulation in cancer cells. It is known that exosome-mediated cell-to-cell communication is the key in the battle between cancer and the immune system [49]. Furthermore, Parolini et al. [50] showed that exosome fusion with target cells occurs more efficiently under acidic conditions, implying that exosomes may be taken up preferentially by tumors (which have an acidic microenvironment) rather than the surrounding healthy tissue. Further investigations are necessary to uncover this mechanism. Our results show that exoPTX demonstrated superior inhibition of pulmonary metastases growth in LLC mouse model. All three mechanisms mentioned here are likely to have significant impact on exoPTX anticancer activity, i.e.: (i) preferential accumulation in cancer cells, (ii) efficient delivery of incorporated cargo into target cancer cells, and (iii) overcoming of Pgp-mediated drug efflux in resistant cancer cells.

Drug-loaded exosomes may well serve as a next generation drug delivery mechanism that combines nanoparticle size with non-cytotoxic effects, a high drug carrying capacity, and a low immunogenic profile. Further tailoring exosomes can provide biologically-active carriers that may be modified in accordance to the disease and produce cytotoxic (for cancer treatment) or neuroprotective (for the treatment of neurodegenerative disorders) effects,

enhancing the therapeutic outcomes. Indeed, some technological, functional and safety features of exosomal-based drug formulations are still to be addressed. A deficiency in our knowledge of the molecular mechanisms of exosomes formation, and lack of methods to interfere with the packaging of cargo or with vesicle release still hampers identification of their physiological relevance *in vivo*. Certainly, the complexity of these therapeutic interventions is challenging, yet they promise an unparalleled efficacy in the treatment of many life-threatening conditions, including those lacking effective pharmacotherapy.

REFERENCES

1. Ratajczak, J., et al., *Membrane-derived microvesicles: important and underappreciated mediators of cell-to-cell communication.* Leukemia, 2006. **20**(9): p. 1487-95.

2. Kalani, A., et al., *Curcumin-primed exosomes mitigate endothelial cell dysfunction during hyperhomocysteinemia.* Life Sciences, 2014. **107**(1–2): p. 1-7.

3. Simpson, R.J., S.S. Jensen, and J.W.E. Lim, *Proteomic profiling of exosomes: Current perspectives.* PROTEOMICS, 2008. **8**(19): p. 4083-4099.

4. Mathivanan, S., H. Ji, and R.J. Simpson, *Exosomes: Extracellular organelles important in intercellular communication.* Journal of Proteomics, 2010. **73**(10): p. 1907-1920.

5. Alvarez-Erviti, L., et al., *Delivery of siRNA to the mouse brain by systemic injection of targeted exosomes.* Nat Biotechnol, 2011. **29**(4): p. 341-5.

6. Wahlgren, J., et al., *Plasma exosomes can deliver exogenous short interfering RNA to monocytes and lymphocytes.* Nucleic Acids Research, 2012. **40**(17): p. e130-e130.

7. Johnsen, K.B., et al., *A comprehensive overview of exosomes as drug delivery vehicles — Endogenous nanocarriers for targeted cancer therapy.* Biochimica et Biophysica Acta (BBA) - Reviews on Cancer, 2014. **1846**(1): p. 75-87.

8. Shtam, T., et al., *Exosomes are natural carriers of exogenous siRNA to human cells in vitro.* Cell Communication and Signaling, 2013. **11**(1): p. 88.

9. Pan, Q., et al., *Hepatic cell-to-cell transmission of small silencing RNA can extend the therapeutic reach of RNA interference (RNAi).* Gut, 2012. **61**(9): p. 1330-1339.

10. Chen, L., et al., *Epigenetic regulation of connective tissue growth factor by MicroRNA-214 delivery in exosomes from mouse or human hepatic stellate cells.* Hepatology, 2014. **59**(3): p. 1118-1129.

11. Maguire, C.A., et al., *Microvesicle-associated AAV Vector as a Novel Gene Delivery System.* Molecular Therapy, 2012. **20**(5): p. 960-971.

12. György, B., et al., *Naturally enveloped AAV vectors for shielding neutralizing antibodies and robust gene delivery in vivo.* Biomaterials, 2014. **35**(26): p. 7598-7609.

13. Hudry, E., et al., *Exosome-associated AAV vector as a robust and convenient neuroscience tool.* Gene Ther, 2016.

14. Zhuang, X., et al., *Treatment of Brain Inflammatory Diseases by Delivering Exosome Encapsulated Anti-inflammatory Drugs From the Nasal Region to the Brain.* Mol Ther, 2011. **19**(10): p. 1769-1779.

15. Sun, D., et al., *A Novel Nanoparticle Drug Delivery System: The Anti-inflammatory Activity of Curcumin Is Enhanced When Encapsulated in Exosomes.* Mol Ther, 2010. **18**(9): p. 1606-1614.

16. Tian, Y., et al., *A doxorubicin delivery platform using engineered natural membrane vesicle exosomes for targeted tumor therapy.* Biomaterials, 2014. **35**(7): p. 2383-2390.

17. Montecalvo, A., et al., *Mechanism of transfer of functional microRNAs between mouse dendritic cells via exosomes.* Blood, 2012. **119**(3): p. 756-66.

18. Goffin, J., et al., *First-line systemic chemotherapy in the treatment of advanced non-small cell lung cancer: a systematic review.* J Thorac Oncol, 2010. **5**(2): p. 260-74.

19. Maemondo, M., et al., *Gefitinib or chemotherapy for non-small-cell lung cancer with mutated EGFR.* N Engl J Med, 2010. **362**(25): p. 2380-8.

20. Vilner, B.J., C.S. John, and W.D. Bowen, *Sigma-1 and sigma-2 receptors are expressed in a wide variety of human and rodent tumor cell lines.* Cancer Res, 1995. **55**(2): p. 408-13.

21. Kim, S.K., M.B. Foote, and L. Huang, *The targeted intracellular delivery of cytochrome C protein to tumors using lipid-apolipoprotein nanoparticles.* Biomaterials, 2012. **33**(15): p. 3959-66.

22. Yang, Y., et al., *Nanoparticle delivery of pooled siRNA for effective treatment of non-small cell lung cancer.* Mol Pharm, 2012. **9**(8): p. 2280-9.

23. Banerjee, V., R.K. Joshi, and H.K. Sehgal, *Influence of adsorption and diffusion rates on the growth of Pb1-x Fex S nanoparticle films.* Phys Rev E Stat Nonlin Soft Matter Phys, 2004. **70**(3 Pt 2): p. 036122.

24. Kooijmans, S.A., et al., *PEGylated and targeted extracellular vesicles display enhanced cell specificity and circulation time.* J Control Release, 2016. **224**: p. 77-85.

25. Thery, C., et al., *Isolation and characterization of exosomes from cell culture supernatants and biological fluids.* Curr Protoc Cell Biol, 2006. **Chapter 3**: p. Unit 3 22.

26. Bhatnagar, S., et al., *Exosomes released from macrophages infected with intracellular pathogens stimulate a proinflammatory response in vitro and in vivo.* Blood, 2007. **110**(9): p. 3234-44.

27. Clayton, A., et al., *Induction of heat shock proteins in B-cell exosomes.* J Cell Sci, 2005. **118**(Pt 16): p. 3631-8.

28. Nolte-'t Hoen, E.N., et al., *Activated T cells recruit exosomes secreted by dendritic cells via LFA-1.* Blood, 2009. **113**(9): p. 1977-81.

29. Lai, R.C., R.W. Yeo, and S.K. Lim, *Mesenchymal stem cell exosomes.* Semin Cell Dev Biol, 2015.

30. Song, J., et al., *Cardiac endothelial cell-derived exosomes induce specific regulatory B cells.* Sci Rep, 2014. **4**: p. 7583.

31. Skogberg, G., et al., *Human thymic epithelial primary cells produce exosomes carrying tissue-restricted antigens.* Immunol Cell Biol, 2015.

32. Benito-Martin, A., et al., *The new deal: a potential role for secreted vesicles in innate immunity and tumor progression.* Front Immunol, 2015. **6**: p. 66.

33. Marcus, M.E. and J.N. Leonard, *FedExosomes: Engineering Therapeutic Biological Nanoparticles that Truly Deliver.* Pharmaceuticals (Basel), 2013. **6**(5): p. 659-80.

34. van der Pol, E., et al., *Particle size distribution of exosomes and microvesicles determined by transmission electron microscopy, flow cytometry, nanoparticle tracking analysis, and resistive pulse sensing.* J Thromb Haemost, 2014. **12**(7): p. 1182-92.

35. Lotvall, J., et al., *Minimal experimental requirements for definition of extracellular vesicles and their functions: a position statement from the International Society for Extracellular Vesicles.* J Extracell Vesicles, 2014. **3**: p. 26913.

36. Aalberts, M., et al., *Identification of distinct populations of prostasomes that differentially express prostate stem cell antigen, annexin A1, and GLIPR2 in humans.* Biol Reprod, 2012. **86**(3): p. 82.

37. Taylor, D.D. and S. Shah, *Methods of isolating extracellular vesicles impact down-stream analyses of their cargoes.* Methods, 2015.

38. Lamparski, H.G., et al., *Production and characterization of clinical grade exosomes derived from dendritic cells.* J Immunol Methods, 2002. **270**(2): p. 211-26.

39. Tauro, B.J., et al., *Comparison of ultracentrifugation, density gradient separation, and immunoaffinity capture methods for isolating human colon cancer cell line LIM1863-derived exosomes.* Methods, 2012. **56**(2): p. 293-304.

40. Taylor, D.D., W. Zacharias, and C. Gercel-Taylor, *Exosome isolation for proteomic analyses and RNA profiling.* Methods Mol Biol, 2011. **728**: p. 235-46.

41. Thery, C., *Exosomes: secreted vesicles and intercellular communications.* F1000 Biol Rep, 2011. **3**: p. 15.

42. van der Pol, E., et al., *Classification, functions, and clinical relevance of extracellular vesicles.* Pharmacol Rev, 2012. **64**(3): p. 676-705.

43. Johnstone, R.M., *The Jeanne Manery-Fisher Memorial Lecture 1991. Maturation of reticulocytes: formation of exosomes as a mechanism for shedding membrane proteins.* Biochem Cell Biol, 1992. **70**(3-4): p. 179-90.

44. Mathivanan, S. and R.J. Simpson, *ExoCarta: A compendium of exosomal proteins and RNA.* Proteomics, 2009. **9**(21): p. 4997-5000.

45. Zomer, A., et al., *Exosomes: Fit to deliver small RNA.* Commun Integr Biol, 2010. **3**(5): p. 447-50.

46. Valadi, H., et al., *Exosome-mediated transfer of mRNAs and microRNAs is a novel mechanism of genetic exchange between cells.* Nat Cell Biol, 2007. **9**(6): p. 654-9.

47. Wolfers, J., et al., *Tumor-derived exosomes are a source of shared tumor rejection antigens for CTL cross-priming.* Nat Med, 2001. **7**(3): p. 297-303.

48. Chen, W., et al., *Efficient induction of antitumor T cell immunity by exosomes derived from heat-shocked lymphoma cells.* Eur J Immunol, 2006. **36**(6): p. 1598-607.

49. Yang, C., et al., *Tumor-derived exosomes confer antigen-specific immunosuppression in a murine delayed-type hypersensitivity model.* PLoS One, 2011. **6**(8): p. e22517.

50. Le, M.T., et al., *miR-200-containing extracellular vesicles promote breast cancer cell metastasis.* J Clin Invest, 2014. **124**(12): p. 5109-28.

51. Harris, D.A., et al., *Exosomes released from breast cancer carcinomas stimulate cell movement.* PLoS One, 2015. **10**(3): p. e0117495.

52. Lv, M.M., et al., *Exosomes mediate drug resistance transfer in MCF-7 breast cancer cells and a probable mechanism is delivery of P-glycoprotein.* Tumour Biol, 2014. **35**(11): p. 10773-9.

53. Prokopi, M., C.A. Kousparou, and A.A. Epenetos, *The Secret Role of microRNAs in Cancer Stem Cell Development and Potential Therapy: A Notch-Pathway Approach.* Front Oncol, 2014. **4**: p. 389.

54. Zhao, L., et al., *The role of exosomes and "exosomal shuttle microRNA" in tumorigenesis and drug resistance.* Cancer Lett, 2015. **356**(2 Pt B): p. 339-46.

55. Schorey, J.S., et al., *Exosomes and other extracellular vesicles in host-pathogen interactions.* EMBO Rep, 2015. **16**(1): p. 24-43.

56. Zitvogel, L., et al., *Eradication of established murine tumors using a novel cell-free vaccine: dendritic cell-derived exosomes.* Nat Med, 1998. **4**(5): p. 594-600.

57. Romagnoli, G.G., et al., *Dendritic Cell-Derived Exosomes may be a Tool for Cancer Immunotherapy by Converting Tumor Cells into Immunogenic Targets.* Front Immunol, 2014. **5**: p. 692.

58. Qazi, K.R., et al., *Antigen-loaded exosomes alone induce Th1-type memory through a B-cell-dependent mechanism.* Blood, 2009. **113**(12): p. 2673-83.

59. Kaur, S., et al., *CD47-dependent immunomodulatory and angiogenic activities of extracellular vesicles produced by T cells.* Matrix Biol, 2014. **37**: p. 49-59.

60. van der Grein, S.G. and E.N. Nolte-'t Hoen, *"Small Talk" in the Innate Immune System via RNA-Containing Extracellular Vesicles.* Front Immunol, 2014. **5**: p. 542.

61. Aucher, A., D. Rudnicka, and D.M. Davis, *MicroRNAs transfer from human macrophages to hepato-carcinoma cells and inhibit proliferation.* J Immunol, 2013. **191**(12): p. 6250-60.

62. Bruno, S., et al., *Microvesicles derived from human bone marrow mesenchymal stem cells inhibit tumor growth.* Stem Cells Dev, 2013. **22**(5): p. 758-71.

63. Morelli, A.E., *The immune regulatory effect of apoptotic cells and exosomes on dendritic cells: its impact on transplantation.* Am J Transplant, 2006. **6**(2): p. 254-61.

64. Colino, J. and C.M. Snapper, *Dendritic cell-derived exosomes express a Streptococcus pneumoniae capsular polysaccharide type 14 cross-reactive antigen that induces protective immunoglobulin responses against pneumococcal infection in mice.* Infect Immun, 2007. **75**(1): p. 220-30.

65. Schnitzer, J.K., et al., *Fragments of antigen-loaded dendritic cells (DC) and DC-derived exosomes induce protective immunity against Leishmania major.* Vaccine, 2010. **28**(36): p. 5785-93.

66. Admyre, C., et al., *Exosomes with immune modulatory features are present in human breast milk.* J Immunol, 2007. **179**(3): p. 1969-78.

67. Zonneveld, M.I., et al., *Recovery of extracellular vesicles from human breast milk is influenced by sample collection and vesicle isolation procedures.* J Extracell Vesicles, 2014. **3**.

68. Gyorgy, B., et al., *Membrane vesicles, current state-of-the-art: emerging role of extracellular vesicles.* Cell Mol Life Sci, 2011. **68**(16): p. 2667-88.

69. Lai, R.C., et al., *Exosome secreted by MSC reduces myocardial ischemia/reperfusion injury.* Stem Cell Res, 2010. **4**(3): p. 214-22.

70. Arslan, F., et al., *Mesenchymal stem cell-derived exosomes increase ATP levels, decrease oxidative stress and activate PI3K/Akt pathway to enhance myocardial viability and prevent adverse remodeling after myocardial ischemia/reperfusion injury.* Stem Cell Res, 2013. **10**(3): p. 301-12.

71. Lee, C., et al., *Exosomes mediate the cytoprotective action of mesenchymal stromal cells on hypoxia-induced pulmonary hypertension.* Circulation, 2012. **126**(22): p. 2601-11.

72. Katsuda, T., et al., *Human adipose tissue-derived mesenchymal stem cells secrete functional neprilysin-bound exosomes.* Sci Rep, 2013. **3**: p. 1197.

73. Xin, H., Y. Li, and M. Chopp, *Exosomes/miRNAs as mediating cell-based therapy of stroke.* Front Cell Neurosci, 2014. **8**: p. 377.

74. Ilmer, M., et al., *Two sides of the same coin: stem cells in cancer and regenerative medicine.* Faseb J, 2014. **28**(7): p. 2748-61.

75. Emanueli, C., et al., *Exosomes and exosomal miRNAs in cardiovascular protection and repair.* Vascul Pharmacol, 2015.

76. Huang, L., et al., *Exosomes in mesenchymal stem cells, a new therapeutic strategy for cardiovascular diseases?* Int J Biol Sci, 2015. **11**(2): p. 238-45.

77. Sahoo, S. and D.W. Losordo, *Exosomes and cardiac repair after myocardial infarction.* Circ Res, 2014. **114**(2): p. 333-44.

78. Ibrahim, A.G., K. Cheng, and E. Marban, *Exosomes as critical agents of cardiac regeneration triggered by cell therapy.* Stem Cell Reports, 2014. **2**(5): p. 606-19.

79. Aminzadeh, M.A., et al., *Therapeutic efficacy of cardiosphere-derived cells in a transgenic mouse model of non-ischaemic dilated cardiomyopathy.* Eur Heart J, 2015. **36**(12): p. 751-62.

80. Hergenreider, E., et al., *Atheroprotective communication between endothelial cells and smooth muscle cells through miRNAs.* Nat Cell Biol, 2012. **14**(3): p. 249-56.

81. Jeyaseelan, K., K.Y. Lim, and A. Armugam, *MicroRNA expression in the blood and brain of rats subjected to transient focal ischemia by middle cerebral artery occlusion.* Stroke, 2008. **39**(3): p. 959-66.

82. Lusardi, T.A., et al., *MicroRNA responses to focal cerebral ischemia in male and female mouse brain.* Front Mol Neurosci, 2014. **7**: p. 11.

83. Liu, F.J., et al., *microRNAs Involved in Regulating Spontaneous Recovery in Embolic Stroke Model.* PLoS One, 2013. **8**(6): p. e66393.

84. Tan, C.Y., et al., *Mesenchymal stem cell-derived exosomes promote hepatic regeneration in drug-induced liver injury models.* Stem Cell Res Ther, 2014. **5**(3): p. 76.

85. Regente, M., et al., *Apoplastic exosome-like vesicles: a new way of protein secretion in plants?* Plant Signal Behav, 2012. **7**(5): p. 544-6.

86. Ding, Y., et al., *Unconventional protein secretion.* Trends Plant Sci, 2012. **17**(10): p. 606-15.

87. Kalani, A., et al., *Curcumin-primed exosomes mitigate endothelial cell dysfunction during hyperhomocysteinemia.* Life Sci, 2014. **107**(1-2): p. 1-7.

88. Kalani, A., A. Tyagi, and N. Tyagi, *Exosomes: mediators of neurodegeneration, neuroprotection and therapeutics.* Mol Neurobiol, 2014. **49**(1): p. 590-600.

89. Sun, D., et al., *A novel nanoparticle drug delivery system: the anti-inflammatory activity of curcumin is enhanced when encapsulated in exosomes.* Mol Ther, 2010. **18**(9): p. 1606-14.

90. Zhuang, X., et al., *Treatment of brain inflammatory diseases by delivering exosome encapsulated anti-inflammatory drugs from the nasal region to the brain.* Mol Ther, 2011. **19**(10): p. 1769-79.

91. Jang, S.C., et al., *Bioinspired Exosome-Mimetic Nanovesicles for Targeted Delivery of Chemotherapeutics to Malignant Tumors.* ACS Nano, 2013.

92. Tian, Y., et al., *A doxorubicin delivery platform using engineered natural membrane vesicle exosomes for targeted tumor therapy.* Biomaterials, 2014. **35**(7): p. 2383-90.

93. Rani, S., et al., *Mesenchymal Stem Cell-derived Extracellular Vesicles: Toward Cell-free Therapeutic Applications.* Mol Ther, 2015.

94. Yang, T., et al., *Exosome Delivered Anticancer Drugs Across the Blood-Brain Barrier for Brain Cancer Therapy in Danio Rerio.* Pharm Res, 2015.

95. Thery, C., M. Ostrowski, and E. Segura, *Membrane vesicles as conveyors of immune responses.* Nat Rev Immunol, 2009. **9**(8): p. 581-93.

96. Waldenstrom, A., et al., *Cardiomyocyte microvesicles contain DNA/RNA and convey biological messages to target cells.* PLoS One, 2012. **7**(4): p. e34653.

97. El Andaloussi, S., et al., *Exosomes for targeted siRNA delivery across biological barriers.* Adv Drug Deliv Rev, 2013. **65**(3): p. 391-7.

98. Lee, Y., S. El Andaloussi, and M.J. Wood, *Exosomes and microvesicles: extracellular vesicles for genetic information transfer and gene therapy.* Hum Mol Genet, 2012. **21**(R1): p. R125-34.

99. Lai, C.P. and X.O. Breakefield, *Role of exosomes/microvesicles in the nervous system and use in emerging therapies.* Front Physiol, 2012. **3**: p. 228.

100. Lai, R.C., et al., *Exosomes for drug delivery - a novel application for the mesenchymal stem cell.* Biotechnol Adv, 2012.

101. Ohno, S., et al., *Systemically injected exosomes targeted to EGFR deliver antitumor microRNA to breast cancer cells.* Mol Ther, 2013. **21**(1): p. 185-91.

102. Kooijmans, S.A., et al., *Electroporation-induced siRNA precipitation obscures the efficiency of siRNA loading into extracellular vesicles.* J Control Release, 2013. **172**(1): p. 229-38.

103. Wahlgren, J., et al., *Plasma exosomes can deliver exogenous short interfering RNA to monocytes and lymphocytes.* Nucleic Acids Res, 2012. **40**(17): p. e130.

104. van der Meel, R., et al., *Extracellular vesicles as drug delivery systems: lessons from the liposome field.* J Control Release, 2014. **195**: p. 72-85.

105. Raposo, G. and W. Stoorvogel, *Extracellular vesicles: exosomes, microvesicles, and friends.* J Cell Biol, 2013. **200**(4): p. 373-83.

106. Haney, M.J., et al., *Exosomes as drug delivery vehicles for Parkinson's disease therapy.* J Control Release, 2015.

107. Jamur, M.C. and C. Oliver, *Permeabilization of cell membranes.* Methods Mol Biol, 2010. **588**: p. 63-6.

108. Pascucci, L., et al., *Paclitaxel is incorporated by mesenchymal stromal cells and released in exosomes that inhibit in vitro tumor growth: a new approach for drug delivery.* J Control Release, 2014. **192**: p. 262-70.

109. Lv, L.H., et al., *Anticancer drugs cause release of exosomes with heat shock proteins from human hepatocellular carcinoma cells that elicit effective natural killer cell antitumor responses in vitro.* J Biol Chem, 2012. **287**(19): p. 15874-85.

110. Lee, J., et al., *Liposome-Based Engineering of Cells To Package Hydrophobic Compounds in Membrane Vesicles for Tumor Penetration.* Nano Lett, 2015.

111. Zhao, Y., et al., *GDNF-transfected macrophages produce potent neuroprotective effects in Parkinson's disease mouse model.* PLoS One, 2014. **9**(9): p. e106867.

112. Haney, M.J., et al., *Blood-borne macrophage-neural cell interactions hitchhike endosome networks for cell-based nanozyme brain delivery.* Nanomedicine (Lond), 2012. **7**(6): p. 815-833.

113. Zeelenberg, I.S., et al., *Targeting tumor antigens to secreted membrane vesicles in vivo induces efficient antitumor immune responses.* Cancer Res, 2008. **68**(4): p. 1228-35.

114. Haney, M.J., et al., *Specific Transfection of Inflamed Brain by Macrophages: A New Therapeutic Strategy for Neurodegenerative Diseases.* Plos One, 2013. **8**((4)): p. e61852.

115. Maguire, C.A., et al., *Microvesicle-associated AAV vector as a novel gene delivery system.* Mol Ther, 2012. **20**(5): p. 960-71.

116. Shtam, T.A., et al., *Exosomes are natural carriers of exogenous siRNA to human cells in vitro.* Cell Commun Signal, 2013. **11**: p. 88.

117. Pan, Q., et al., *Hepatic cell-to-cell transmission of small silencing RNA can extend the therapeutic reach of RNA interference (RNAi).* Gut, 2012. **61**(9): p. 1330-9.

118. Liu, Y., et al., *Microvesicle-delivery miR-150 promotes tumorigenesis by up-regulating VEGF, and the neutralization of miR-150 attenuate tumor development.* Protein Cell, 2013. **4**(12): p. 932-41.

119. Nordin, J.Z., et al., *Ultrafiltration with size-exclusion liquid chromatography for high yield isolation of extracellular vesicles preserving intact biophysical and functional properties.* Nanomedicine, 2015.

120. Yeo, R.W., et al., *Mesenchymal stem cell: An efficient mass producer of exosomes for drug delivery.* Adv Drug Deliv Rev, 2012.

121. Ban, J.J., et al., *Low pH increases the yield of exosome isolation.* Biochem Biophys Res Commun, 2015.

122. Portner, R., et al., *Bioreactor design for tissue engineering.* J Biosci Bioeng, 2005. **100**(3): p. 235-45.

123. Muller, F.J., E.Y. Snyder, and J.F. Loring, *Gene therapy: can neural stem cells deliver?* Nat Rev Neurosci, 2006. **7**(1): p. 75-84.

124. Chen, T.S., et al., *Enabling a robust scalable manufacturing process for therapeutic exosomes through oncogenic immortalization of human ESC-derived MSCs.* J Transl Med, 2011. **9**: p. 47.

125. Mignot, G., et al., *Prospects for exosomes in immunotherapy of cancer.* J Cell Mol Med, 2006. **10**(2): p. 376-88.

126. Escudier, B., et al., *Vaccination of metastatic melanoma patients with autologous dendritic cell (DC) derived-exosomes: results of thefirst phase I clinical trial.* J Transl Med, 2005. **3**(1): p. 10.

127. Morse, M.A., et al., *A phase I study of dexosome immunotherapy in patients with advanced non-small cell lung cancer.* J Transl Med, 2005. **3**(1): p. 9.

128. Dai, S., et al., *Phase I clinical trial of autologous ascites-derived exosomes combined with GM-CSF for colorectal cancer.* Mol Ther, 2008. **16**(4): p. 782-90.

129. Greenwald, R.B., et al., *Drug delivery systems: water soluble taxol 2'-poly(ethylene glycol) ester prodrugs-design and in vivo effectiveness.* J Med Chem, 1996. **39**(2): p. 424-31.

130. Kim, M.S., et al., *Development of exosome-encapsulated paclitaxel to overcome MDR in cancer cells.* Nanomedicine: Nanotechnology, Biology and Medicine.

131. Zhao, Y., et al., *Polyelectrolyte complex optimization for macrophage delivery of redox enzyme nanoparticles.* Nanomedicine (Lond), 2011. **6**(1): p. 25-42.

132. Batrakova, E.V., et al., *A macrophage-nanozyme delivery system for Parkinson's disease.* Bioconjug Chem, 2007. **18**(5): p. 1498-506.

133. Laulagnier, K., et al., *Characterization of exosome subpopulations from RBL-2H3 cells using fluorescent lipids.* Blood Cells, Molecules, and Diseases, 2005. **35**(2): p. 116-121.

134. Jang, S.C., et al., *Bioinspired exosome-mimetic nanovesicles for targeted delivery of chemotherapeutics to malignant tumors.* ACS Nano, 2013. **7**(9): p. 7698-710.

135. Peng, Q., et al., *Preformed albumin corona, a protective coating for nanoparticles based drug delivery system.* Biomaterials, 2013.

136. Mulcahy, L.A., R.C. Pink, and D.R.F. Carter, *Routes and mechanisms of extracellular vesicle uptake.* Journal of Extracellular Vesicles, 2014. **3**: p. 10.3402/jev.v3.24641.

137. Johnsen, K.B., et al., *A comprehensive overview of exosomes as drug delivery vehicles - endogenous nanocarriers for targeted cancer therapy.* Biochim Biophys Acta, 2014. **1846**(1): p. 75-87.

138. Hayeshi, R., et al., *The potential inhibitory effect of antiparasitic drugs and natural products on P-glycoprotein mediated efflux.* European Journal of Pharmaceutical Sciences, 2006. **29**(1): p. 70-81.

139. Bauer, K.S., et al., *A phase I and pharmacologic study of idarubicin, cytarabine, etoposide, and the multidrug resistance protein (MDR1/Pgp) inhibitor PSC-833 in patients with refractory leukemia.* Leukemia Research. **29**(3): p. 263-271.

140. Koziara, J.M., et al., *In-vivo efficacy of novel paclitaxel nanoparticles in paclitaxel-resistant human colorectal tumors.* Journal of Controlled Release, 2006. **112**(3): p. 312-319.

141. De Jong, W.H. and P.J.A. Borm, *Drug delivery and nanoparticles: Applications and hazards.* International Journal of Nanomedicine, 2008. **3**(2): p. 133-149.

142. Batrakova, E.V., et al., *Mechanism of sensitization of MDR cancer cells by Pluronic block copolymers: Selective energy depletion.* Br J Cancer, 2001. **85**(12): p. 1987-1997.

143. Batrakova, E., et al., *Fundamental Relationships Between the Composition of Pluronic Block Copolymers and Their Hypersensitization Effect in MDR Cancer Cells.* Pharmaceutical Research. **16**(9): p. 1373-1379.

144. Batrakova, E.V., et al., *Optimal Structure Requirements for Pluronic Block Copolymers in Modifying P-glycoprotein Drug Efflux Transporter Activity in Bovine Brain Microvessel Endothelial Cells.* Journal of Pharmacology and Experimental Therapeutics, 2003. **304**(2): p. 845-854.

145. Batrakova, E.V., et al., *Sensitization of Cells Overexpressing Multidrug Resistant Proteins by Pluronic P85.* Pharmaceutical research, 2003. **20**(10): p. 1581-1590.

146. Cascorbi, I., *Role of pharmacogenetics of ATP-binding cassette transporters in the pharmacokinetics of drugs.* Pharmacology & Therapeutics, 2006. **112**(2): p. 457-473.

147. Kalra, H., et al., *Comparative proteomics evaluation of plasma exosome isolation techniques and assessment of the stability of exosomes in normal human blood plasma.* Proteomics, 2013. **13**(22): p. 3354-64.

148. Safaei, R., et al., *Abnormal lysosomal trafficking and enhanced exosomal export of cisplatin in drug-resistant human ovarian carcinoma cells.* Mol Cancer Ther, 2005. **4**(10): p. 1595-604.

149. Yamagishi, T., et al., *P-glycoprotein mediates drug resistance via a novel mechanism involving lysosomal sequestration.* J Biol Chem, 2013. **288**(44): p. 31761-71.

150. Jemal, A., et al., *Cancer statistics, 2007.* CA Cancer J Clin, 2007. **57**(1): p. 43-66.

151. Klyachko, N.L., et al., *Macrophages offer a paradigm switch for CNS delivery of therapeutic proteins.* Nanomedicine, 2014. **9**(9): p. 1403-1422.

152. Brynskikh, A.M., et al., *Macrophage delivery of therapeutic nanozymes in a murine model of Parkinson's disease.* Nanomedicine (Lond), 2010. **5**(3): p. 379-96.

153. Batrakova, E.V., et al., *Effects of pluronic and doxorubicin on drug uptake, cellular metabolism, apoptosis and tumor inhibition in animal models of MDR cancers.* J Control Release, 2010. **143**(3): p. 290-301.